Experimental Study on Mixing of Activated Sludge with or without Air in a Mixing Tank through Electrical Resistance Tomography (ERT) and Response Surface Methodology (RSM)

By

Divya Malik

Bachelor of Technology (Biotechnology)

Sardar Vallabhbhai Patel University of Agriculture & Technology,

Meerut, India, 2015

Supervisor: Dr. Leila Pakzad

A Thesis Submitted to Department of Chemical Engineering

in Partial Fulfillment of the Requirements for the

Degree of Masters of Science in Environmental Engineering at

Lakehead University

Thunder Bay, Ontario, Canada

April, 2017

ABSTRACT

Experimental Study on Mixing of Activated Sludge with or without Air in a Mixing Tank through Electrical Resistance Tomography (ERT) and Response Surface Methodology (RSM)

MSc, Environmental Engineering, Lakehead University, ON, 2017

Divya Malik

In such industrial processes as oxidation, hydrogenation, and biological fermentation gas and liquid are contacted and mixed to reach steady condition. The unit operations applied for gas/liquid processes include but are not limited to bubble column, plate column, mechanically agitated vessels, in-line static mixers, jet mixing devices/jet mixers, and surface aerators. Among aforementioned unit operations, aerated mixing vessels are mostly employed for the gas-liquid processes in such industry as biochemical, pharmaceutical, cosmetics, and waste water treatment. While gas-dispersion in Newtonian fluids, especially in low-viscosity systems, has been successfully understood, not enough information may be found in the literature about this process in non-Newtonian fluids. Therefore, in this study electrical resistance tomography (ERT) was utilized to assess the mixing of the activated sludge as shear thinning non-Newtonian fluid in presence of aeration. ERT results revealed that shorter mixing time can be achieved in presence of aeration. The following three central impellers were employed: ASI (a combination of A200 and the Scaba impellers), ARI (a combination of A200 and the Rushton impellers), and Rushton (fully radial impeller). An ERT system with a two-plane assembly equipped with 16 sensors on each plane was employed to assess the impact of the impeller type, impeller speed, and gas flow rate on the mixing of activated sludge in terms of mixing time, specific power consumption, and gas flow number. A statistical-based experimental design with RSM (response surface methodology) was applied to evaluate the individual and interactive effects of the design parameters and operating conditions. Experiments and RSM demonstrated that among all independent variables in this study, impeller speed was the common independent variable which impacts mixing time, specific power consumption and gas flow number significantly.

Acknowledgements

I would like to offer my deepest gratitude to my supervisor, Dr. Leila Pakzad for her continuous guidance and motivation during my course and research work. This thesis work would not have been possible without her knowledge, guidance and helpful tips. Thank you from the bottom of my heart as well as on behalf of my parents for your attention, support and care during this journey. She is an idol to me and it would be my pleasure to follow her footsteps and advices for the rest of my life.

I am grateful to Dr. Amir H. Azimi from Department of Civil Engineering and Dr. Ebrahim Rezaei from Department of Chemical Engineering at Lakehead University for reviewing my research work.

I also owe a great debt to Nancy Gallo and Laura Pudas from International office at Lakehead University for their emotional support as well as motivation during this journey.

My special thanks and lots of love goes to my parents and the most loveable person, my brother. Without their love, affection, and support I would not be able to face any challenge in my life. My mother deserves my wholehearted thanks for her unconditional love, encouragement, and moral support. Also, I can't express my feelings in words how thankful I am to my father for fulfilling my dreams and supporting me on each and every step. Thanks a lot. I will always make you feel proud.

Finally, thank you, Godhead, for always being there for me.

Table of Contents

List of Figures

List of Tables

1. Introduction

High efficiency mixing in the gas/liquid systems requires high interfacial area, high mass transfer coefficient, and high turbulent flow which can be achieved through different unit operations. The unit operations applied for gas/liquid processes include but are not limited to bubble column (Babaie et al., 2015(a)), mechanically agitated vessels (Hashemi et al., 2015), in-line static mixers (Ramsay et al., 2016), jet mixing devices/jet mixers (Amiri et al., 2010), and surface aerators (Middleton, 1985). Previously mentioned unit operations work on the different principles such as in the bubble column (Babaei et al., 2015(a)), the gas is sparged into the liquid at the bottom of the column whereas in jet mixing devices (Amiri et al., 2010), the gas is dispersed into the liquid with the help of liquid jets. At industrial level such as waste-water treatment, food, pharmaceutical, cosmetic, paint, and polymer, aerated mixing vessels (Hashemi et al., 2015) are mostly employed for the gas-liquid processes.

The two-phase gas/liquid mixing in the stirred vessels yields significant complexity which is of great importance in manufacturing of a variety of key chemical intermediates (Lamont, 1958). To create a dispersion of gas in a continuous liquid phase, a mechanical agitation system is highly recommended (Wang et al., 2000). To maximize the efficiency of such aerated mixing vessels, it is important to identify the effective parameters. Such parameters include: **(a)** rheological properties of the liquid; **(b)** mixing operation conditions such as impeller speed, power and tip speed, level of mixing achieved, flow pattern existing in the vessel, and distribution of turbulence intensity in the vessel; **(c)** geometric parameters such as vessel diameter; liquid height: bottom or head geometry, such as flat, dished, or cone-shaped; impeller type, geometry, diameter, and bottom clearance; and baffle number, type, and geometry, **(d)** gas phase conditions such gas flow rate, superficial gas velocity, and sparger type and size. For a successful design and scale-up, it is crucial to have a better understanding on the mixing parameters related to this system such as the hydrodynamic parameters, power consumption, and mixing time.

The purpose of the mixing in gas-liquid system is to increase the contacting area by dispersing the gas bubbles into the liquid. This task will be more difficult in case of non-Newtonian fluids such as activated sludge. While gas-dispersion in Newtonian fluids, especially in low-viscosity systems,

has been successfully understood, not enough information may be found in the literature about this process in non-Newtonian fluids. One concern in gas dispersion in non-Newtonian fluids is to increase the effectiveness of the mixing system in dispersing the gas bubbles into the viscous fluid. In fact, design criteria incorporating mixing effectiveness are needed so that acceptable mixing responses can be attained from the applied mixing systems.

The involved processes in gas/liquid mixing system are agitation and aeration with the mutual effects. Based on these processes, two flow regimes are determined as: **(1)** if the impeller speed is high and gas flow rate is low, loading regime takes place in which impeller disperses the gas towards the walls of the vessel; **(2)** if the impeller speed is low and gas flow rate is high, flooding regime occurs in which the impeller is not able to disperse the gas (Ali, 2014). Therefore, it is essential that the gas is effectively captured and dispersed by the agitator in the aerated mixing vessels (Hashemi et al., 2015). In order to have an optimum process, selection of the impeller type and impeller speed corresponding to the gas flow rate is a challenging task in chemical industries. However, the optimal agitation strategies are fully influenced by liquid rheology (Williams et al., 1999; Vlaev et al., 1999; Bolton et al., 2004; Fransolet et al., 2005).

One of the most important application of the aerated mixing vessels is in treatment of the activated sludge (Papa et al., 2015). Aeration is utilized in activated sludge bioreactors to supply oxygen to the biomass and conservation of mixed conditions inside the bioreactor (Braak et al., 2011). During the agitation of the activated sludge, it exhibits complex rheology depending on several different parameters such as pH, temperature, particle dimensions, concentration of solid, fluid consistency coefficient, yield stress, and sludge treatment process (Novarino et al., 2010) which makes the mixing process more challenging and difficult. Sanin (2002) studied the effect of pH, conductivity, solid concentration and flocculation properties on colloidal properties of sludge. Mori et al. (2006) contributed a study on the rheological parameters for various total suspended solid (TSS) values in activated sludge and Guibaud et al. (2004) determined the Bingham's viscosity and shear stress for various total suspended solid (TSS) in the activated sludge samples.

Mixing performance is generally evaluated by measuring mixing times. Although several studies have been performed to understand the effect of aeration on mixing time in the aerated mixing

vessels, still there is not an exact answer especially in case of non-Newtonian liquids such as activated sludge. It was shown that the high amount of aeration decreases the mixing time due to the giant motion inside the vessel (Vasconcelos et al., 1995) however, some other literature concluded that a fluctuation can be observed in mixing time by applying a dominant amount of aeration (Machon & Jodha, 2000). There are various methods to measure mixing time (Kraume & Zehner, 2001) such as applying conductivity method (Jaworski et al., 2002), pH meter (Gullard & Tragardh, 2003), tomography technique (Pakzad et al., 2008, Pakzad et al., 2013, Kazemzadeh et al., 2016), and the decolorization method (Kuzmanic & Ljubicic, 2000). Among the aforementioned techniques, electrical resistance tomography (ERT) was found as the most widely utilized technique because of its fast speed in capturing the real-time data of the extremely fluctuating flow in gas-liquid systems without interrupting the developed flow (Hashemi et al., 2015)

In this study, electrical resistance tomography (ERT) was employed to study the level of homogeneity inside an aerated mixing vessel applied in agitation of activated sludge, pseudoplastic fluid. Therefore, the main objective of this study was to assess the mixing time, specific power consumption, and gas flow number of three different impellers namely, ARI (an axial-radial impeller), Rushton (a radial impeller), and ASI (a combination of the A200 and the Scaba impeller) in the mixing of activated sludge, a non-Newtonian fluid. Using ERT, for the first time the performance of an impeller called ASI (Pakzad et al., 2013) in agitation of activated sludge in presence of air was studied and compared with two other impellers. Also, the effect of the impeller speed and air flow rate was assessed. The rheological properties of activated sludge were also determined using a rheometer. Design of experiments (DOE) and response surface methodology (RSM) was also applied to analyze the data, evaluate the possible interaction among the variables, and define the most effective factor. Using three-factor three-level Box-Behnken combined with RSM, two quadratic models were established in terms of mixing time and specific power consumption, respectively as the functions of impeller type, impeller speed, and gas flow rate.

Chapter two provides a brief literature review in order to understand fundamentals in non-Newtonian fluids mixing with or without air such as fluid behavior, gas-liquid dispersion, flow

patterns, mixing time, power consumption, and gas flow number. Lastly, a brief section is presented which includes some techniques to evaluate mixing time.

Chapter three is organized with the detailed design, specification, structure and operation of electrical resistance tomography (ERT). At the end, applications of ERT are presented.

Chapter four is concerned with the experimental set up employed in this study as well as detailed discussion on the procedure is presented.

Chapter five provides the experimental results from ERT and response surface methodology (RSM) found in this research work as well as the thorough discussions.

Finally, Chapter six summarize the conclusions obtained in this study and provides recommendations for future work.

2. Literature Review

2.1 Introduction

The main objective of mixing in all systems is homogenization. The system to be mixed can be multiphase system such as liquid-gas, liquid-solid, and liquid-gas-solid. Among multiphase mixing systems, the gas-liquid mixing in mechanically agitated vessels are very common industrial operations used in such industries as pharmaceutical, cosmetic, waste water treatment, food, chemical, and biochemical. One example of such system is the injection of compressed air into ambient water which is one of the best available lake, river, and wastewater remediation methods to intensify aeration without the necessity of applying porous diffusers. In different industries like pharmacies, foods, refineries and chemical process, mixing time examines as an important parameter in stirred tanks. Mixing time must adapt the reactant which react very fast (Holley, 1996).

The term two-phase flow covers a wide range of flow regimes. Two-phase flows should be reviewed through two concepts, **(a)** the physical state of the constituent components and **(b)** topology of the interfaces. Through the physical state, two-phase flows can be defined as gas-liquid, gas-solid, solid-liquid, or liquid- liquid (two immiscible liquids) whereas on the basis of topology of interfaces, a flow can be divided as separated, dispersed, or transitional. In biochemical engineering, gas-liquid systems have considerable applications due to the utilization of gas phase in the complex fermentation process (Hashemi et al., 2015). The reason is attributed to the agitation in such multiphase complex process since agitation provides the high mass transfer rate along with the significant degree of homogeneity in the shortest mixing time. In complex fluids such as activated sludge gas phase has a significant impact on hydrodynamics characteristics and mass transfer rate throughout the mixing tank (Babaei et al., 2015(b)).

In designing of chemical engineering reactors, the efficiency of mixing performance is one of the most crucial parameter although it has impact on scaling up process. Therefore, it is important to design an efficient mixing system equipped with appropriate equipment (type of impellers, sparger). The mixing time and power consumption are the two most considerable parameters to

assess the mixing performance of the reactor. However, impeller type, impeller speed, and gas flow rate are the three independent factors which has a significant effect on the above mentioned parameters and the performance of such independent factors should be determined in detail.

The main objective of this chapter is to give a precise knowledge regarding gas-liquid mixing, mixing in presence or absence of aeration, mixing of activated sludge with different types of impellers, mixing time, specific power consumption, and gas flow number. In continuation, some applications of ERT in mixing of activated sludge and the research objectives are presented.

2.2 Activated Sludge

2.2.1 Rheology

Rheology is the science which is necessary to study the behavior of every fluid in certain mechanical conditions. Sanin et al. (2011) defined rheology as "the science that deals with the relationship between an imposed shear stress and the resultant shear rate under different conditions".

Figure 2.1 shows the fluid behavior when the force is applied. There are two plates parallel to each other with area (A), and a specific distance (d_y), and the fluid is flowing between two plates. To produce the velocity (dV_x) to the upper plate, the force is applied whereas the lower plate is in the stationary form, which demonstrates that the fluid near to the upper plate flows at velocity, dV_x whereas the velocity is zero for the fluid near to the lower plate. However, because of the uniform shearing force F, on distance d_y, a uniform velocity gradient of magnitude $\frac{dV_x}{d_y}$ is produced within the fluid (Chhabra & Richardson, 2008).

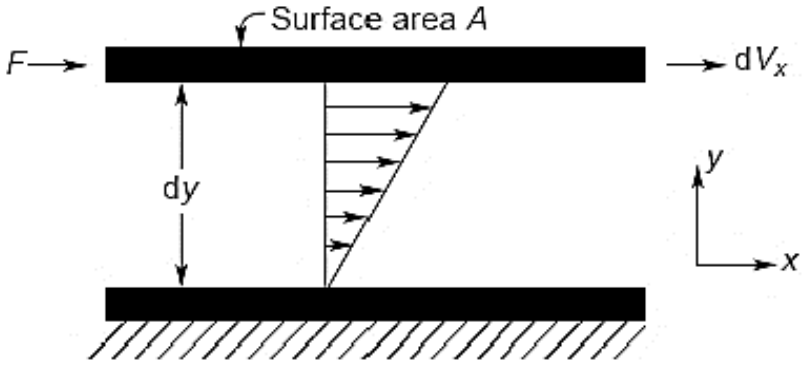

Figure 2.1. Unidirectional Flow (Chhabra and Richardson, 2008).

The experiment based on unidirectional flow can be explained by using the following equation:

$$\frac{F}{A} = \tau = \frac{\eta dV_x}{d_y} = \mu\dot{\gamma} \tag{2.1}$$

where $\frac{dV_x}{d_y}$, the velocity gradient termed as the shear rate ($\dot{\gamma}$), the shearing force per unit area is known as shear stress (τ) and μ is the constant which is known as the Newtonian viscosity (Chhabra & Richardson, 2008).

The rate at which the shear rate depends not only on the magnitude of shear stress but also on the property of the fluid which is called viscosity (Wilkes, 2006). Viscosity is the characteristic of liquid to oppose flow or a change in shape through internal forces and molecular attraction (Holland & Chapman, 1966). Fluids can be described as Newtonian and non-Newtonian fluids due to the effects generated by shear stress. For better understanding of the gas-liquid mixing process, it is more advantageous to subdivide liquids further into Newtonian and non-Newtonian fluids. In case of Newtonian fluids, the shear stress is directly proportional to that of the shear rate. Newtonian's law of viscosity can be expressed by the following equation:

$$\tau = \mu\dot{\gamma} \tag{2.2}$$

In the above equation, shear stress is denoted by $\boldsymbol{\tau}$, Newtonian viscosity is denoted by μ, and shear rate is denoted by $\dot{\gamma}$. The rate of shear stress to shear rate is termed as the Newtonian viscosity which determine the resistance to flow. There are various factors which affects the Newtonian viscosity such as material/fluid, temperature and pressure of the fluid.

"A non-Newtonian fluid may defined as a fluid whose apparent viscosity is not constant at a given temperature and pressure, but differs depending on the flow (example, flow geometry, shear rate etc.)" (Markis F., 2015). For non-Newtonian fluids, the flow curve i.e. shear stress versus shear rate plot is non-linear. This type of material can be generally characterized as follows:

1. Time-dependent fluids: In the case of time-dependent non-Newtonian fluids the shear stress and the viscosity increases or decreases with the time-period of shearing.

2. Time-independent fluids: The shear rate for these types of fluids at any point is calculated by the shear stress at that point and does not depend on time-period of shearing.

3. Viscoplastic fluids: These kinds of fluids shows the characteristics of both solids and ideal viscous fluids after deformation.

To determine important rheological parameters such as shear stress, yield stress, flow index, infinite and zero-rate viscosities and flow consistency index several rheological models have been developed as follows (Sokolov, 2013):

2.2.2 Non-Newtonian Fluid Models

Different fluid models can be used to identify the non-Newtonian fluids by determining their behavior. The power-law (or Ostwald model), the Bingham model, the Herschel-Bulkey model, the truncated power law model, the Sisko model, the Casson model, and the Cross model are the most commonly used models to determine the fluid behavior (Chhabra & Richardson, 2008). The power- law model is known as the pseudoplastic model which shows the shear-thinning behavior of the fluid. The equation for power- law model is as follows:

$$\tau = K\dot{\gamma}^n \tag{2.3}$$

where $\boldsymbol{\tau}$ is the shear stress, $\dot{\boldsymbol{\gamma}}$ shows the shear rate, K is the fluid consistency and n shows the flow index which is dimensionless measure of the fluid behavior (Chhabra & Richardson, 2008). **Figure 2.2** shows the different flow curves or rheograms for Newtonian and non-Newtonian fluids. The pseudoplastic curve for the power law model passes through the origin. However, the fluid is called as Newtonian, when the value of n equals to 1 and the curve shows the straight line through the origin. When n is less than 1 and n is greater than 1, the fluid is termed as shear thinning and shear thickening (dilatant) fluid respectively. Therefore, for shear thinning flow the curve displays a concave upward direction whereas for dilatant fluid, the stress-shear rate curve is concave downward (Chhabra & Richardson, 2008).

A model which outlines the viscoplastic behavior of the fluid and is a two-parameter modification of the power law model is known as the Bingham model. The Bingham fluid shows a linear flow curve on stress-shear rate plot (Chhabra & Richardson, 2008). The combination of power law model and the Bingham model (exhibits the viscoplastic and shear thinning or thickening behavior)

is termed as the Herschel-Bulkley model. The Herschel-Bulkley fluid at low stress behaves such as solid, and shows a shear thinning fluid behavior until a yield stress stage is reached. After removing the applied stress this kind of fluid goes back to the solid state. The Herschel-Bulkley model explains the properties of viscous as well as plastic fluids. These kind of fluids displays a "yield pseudoplastic" concave curve (Chhabra & Richardson, 2008).

To characterize the viscoplastic fluids which possess pseudo-plastic shear thinning behavior Bingham **(Equation 2.4)**, Ostwald **(Equation 2.5)**, Hershel-Bulkley **(Equation 2.6)**, Sisko **(Equation 2.7)**, Careau **(Equation 2.8)** and cross models **(Equation 2.9)** have been employed (Ratkovich et al., 2013, Mori et al., 2006, Khalili et al., 2011). The following equations can be used for the respective models:

$$\tau = \boldsymbol{\tau_y} + \eta_B \dot{\gamma}^n \tag{2.4}$$

$$\tau = K\dot{\gamma}^n \tag{2.5}$$

$$\tau = \boldsymbol{\tau_y} + K\dot{\gamma}^n \tag{2.6}$$

$$\mu = \mu_\infty + K\dot{\gamma}^{n-1} \tag{2.7}$$

$$\frac{\mu - \mu_\infty}{\mu_0 - \mu_\infty} = [1 + (\lambda\dot{\gamma})^2]^{\frac{n-1}{2}} \tag{2.8}$$

$$\frac{\mu - \mu_\infty}{\mu_0 - \mu_\infty} = \frac{1}{1 + (\lambda\dot{\gamma})^m} \tag{2.9}$$

$$\mu(T) = \mu_0 e^{\left(\frac{E}{RT}\right)} \tag{2.10}$$

where $\boldsymbol{\tau}$ is the shear stress, $\boldsymbol{\tau_y}$ is the yield stress, $\dot{\boldsymbol{\gamma}}$ is the shear rate, K is the fluid consistency and n is the flow index which is dimensionless measure of the fluid behavior (Chhabra & Richardson, 2008), η_B is the high-shear thinning limiting viscosity, μ_∞ is the infinite rate apparent viscosity, μ_0 is the zero-shear rate apparent viscosity, λ is the time constant, m is the cross-rate constant. In **Equation (2.10)**, T is the temperature, μ_0 is the coefficient which is termed as frequency factor, E is the activation energy and R is the universal gas constant (8.314 J $mol^{-1}K^{-1}$). **Equation (2.10)** shows the effect of temperature at specific shear rate of the fluid and can be described by the Arrehenius relationship obtained from Ostwald model (Rao et al., 2010).

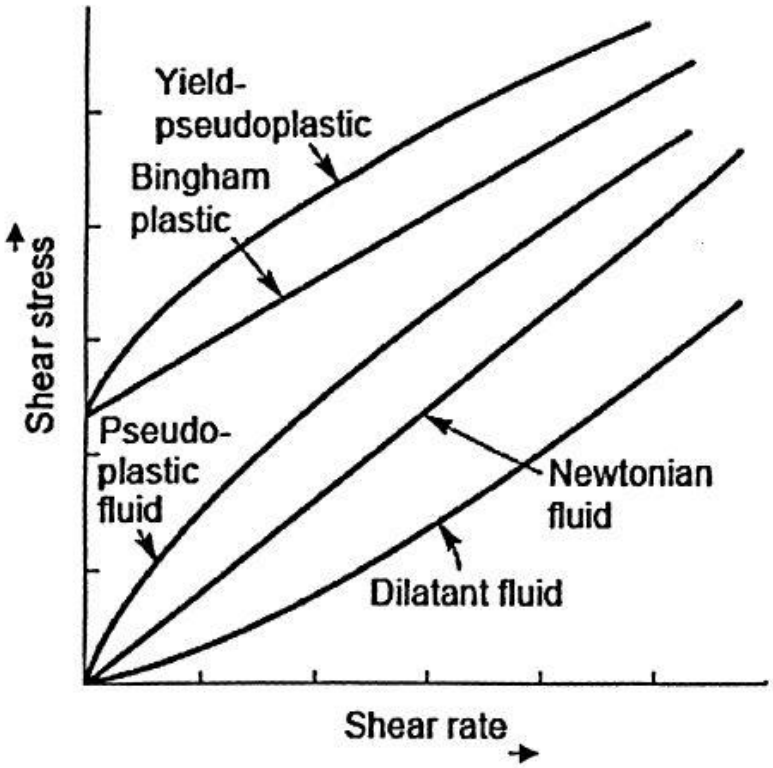

Figure 2.2. Flow Curves of Newtonian and non-Newtonian Fluids (Chhabra and Richardson, 1999).

2.2.3 Activated Sludge and Rheological Modeling

The word 'sludge' describes the water and a semi-solid residue which assembles from industrial waste, hospital waste, farmlands and landfill leachates etc. (Sanin et al., 2011). 'Fresh' sewage sludge is a collection of water, mineral particles, dead/alive bacteria (Bhattacharya, 1981, Baudez et al., 2013). The flow behavior and properties of sludge are not constant, which resembles that the behavior of flow depends on various unit operations such as storage and handling, mixing, pumping, transportation, and etc. Also, the shape and structure of the sludge altered with the concentration of solids, temperature, particle interactions, and water content (Markis F., 2015).

The total solids concentration, water content and particle interactions have also impact on the apparent viscosity, yield stress, thixotropic, and viscoelastic characteristics of sludge (Markis F., 2015).

Rheology of activated sludge has a major role to understand the sludge behavior through the treatment process (Slatter, 1997). The rheology of activated sludge depends on several different factors such as pH, temperature, particle dimensions, concentration of solids, fluid consistency coefficient, yield stress, type of sludge, sludge treatment process and etc. (Novarino et al., 2010). One of the most important parameter is the viscosity which gives an idea about the characteristics of sludge flow under deformation in flow conditions. The ratio of shear stress to shear rate is termed as viscosity. The viscosity of activated sludge changes with shear stress and shear rate (Novarino et al., 2010).

Many studies have been done in regards to these parameters and how these parameters have effects on rheological properties of activated sludge (Sanin, 2002; Dentel., 1997; Mori et al., 2006; Guibaud et al., 2004; Forster, 2002). According to Sanin's research, the viscosity of the dispersion medium, the particle concentration, size and shape of particle and particle-dispersion medium interactions influence the rheological behavior of activated sludge. As the solid concentration influence the activated sludge viscosity such that with the increase in solid concentration, the non-Newtonian sludge behavior also increases instead of the Newtonian (for example, water and fluids with low solid concentration).

Table 2.1 presents the literature data on the rheology of activated sludge for the same range (approximately) of mixed liquor suspended solids (MLSS)[1] concentration and shear rate collected by different researchers. The results shown in **Table 2.1** are not consistent due to the complex rheological behavior of activated sludge as rheology of sludge affected by several factors such as MLSS concentration, conductivity, pH, floc structure and temperature as well as the measurement process in the mentioned studies was also varied (Ratkovich et al., 2013).

[1] **MLSS:** concentration of suspended solid particles in an aeration tank which occurs during the activated sludge process while treatment of wastewater.

Table 2.1. Rheological Properties of Activated Sludge in Different Studies.

Sludge Source	**Shear Rate (s^{-1})**	**MLSS (g/L)**	**Rheological Model**	**Range of Model Parameters τ (mPa)**	**References**
Wastewater treatment plant	20-200	2-10	$\tau = a\ln(\dot{\gamma}) - b$	a: 4615.4-14.425 b: 11,095-32,411	Jin et al. (2006)
Wastewater treatment plant	1.8-73.4	2-18	power law	MLSS= 3.68 g/L (*K*= 4, *n*= 0.77) MLSS=10.76g/L (*K*= 20.9, *n*= 0.595)	Sanin et al. (2004)
Membrane bioreactor & aeration tank	10-600	10	power law	MBR: *K*=13, *n*= 0.62 Aeration tank: *K*= 52, *n*= 0.62	Defrance et al. (2000)
Membrane bioreactor	0.1-100	15	power law	*K*= 1660 *n*= 0.11	Barbot et al. (2010)
Membrane sequencing batch reactors	NM	0.39	Casson Hershel-Bulkley power law	$\tau_y = 9.6$, *K*= 27.7 $\tau_y = 9.6$, *K*= 4.1, *n*= 0.7471 *K*= 8.9, *n*= 0.5894	Shariati et al. (2011)
Bubble column bioreactor	NM	0.712-15.86	Newtonian Bingham power law	μ= 0.00107-0.00267 $\tau_y = 0.0289 - 0.1622$, *K*= 0.00088-0.00165 *K*=0.00528-0.05371, *n*= 0.6887-0.4136	Babaei et al. (2015(a))

There are various kinds of rheometers available to study the rheological properties of non-Newtonian fluids (suspensions and sludge). Rotational, tube, or systematic rheometers can determine the properties of fluid. The plot of shear rate versus shear stress is known as rheograms, which can be determined by flow measurements. To study the sludge rheology, the concentric cylinder geometry is one of the most popular rotational rheometer which consists of a cup and a bob (one of which rotating at a constant rate) (Markis F., 2015). The resistant torque of one of two cylinders determine the shear stress. To study the flow properties of the sludge, rotational

rheometers have been used by various researchers such as Campbell and Crescuolo, (1982) and Forster, (1982).

Novarino et al. (2010) studied the rheology of activated sludge in account of heterogeneous composition and interaction between solid-liquid and solid-solid with the help of Anton Paar Physica rheometer endowed with coaxial cylinder. Later, to determine the thixotropic behavior of their sludge Anton Paar Physia rheometer equipped with the double gap measuring system was used by Tixier et al. (2003a). To study the activated sludge behavior during several steps of treatment Lotito et al. (1997) used the rotational rheometer equipped with the concentric cylinder geometry.

To correlate the rheological properties of activated sludge with sludge pumping processes Slatter (1997) have been used tube viscometers. To minimize the problems related to size of flocculated structures. Slatter (1997) have been employed balance beam rheometer. The balance beam rheometer measured the flow from mass very accurately. Poitou et al. (1997) employed the capillary rheometer to study the rheological and mechanical characteristics of pasty sludge.

However, there is not any particular rheometer available to study the rheological properties of activated sludge because sludge has the complex nature and each rheometer produce some kind of errors. Such that the rheological properties of the activated sludge depend on the background of the material and sensitivity of rheometer.

2.2.4 Literature on Mixing of Activated Sludge

Activated sludge has a major application in wastewater treatment. Sludge flocs contains different kind of bacteria, fungi, and protozoa which provides the ability to activated sludge process of complete mineralization of pollutants (Sahinkaya et al., 2005). In the activated sludge bioreactors, aeration is utilized for supply of oxygen to the biomass as well as the maintenance of proper hydrodynamics environment throughout the bioreactor (Braak et al., 2011). Such that the role of aeration and its distribution within the bioreactor are the mixing characteristics in the activated sludge process (Babaei et al., 2015(b)).

A comprehensive knowledge regarding impact of rate of aeration and rheological properties of activated sludge on mixing is very essential. There are several experimental and modelling studies have been performed in this regard but due to the drawback of opacity activated sludge the fluid

has been eliminated by water, yeast suspension, carboxylmethyl cellulose (CMC) solution in their studies (Fayolle et al., 2007; Prieske et al., 2010; Rosenberg et al., 2002; Prakash et al., 2001; Ratkovich et al., 2010).

There are only few studies which have been performed by utilizing the activated sludge in a bioreactor. For instance, Jin et al. (2006) studied the hydrodynamics and mass transfer coefficient in three-phase air-lift bioreactors containing activated sludge. They found a better performance of liquid circulation, gas holdup, residence time and mass transfer coefficient in external air-lift reactor (EALR) as compare to the internal air-lift reactor (IALR).

Duran et al. (2016) reported a study on the impact of suspended solid particles on non-Newtonian behavior of activated sludge and oxygen transfer coefficient. In the following study they found that with the increase in suspended solids, the oxygen transfer coefficient was decreased whereas an increase in suspended solid concentration cause the increment in shear-thinning behavior of activated sludge. Rosenberg et al. (2002) studied the rheology of activated sludge in membrane bioreactors. Effects of aeration patterns on the flow characteristics in wastewater aeration tanks was studied by Gresch et al. (2011).

An experimental study on inhibition of oxygen transfer under fine bubble aeration in activated sludge was reported by Fan et al. (2015) in which it was demonstrated that with the increase in activated sludge concentration, rise in apparent viscosity was demonstrated, causing the reduction in turbulence strength and gas holdup in the reactor.

Pitoors et al. (2014) reported a model-based study on the dissolved oxygen concentration and reduction of oxygen consumption in activated sludge process. This study reported that dissolved oxygen in combination of dissolved oxygen control strategies can provide less power consumption, aeration reduction, stability of the system, increased operation life of an aeration equipment and improved activated sludge quality.

The characterization of gas holdup inside a bubble column bioreactor containing activated sludge was studied by Babaei et al. (2015(a)) in which they utilized electrical resistance tomography (ERT). This study reported that overall gas holdup showed some variation with initially increasing followed by decreasing with increasing MLSS concentration. The radial distribution of gas holdup within the bubble column was also modeled in this study.

Babaei et al. (2015(b)) analyzed the gas phase characterization and mixing performance in an activated sludge bioreactor using electrical resistance tomography (ERT). In this study, it was found that with the increase in mixed liquor suspended solid (MLSS) particles, the rise velocity and mixing time decreases. They also reported that to achieve the lowest mixing time gas-liquid mixing system should be employed.

By utilizing an impeller in a stirred vessel, the mixing of activated sludge was achieved by Yang et al. (2015) in which the dual dislocated-blade Rushton impeller and a standard Rushton impeller was employed for the mixing of activated sludge in a stirred vessel in presence of gas. This study reported that the dual dislocated-blade Rushton impeller has the superior performance characteristics in mixing, power consumption and gas hold up of activated sludge.

2.3 Gas-Liquid Mixing

Gas-liquid mixing begins from complex interactions between molecules and thus affects the chemistry of products formed. It is therefore, necessary to understand the mixing parameters related to this system such as the hydrodynamic parameters such as gas holdup and liquid circulation velocity, transport properties such as heat and mass transfer coefficients, power consumption per unit volume and mixing time for a successful design and scale-up. When scaling-up the mixing process to industrial level, one should be able to predict the performance comparable to that of laboratory scale. When scaling-up fails, it implies inefficient mixing, which compromises product quality (Gumery, 2005). The cost of correcting this anomaly is high. It was estimated that the US chemical industry alone spent up to $10 billion extra due to poor mixing (Smith, 1990). Bissell (1938) noted the need for mixing criteria and recommended side-by-side comparisons of mixer designs for evaluating performance.

2.3.1 Gas-Liquid Dispersion System

The dispersion of gas in liquids by mechanical agitation has been the subject of numerous studies. The dispersion or mixing of one phase into another phase plays a significant role in heat and mass transfer of chemical engineering performance. The dispersion of one fluid into another takes place via jet when the surface tension cause latter to subside into a dispersion of bubbles. The mixing

and interdispersion of two immiscible fluids is a common operation which is designed to create high interfacial areas for both mass transfer and chemical reaction (Vincent and Mason, 1967)

In the performance of different industrial processes, such as oxidation, hydrogenation, and biological fermentation, contact of gas and liquid takes place; and for most of the cases, gas-liquid are mixed to supply a steady foam. Mass transfer takes place beyond the gas-liquid interface and chemical reaction supports the mass transfer in the liquid-phase. However, in case when agitation is obstructed, all types of mixture are usually unstable and separated. To create a dispersion of gas bubbles in a continuous liquid phase, mechanical agitation system is the main method used (Wang et. al., 2000).

Warmoeskerken et al. (1981) studied the gas-liquid dispersion by using pitched blade turbines. According to their studies, there are two distinct regimes by which gas leaving the sparger reaches the impeller. The first regime is at low gas flow rates, when the flow is indirect via the recirculation loops. The second regime is at higher gas flow rate, when the flow is direct

Also, the dispersion of liquid in gases and dispersion of gases in liquid has a major role in mixing as well as in the formation of bubbles and the process of dispersion system in both cases (dispersion of liquid in gases and gases in liquids) which is described as follows:

2.3.2 Dispersion of Liquids in Gases

Spraying the liquid phase into gaseous phase is called the dispersion of liquid in gas. Atomization of liquids into gases requires overcoming the surface tension, and this atomization is effected by nozzles, two-component nozzles, and centrifugal atomizers. Due to the formation of droplets, the original amount of liquid surface tends to increase. The energy required for dispersion in nozzle is produced by exerting a pressure on the liquid. In the case of two-component nozzles, atomization of liquid is brought about by gas emerging from the nozzle at high velocity. The liquid to be dispersed into gas is accelerated by a rotating disk in centrifugal atomizers. The droplets dispersed in the gas extend in a downward direction due to higher specific gravity and if these droplets are adequately fine then the velocity to move them downward is approximation by Stokes' equation:

$$u = \frac{d^2(\rho_l - \rho_g)}{18\eta} \tag{2.11}$$

where d is the diameter of the droplet, $\rho_l$is the density of the liquid, $\rho_g$is the density of the gas, and η is the viscosity of the gas. Therefore, the smaller the size of the droplets, the slower they move in a downward direction and longer the heterogeneous mixture is preserved (Sterbacek & Tausk, 1965)

2.3.3 Dispersion of Gases in Liquids

When gases are dispersed in liquids, dispersion is effected by bubbling the gas throughout the liquid. In two-phase mixing, the gas may be insoluble in liquid, the gas is mixed in the liquid either by physical means or reacts with it chemically.

In dispersion of gases in the liquid, the formation of bubbles at the opening through which the gas enters the liquid plays a major role. To determine the formation of bubbles in the liquid it may be assumed that the gas flowing under pressure through pipe enters the liquid with the help of a single inlet. The formation of a bubble may prevent by the pressure of the liquid column above the inlet, which must be controlled by either the pressure of the gas or by the surface tension. As the bubble begins to form and acted upon by buoyancy and when the buoyancy goes beyond the surface tension, the bubble isolated from the opening and moves in an upward direction. However, the formation of bubble depends on the surface tension and size of the inlet opening. In this study, we will focus on dispersion of gases in liquid.

2.3.4 Liquid-Gas Mixing Process

Slow mixing is always effected by the molecular diffusion. The penetration of fluid elements into each other by the action of turbulent diffusion increases the technical mixing operations. Vessels used for gas-liquid mixing may be designed for either continuous or batch operation in which mixing is generally achieved by forced convection. In fact, the motion of the liquid inside the vessel should be intense enough to bring about turbulence and thus turbulent diffusion. However, it is not possible to attain the same intensity of turbulence throughout the entire contents of the vessel especially in case of non-Newtonian fluids. The motion close to the vessel's walls is less intense. Such problems can be overcome by proper design of the mixing system especially in case of liquid-gas mixing. The proper design includes but not limited to design for impeller's type, size,

rotational speed, bottom tank clearance, gas sparger type and location, gas flow rate, and so on (Sterbacek & Tausk, 1965).

Air agitation happens due to the energy supplied by the compression of air prior to its introduction into the vessel. In this case, the gas pressure should be greater than that of the hydrostatic head of liquid at the gas inlet. The energy required for isothermal compression of the gas from the volume and pressure at the surface to the volume and pressure at the bottom is equal to the energy transmitted to the surrounding liquid by expanding bubbles (Lamont, 1958). This can be expressed by the simple equation:

$$\mathrm{P} = P_1 Q_g ln \frac{P_2}{P_1} \tag{2.12}$$

where P is the power transmitted by the gas, P_1 is the gas pressure at the free space, P_2 is the gas pressure at the bottom of the vessel, and Q_g is the volumetric flow rate of the gas at the free surface.

In gas-liquid system, gas is introduced from the sparger by a compressor to the stirred tank. There are three hydrodynamic regimes with respect to the distribution of the gas phase in stirred tank which are as follows; flooding, loading and complete dispersion. The transition conditions are determined by increasing and decreasing the gas flow rates and impeller speed. When the impeller speed is low and gassing rate is constant, bubbles pass through the impeller without being affected by the fluid flow which is introduced by a rotating stirrer. However, the gas dispersion is undesirable in this condition and power loss is not observed when compared to ungassed conditions. In this condition, the impeller is known as to be flooded. When the speed increases gently, a cavity is formed behind the blades which affects the bubbles; at the same time the loading condition takes place and large cavities aggregation brings about reduction of the gassed power consumption. At the minimum speed of the impeller, complete dispersion regime takes place for the complete dispersion of gas in the vessel.

2.4 Flow Patterns and Flow Regime in Gas-Liquid Stirred Vessel

The configuration of the vessel and the characteristics of the fluid used will directly affect all the flow regimes with different gas flow rates. Different regimes can be determined while sparging

the gas from the bottom of the vessel with different gas flow rates. **Figure 2.3** shows the different kinds of flow regimes.

There is little or no interaction in between the bubbles when the bubbles flow straight up in the vessel and the gas flow rate is low. This kind of flow is called bubbly flow or homogenous bubble flow **(Figure 2.3(a))** which creates a large amount of surface area for mass transfer, however the velocity of gas phase and liquid phase is equal to each other which basically gives less or no turbulence (Hamood-Ur-Rehman, 2012).

As can be seen in **Figure 2.3(b)** there is another flow known as the churn turbulent flow or heterogeneous turbulent flow, in which the formation of bubbles of different sizes takes place and the interaction in between the bubbles also increases due to the increase in gas flow rate. This type of flow can be noted either during the increase in gas flow rate or with a greater diameter of the vessel. The mass transfer rate is limited in heterogeneous turbulent flow whereas the gas flow rate will be low (Kee et al., 1988).

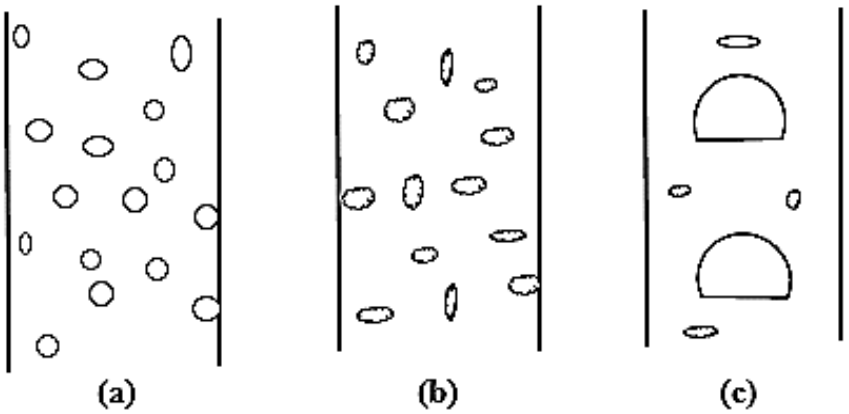

Figure 2.3. Fluid flow regimes **(a)** Homogenous bubble flow, **(b)** Heterogeneous turbulent flow, **(c)** Slug flow (Hamood-Ur-Rehman, 2012).

Lastly, the slug flow shown in **Figure 2.3(c)** is produced in high viscous fluids at high gas flow rates, in which the shape and size of the spherical cap bubbles differs from each other. In case of the column/vessel having small diameter, the spherical cap shaped bubbles adjusts their shape and size according to the column they are rising.

Mechanical agitation plays a significant role in the conversion of gas into small bubbles which allows for a high interfacial area. In gas-liquid stirred reactors, it is very important to disperse the

bubbles throughout the liquid, keep the bubbles inside the liquid to provide good gas hold-up, mix the liquid inside the vessel, maximize the heat and mass transfer coefficients, and to maintain particles in suspension. Mechanical agitation plays a major role which occurs by providing high energy turbulence as well as high flow rate (Scargiali, 2007). **Figure 2.4** shows various agitators which can be utilized in gas-liquid dispersion. The most widely used and effective impeller is the 6-blade disc turbine, also called the Rushton turbine, which can be used in gas-liquid stirred reactors (Scargiali, 2007).

However, with concave blades and 12 or 18 blades improved disc turbine agitators proven to have good gas holding capacity as compared to the Rushton turbines as well as they are increasingly employed (Gibilaro, 1985).

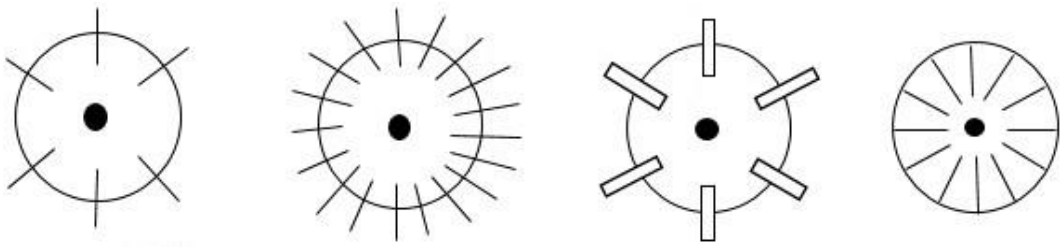

(a) **(b)** **(c)** **(d)**

Figure 2.4. Agitators for gas-liquid dispersion **(a)** 6-blade disc turbine, **(b)** 18-blade disc turbine, **(c)** 6-concave blade disc turbine, **(d)** 18-blade vaned disc (Middleton, 1985).

If the gas is effectively captured and dispersed by the agitator, the nature of gas inlet device does not have any effect in the gas-liquid mixing process. To obtain efficient mass transfer, multiple orifice ring sparger is recommended (Scargiali, 2007). To process the entering gas immediately by the impeller, the distance between the impeller plane and inlet distance should be smaller than $D/2$, where D is the diameter of impeller. There are different of flow regimes produced during the increase in agitation speed. There are five flow regimes in the vessel which can be defined for six bladed disc turbine impellers as shown in **Figure 2.5** (Nienow et al., 1978).

In case of flooding, when the agitation speed (N) is relatively low **(Figure 2.5(a))**, the gas passes through the agitator region and large bubbles which are not converted into smaller bubbles by the impeller action. In the first loading regime, with an increase in N as can be seen in **Figure 2.5(b)**, the gas phase dispersed in smaller bubbles, which basically spread in the reactor. In second loading

as shown in **Figure 2.5(c)**, the gas phase disperses into smaller bubbles. Due to the downward liquid velocity, the bubbles are entrained and recirculate to the impeller region.

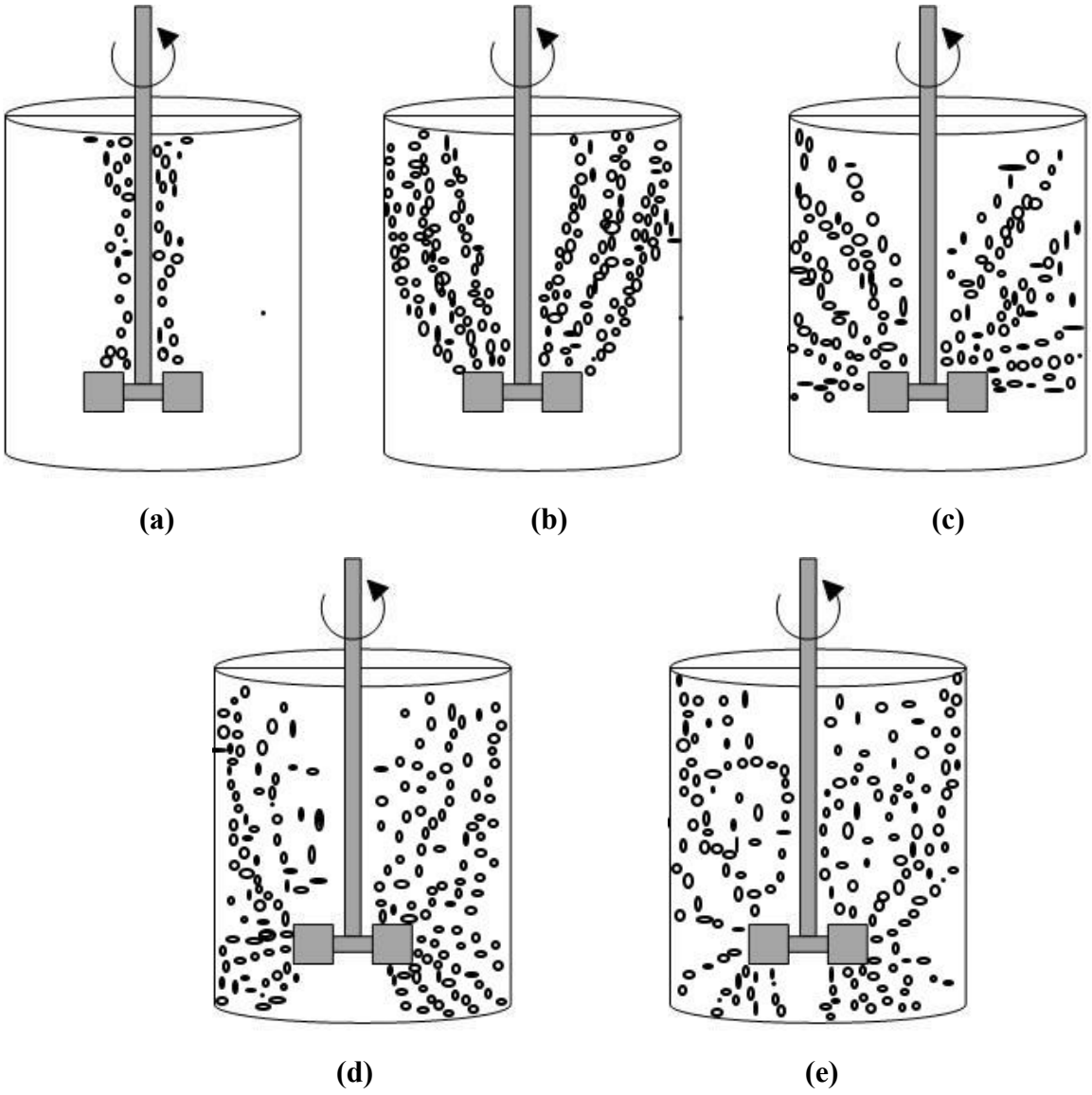

Figure 2.5. Flow patterns with increasing impeller speed (*N*) in presence of gas (*Q*) (Nienow, 1978).

The next stage in which the *N* increases has complete aeration. Recirculation of gas takes place in both top and bottom of the impeller as presented in **Figure 2.5(d)**. Lastly, the secondary recirculation stage takes place when the impeller speed at the peak shown in **Figure 2.5(e)**, due to which impeller is oversupplied with gas. Inside the reactor, the secondary gas recirculation loops appear.

2.4.1 Flow Patterns Created by Impellers

Flow pattern created by an agitator is the first indication of its suitability for a particular application. In case of types of flow, based on the directions of the streamline (a fictitious line that illustrates the path of a given elementary particle in its flow), there are basically three principal types of flow:

1. Tangential flow, in which the liquid from the agitator into the surroundings and its entrainment into the impeller are small. In tangential flow dominant flow, the vertical transfer is insignificant. When the rotational movement of the liquid attains the same value as that of the mixer so the effect of the mixing is lowest in the extreme case. However, **Figure 2.6(a)** shows the diagram of tangential flow.

2. Radial flow, in which liquid discharges from the impeller at right angles towards the tank walls. The resistance is offered by the velocity to the flow into the surroundings, and the overcoming of this resistance requires a certain force. The impeller produced the centrifugal force which depends on the diameter and speed of impeller. However, as soon as the centrifugal force overcomes the resistance of the medium, radial flow from the impeller sets in. In radial flow, the bottom part entrains the liquid in upward direction and displaces it at right angles to the axis of the impeller whereas in the upper part of the vessel, liquid entrains in downward direction, displacing it perpendicular to the impeller axis as can be seen in **Figure 2.6(b)**.

3. Axial flow, in which the liquid is perpendicular to the axis of the impeller through which it enters. There are basically two possible axial flow patterns in accordance to the pitch of the impeller with regard to the direction of the impeller's rotation. Therefore, the axial flow impellers can pump liquid from downward to upward direction and from upward to downward direction as shown in **Figure 2.6(c)**

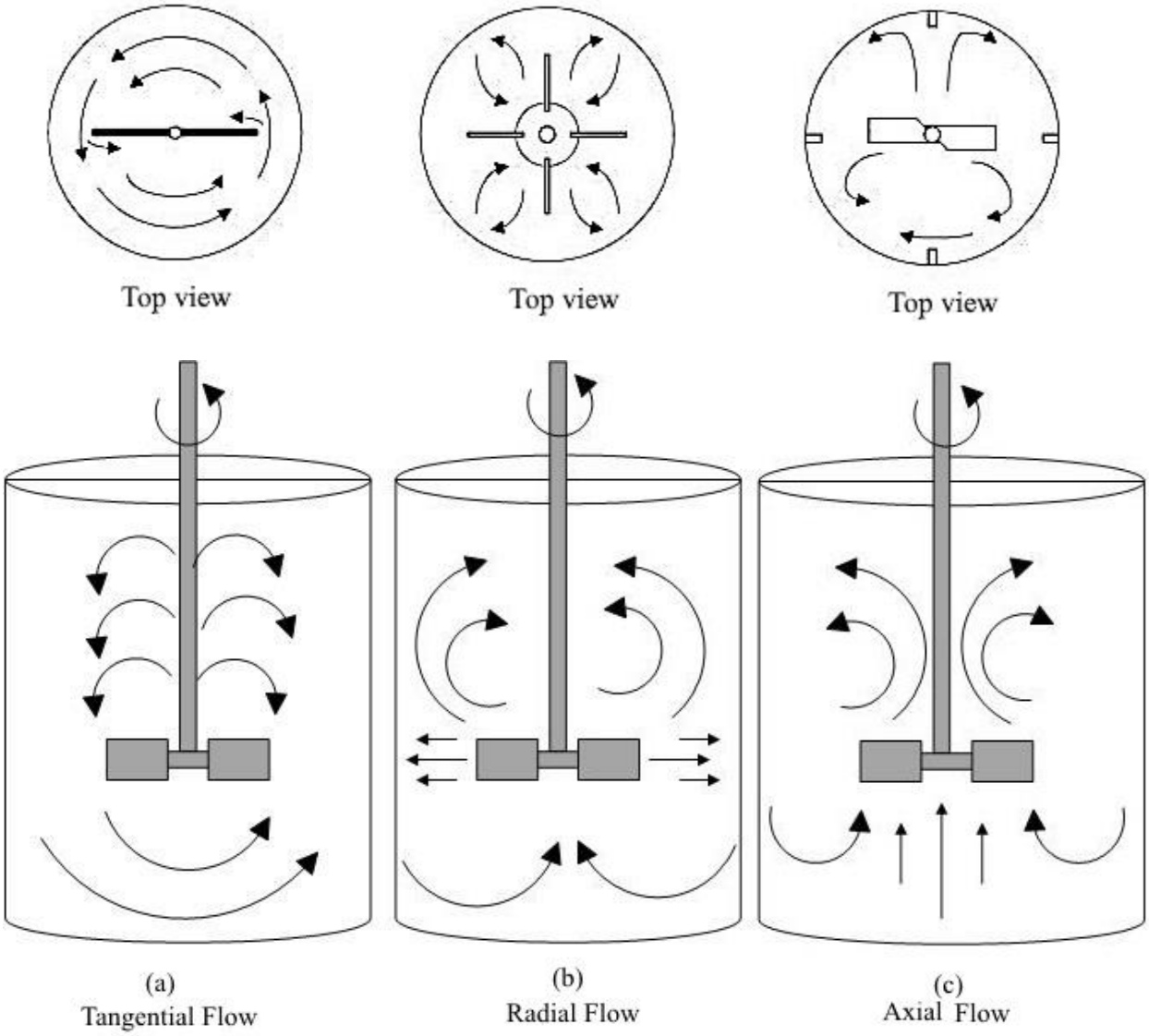

Figure 2.6. Flow patterns created by impellers: **(a)** Tangential flow, **(b)** Radial flow, and **(c)** Axial flow (Starbacek & Tausk, 1965).

Such that these three kinds of flow pattern either separately or in combination are encountered in mixing vessels. The primary flow pattern existing the mixing vessel not only depends on the impeller type and geometry but also on the presence of baffles. However, impeller clearance, liquid height, and baffle length are important as well. However, such parameters as impeller's blade number and width, the baffle width, and the tank geometry, e.g. dished or flat bottom can also have effect on the flow pattern. It was found that in the turbulent flow the flow patterns can be considered independent of fluids viscosity (Tatterson, 1991).

By using radial disc turbines, such as the Rushton turbine or other type of impellers, gas dispersion can be carried out in agitated vessels. In gas-liquid application, to reduce the weakness of disc turbines, an axial flow impeller has evolved. The axial flow impellers are basically used in down-pumping mode and provided a significant advantage as compared to the radial flow agitators (Mc Farlane, 1996). The propeller is considered to be a general purpose impeller because of a good balance of pumping and shear capabilities. When the impeller diameter and liquid viscosity is increased the flow pattern with a propeller becomes closer to radial (Edward L., 2004).

To carry out the bacteria and cell cultivation operations in biochemical industries stirred vessel is the most common reactors (Kadic et al., 2014, Grebe et al., 2014) in which with the help of impellers fluids can be agitated. In gas-liquid mixing process, impeller is the essential requirement for complete dispersion of gas throughout the vessel (Yang et al., 2015). To improve the gas dispersion within the stirred vessel several studies have been reported.

The perforated Rushton impeller which has a reduced power consumption and improved oxygen transfer efficiency was designed by Roman et al. (1996). It was also reported that at same Reynolds number, minimum power consumption of the Scaba impeller can be achieved due to aeration (20-50%) which was smaller than the power consumption of Rushton impeller (Galindo & Nienow, 1993).

Warmoeskerken & Smith (1989) designed the CD-6 impeller which has concave blade as cutting from pipe sections. However, Bakker et al. (1994), Tanphasana et al. (2014), Gimbun et al. (2009) confirmed that this impeller has the better performance in gas-liquid mixing as compare to the traditional Rushton turbine.

A novel impeller which is a combination of A200 and Scaba impeller named ASI was designed by Pakzad et al. (2013) which has a superior performance ability in mixing of non-Newtonian fluids.

The coaxial mixer was utilized in mixing of corn syrup solution (a Newtonian fluid) by Hashemi et al., 2015 in which they reported that PBU-anchor coaxial combination in co-rotating mode has significant ability to give the shorter mixing time and minimum power consumption.

The information presented in the literature shows that the knowledge related to the mixing of activated sludge, a non-Newtonian fluid is still inadequate and require more information.

2.5 Gas Flow Rate and Gas Flow Number

Gas flow rates are often referenced to vessel size, either as a superficial velocity (V_s) based on the cross-sectional area of the vessel, or as tank volumes per minute (vpm). For a constant gas flow rate, the minimum mixing requirement for the gas phase is the impeller speed at which the gas is just dispersed throughout the vessel.

The gas flow number (Fl_g) is a dimensionless number which is the characterization of gas-liquid dispersion inside the mixing tank and can be represented by the ratio of gas inlet rate to that of impeller pumping rate. It can be expressed as follows:

$$Fl_g = \frac{Q_g}{ND^3} \tag{2.13}$$

where Fl_g is the gas flow number, Q_g is the rate of flow, N is impeller speed, and D is the diameter of the impeller.

2.6 Power Consumption

The impeller power for homogenous liquids is basically depends on different factors such as, impeller and tank geometry, different properties of liquid such as density and viscosity, rotational speed of impeller and the gravitational force (Tatterson, 1991)

The equation for the relation between impeller power and factors on which it depends is as follows:

$$P = f(\mu, \rho, N, D, T, g) \tag{2.14}$$

In the above equation, impeller power is denoted by P, fluid viscosity is denoted by μ, fluid density is shown by ρ, impeller rotational speed is denoted by N, and impeller diameter and tank diameter are denoted by D and T, gravitational acceleration is shown by the symbol g.

- **Power Number:**

The power number N_P plays a major role in distinguishing the process of mixing in the mechanical mixing vessels and report the requirement of power for the performance of an impeller as well as the power consumption throughout the mixing process. It also helps in calculating of the elements

of mixing vessel, such as, shaft dimension, impeller design and so on (Wojtowicz, 2014). The power number may be defined as the dimensionless number relating the resistance force to the inertia force. The equation for power number is as follows:

$$N_P = \frac{P}{\rho N^3 D^5} \tag{2.15}$$

In the above equation, P is the power, ρ is the fluid density, N is the rotation speed, and D is the diameter of stirrer.

- **Reynolds Number:**

The Reynolds number (*Re*) is the ratio of inertial to viscous forces. Both Reynolds number and power number, whether in two or three phase systems, are calculated on the basis of liquid properties.

$$N_{Re} = \frac{D^2\, N\rho}{\mu} \tag{2.16}$$

where N_{Re} is the Reynolds number, D is the impeller diameter, N is impeller speed, μ is the fluid viscosity, and ρ is the fluid density.

There is a relation in between Power number and Reynolds number which has three different parts (Skelland, 1967). The first part consists of Reynolds number at small values (< ~10) in which the laminar flow takes place and the slope of power curve on log-log coordinates is -1. However, when the flow is turbulent so we can say that the value of Reynolds number is very high (>10^4), in which the Power number is constant and the value of Power number do not vary with Reynolds number. Therefore, a transition zone exists in between the turbulent and laminar zone. The transition zone is basically dependent on the vessel geometry and type of impeller.

2.6.1 Power Requirement for Non-Newtonian Fluids

Metzner and Otto (1975) introduced a method to determine the Reynolds number (Re) for non-Newtonian fluid in laminar flow regime. This method is based on the variation of shear rate in mixing system. However, they described an apparent viscosity for the Newtonian fluid as the viscosity, which basically follows the same amount of power input under the same conditions of size and speed in the laminar flow regime. In the next step, they checked this with the other important factors of the system and found that the motion of the fluid in the impeller region is

characterized by an average shear rate and this shear rate is directly proportional to that of the impeller rotational speed, the equation is as follows:

$$\dot{\gamma}_{ave}\, \alpha\, N = K_s N \tag{2.17}$$

In the above equation impeller rotational speed is denoted by N and K_S is the function of the type of impeller and the vessel configuration. The apparent viscosity, which is the ratio between shear stress and shear rate can be calculated by rearrangement of power law equation:

$$\eta_{app} = \frac{\tau}{\dot{\gamma}_{ave}} = K(\dot{\gamma}_{ave})^{n-1} \tag{2.18}$$

The Reynolds number for non-Newtonian fluids can be defined as:

$$Re = \frac{\rho D^2 N^{2-n}}{K K_s^{n-1}} \tag{2.19}$$

where η_{app}, τ , $\dot{\gamma}_{ave}$, N , D, ρ, K , K_s and n are apparent viscosity, shear stress, averaged shear rate, impeller speed, impeller diameter, fluid density, shear rate independent constants, respectively.

Metzner and Otto (1957) determined the K_S value i.e. 13 for the disk flat blade turbine. Later on Calderbank & Moo-Young (1959) determined the value of K_S as 10 after further studies of variety of sizes and types of impeller for Bingham and Pseudoplastic fluids (suggested by Metzner and Otto, 1957). For Pseudoplastic fluids, Skelland (1967) determined the K_S value ranging from 10 to 13 for several types of impeller, whereas in case of anchors and helical ribbons the value of K_S lies in between 25 to 30 (Bakker & Gates,1995).

Table 2.2 represents the Metzner-Otto constants for a range of the most common agitators and further developments demonstrated in other studies.

Table 2.2. Shear rate constants based on different studies.

Agitators	K_s value	Reference
Propeller	10	Skelland (1967)
Disc and flat blade turbine	11.5	Metzner and Otto (1957)
Angled blade turbine	13	Skelland (1967)
Anchor	20-25	Bakker and Gates (1995)
Helical ribbon	30	Bakker and Gates (1995)
Scaba 6SRGT	10.5	Pakzad et al. (2013)a
Rushton	11.5	Skelland (1967)
A200	13	Skelland (1967)
ARI	12	Ascanio et al. (2003)
Spiral	11	Skelland (1967)
ASI	11.3	Pakzad et al. (2013)

2.7 Mixing Time

Mixing performance is generally evaluated by measuring mixing times. Although several studies have been performed to understand the effect of aeration on mixing time in the aerated mixing vessels, still there is not an exact answer especially in case of non-Newtonian liquids such as activated sludge. It was shown that the high amount of aeration decreases the mixing time due to the giant motion inside the vessel (Vasconcelos et al., 1995) however, some other literature concluded that a fluctuation can be observed in mixing time by applying a dominant amount of aeration (Machon & Jodha, 2000). There are various methods to measure mixing time (Kraume & Zehner, 2001) such as applying conductivity method (Jaworski et al., 2002), pH meter (Gullard & Tragardh, 2003), tomography technique (Pakzad et al., 2008, Pakzad et al., 2013, Kazemzadeh et al., 2016), and the decolorization method (Kuzmanic & Ljubicic, 2001). Among the aforementioned techniques, electrical resistance tomography (ERT) was found as the most widely utilized technique because of its fast speed in capturing the real-time data of the extremely fluctuating flow in gas-liquid systems without interrupting the developed flow (Hashemi et al., 2015)

Mixing of gas-liquid phase in a vessel is one of the most important parameter. Good mixing is very important when the non-uniform silhouette of concentration or temperature create some side reaction or decrease the rate of chemical reaction. In gas-liquid mixing, sparged air is used to attain the mixing process.

The mixing time is defined as the time required to attain a certain homogeneity of two or more content of material that are to be mixed. The mixing time is commonly considered as one of the most important parameter. In different industries such as pharmacies, food, refineries and chemical process, stirred tanks are majorly used. For proper mixing suitable impellers, impeller ratios should be optimized. In case of high- volume industrial scale mixers, to satisfy maximum allowable mixing time requirements. Mixing time may examine as the time required for a tracer to reach a certain level (98%) of homogeneity. And the tracer may be a chemical species, an electrolyte, or may be a thermal species. The level of homogeneity (t_m) can be evaluated as:

$$t_m = \frac{c - c_\infty}{c_\infty} \tag{2.20}$$

where c and c_∞ are the tracer initial and main concentration respectively.

There are several methods and evaluation techniques for mixing time of gas-liquid phase in a stirred vessel which are described as follows:

2.7.1 Measuring Techniques to Evaluate Mixing Time

The mixing time required to achieve 90% of homogenization (t_{90}) is the time it takes for the fluctuation of the response signal to be below 10% of the concentration achieved at perfect mixing, which is adequate for the most systems (Ali, 2014). There are various ways to determine the time of mixing such as using a conductivity method (Jaworski et al., 2002), by using a measuring tool named as pH meter (Guillard & Tragardh, 2003), and applying the tomography techniques (Pakzad et al., 2008), dilution-based technique, reaction-based technique, and the decolourization method (Kuzmanic & Ljubicic, 2000).

The tracer response technique can be used to measure liquid velocity. This technique measures the pH and conductivity over time. In the following technique, the probes which are connected to sensors and microprocessors are inserted into the vessel to determine the pH and conductivity after addition of a tracer. The velocity and time taken for the tracer to migrant from one probe to the

other can be calculated by the recorded peaks of the time taken to record consecutive peaks (Onken & Weiland, 1980). In case of measuring the pH, an acid or base behaves such as the tracer whereas in measuring the conductivity.

Another technique is the thermos anemometry, in which a thin wire film probe which is made up of platinum is used along with heat generated by electricity. This technique works on the principle, as the liquid flows, the heat is transformed to the liquid and the film is cooled down. This technique gives good result for fluctuation velocities because the time interval is very short. If the probe is frequently calibrated and the position of sensor is also proper to the maximum flow direction during measurement so results will be excellent (Brunn, 1996)

In dye or coloring method, iodine or methylene blue are added and the dispersion of the dye can be visualized by spectrophotometer and reserved for the detection of stagnant regions. The drawback of this technique is that it is not applicable to the fermentation broths due to the absorption of dye in the fermentation process.

The Ultrasonic Doppler velocimetry technique can also be employed to determine the mixing time in which tracer particles are added to the medium to generate echo to determine the Doppler frequency. When tracer particles are loaded and starts to move they transmit the ultrasound beams which are scattered and emitted by the probe generating backscattering at all angles. To determine the Doppler frequency, the generated frequency is used and then the particle velocity can be estimated.

Dilution-based and reaction-based technique can be used for both single-phase flow as well as two-phase flow and provide qualitative information on mixing quality. In this technique, two immiscible liquid streams are first contacted together and then contacted with the gas phase to create the gas-liquid dispersion. However, for dilution-based methods, one of the liquid stream contains the tracer; whereas for the reaction based the liquid streams contains the reactants. And the mixing is judged complete when the concentration of the dye or product is uniform within the liquid slug. Gunther et al. (2004) used a fluorescence tracer (Rhodamine B) in ethanol to study mixing in the liquid-phase of a gas-liquid dispersion in straight and meandering microchannel. And he demonstrated that mixing in the liquid slug is faster in the meandering channel in the straight geometry.

Kraume & Zehner (2001) took the decolourization point equivalent to the 95% homogenization level, whilst obtained using a conductivity meter. It has been also determined that the location of a probe has no influence on mixing time (Rao and Joshi, 1988). However, most recent studies illustrate that the mixing time depends on the injection location, probe size (Bouaifi & Roustan, 2001), and tracer concentration. Homogenization energy, which is a product of mixing time and the corresponding power dissipated has been used to evaluate the mixing efficiency (Bouaifi & Roustan, 2001). The mixing time is decreased by increasing of impeller speed, low aeration lead to increasing of mixing time (Ali, 2014).

The tomography technique measures signals from electrode located around a process vessel (Williams & Beck, 1995). The data input obtained by the help of these electrodes is fed to the host computer to show variations of conductivity with a vessel. These variations of conductivity provide information on distribution of phases and mixing zones in a vessel. Process tomography is one of the fast imaging tool whose sensing techniques and methods of data collection is basically based on electromagnetic radiation, acoustic and electrical distribution inside the vessel. The use of electromagnetic radiation on a daily basis is expensive as well as hazardous to health. However, on the other side, acoustic and electrical methods (light, sound, and electricity are less expensive as well as alternatives for tomography techniques. Moreover, the use of light for tomography is restricted to non-opaque vessels.

The electrical tomography provides distribution of electrical properties such as conductivity or resistance, magnetic inductance and capacitance. Electrical impedance tomography (EIT), electrical inductance (magnetic) tomography (EMT), and electrical capacitance tomography (ECT) produce images based upon the variations in the conductivity and permittivity. The electrical resistance tomography (ERT) is an example of EIT. The electrical tomography remains popular due to their simplicity, high speed capacity and most importantly can be used for real online imaging during manufacturing processes (Mann et al., 1997).

2.8 Research Objectives

Many researchers have expanded their research in the field of rheology and mixing of gas-liquid in bubble column (Babaei et al., 2015(b)), aerated mixing vessel equipped with coaxial mixers (Hashemi et al., 2015), diffuser aeration tank (Pitoors et al., 2014), bubble column bioreactor with different MLSS (mixed liquor suspended solid) contents of activated sludge (Babai et al, 2015(a)), aeration tank (Fan et al., 2015), baffled aeration tank with dual dislocated-blade Rushton impellers (Yang et al., 2015). Despite this strategic direction, the literature review reveals that there is still a lack of information on improving the knowledge regarding the performance of agitation processing in an aerated mixing tank with non-Newtonian fluid. An activated sludge is an example of a non-Newtonian fluid and the dilution rate also increases with the increase in shear stress (Krylow et al., 2007) which makes the mixing process very complex and requires various equipment at appropriate levels to reach the hydrodynamics. Thus, the open literature proposes that a very few researches have explored the mixing of activated sludge in the stirred vessel. In addition, no information is available regarding the mixing of activated sludge in presence or absence of gas.

There are some issues which have not been reported in regards to the mixing of activated sludge:

- There are very few studies in which agitators have been employed in mixing of activated sludge. It is not resolved that which impeller performs the better performance in regards to mixing time and power consumption to mix the activated sludge.
- The previous researchers have utilized aeration in their work therefore, no study have been done in regards to the mixing performance of the impellers at various gas flow rate and in absence of gas.
- The mixing performance of ARI and ASI in activated sludge has not been reported as well as compared with other agitators.
- No study has been done related to an advanced flow visualization technique such as electrical resistance tomography (ERT) to assess the mixing performance of different type of agitators in presence and absence of gas.
- There is not any study has been reported related to the Reynolds number and Power number for the more complex fluids such as activated sludge. Therefore, new correlations for the generalized Reynolds number and power number should be developed.

This research aims to narrow this research gap and perform empirical studies into behavior of several different variables during mixing of the activated sludge. From last few decades, electrical resistance tomography (ERT) became one of the most common technique to investigate mixing process. The non-intrusive and optical behavior of this technique makes it more attractive. Therefore, there is still a lack of information on performance of ERT to compare the performance of different variables at different standard levels.

The aim of this study will be accomplished by fulfilling the following objectives:

- To assess the mixing performance of the activated sludge in two separate conditions: **(a)** in presence of air, **(b)** in absence of air.
- To estimate and compare the performance of three different type of impellers named as: **(a)** ASI (a combination of A200 and Scaba impeller), **(b)** ARI (a combination of A200 and Rushton impeller, and **(c)** Rushton impeller with or without air through electrical resistance tomography (ERT) and response surface methodology (RSM).
- To analyze the individual and interactional effects among various variables such as impeller speed, impeller type and gas flow rate on the mixing time, specific power consumption and gas flow number with the help of ANOVA and RSM.
- To observe the flow patterns within the mixing tank in agitation of activated sludge by impeller type at various rotational speed and various gas flow rate.
- To demonstrate the effect of aeration on formation and destruction of cavern.

3. Electrical Resistance Tomography

3.1 Introduction

Tomographic technology is the study of measurement attainment of signals produced from sensor which are located around a cross-sectional plane of an object which can be a process vessel or a pipeline (Williams & Beck, 1995). By the help of this, the distribution of components can be known within the sensing zone. In order to examine the process space, it is suggested to fix a number of non-intrusive sensors throughout the vessel or pipeline (Huang et al., 1992).

A computer system plays a major role to reconstruct the tomographic image of the cross-section observed by the sensors. There are different kinds of sensing methods for process tomography such as electrical measurements (Yu et al., 1993). Tomography based on X-rays finds its basic use in laboratory of nuclear engineering as a popular experimental device (Lahey & Ohkawa, 1989). However, in chemical and food industries the routinely use of X-rays should be limited in order to ensure the sensitivity of experiment and safety of the person who is performing experiments (Mann et al., 1997). For the routine use, the techniques based on electrical, optical, and ultrasound principles are developed (Dyakowski, 1996). The use of instruments based on the optical techniques is not possible in case of opaque materials. The electrical tomography is basically depending on the electrical properties, for example, capacitance, resistance, eddy current, permeability etc. (Williams & Beck, 1995). These electrical properties are simple rugged constructed and also plays a significant role in real-time imaging of industrial process (Mann et al., 1997). Electrical resistance tomography (ERT) is one of the most common techniques in electrical tomography

3.2 Principles of ERT

The general idea of ERT is that the conductivity of two media is differentiate from each other (Aw et al., 2014). The ERT model provides the sensing field with voltage and measure the potential current via electrodes which are mounted on the boundary of the sensing field (Hosseini et al., 2010 & Zhao et al., 2008). The operating principle of ERT system is based on the current excitation

and measurement of voltage. Generally, the exciting current is applied to the field of measurement with the help of a pair of electrodes which excites the sensing field. These sensing field varies with the variation in distribution of conductivity which result in variation in electric potential distribution. At the same time, the boundary voltage of sensing field also changes. However, the voltage which is determined also contains the statistics on the conductivity in the sensing field as well as the status of the flow inside the vessel can also be determined from further processing information (Tan et al., 2009).

The basic structure of ERT involves the multiple electrodes which are arranged throughout the periphery of the vessel or pipeline which is to be process. The electrodes are in contact with the fluid to be processed but they do not create any disturbance in the process flow pattern (Bolton and Primrose, 2005). Following is the block diagram which shows a typical ERT system **(Figure 3.1)**. An ERT system consists of three important parts as sensors (electrodes), a data acquisition system (DAS), and a host computer or image reconstruction system.

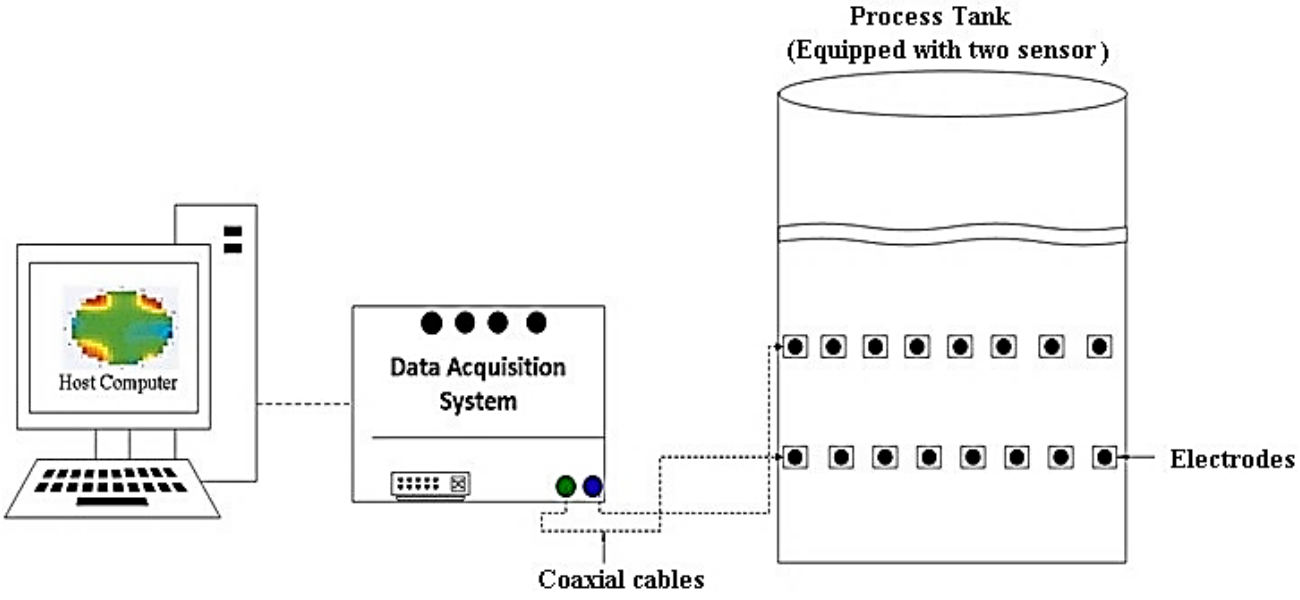

Figure 3.1. The structure of a typical electrical resistance tomography system.

3.2.1 Sensors Selection

Sensors are the backbone of ERT system. The main objective of ERT is to acquire the distribution of resistance in the field of interest. The main characteristics of electrodes which plays a major role in ERT system are the shape and size of the electrodes, the number of electrodes and the

position of electrodes (Aw et al., 2014). A number of spaced electrodes mounted non-invasively on the boundary of field of interest through which current is injected and measure the voltages, by which resistance distribution in a cross-section can be obtained.

The design of electrodes is one of the most important step, which maximize the capacity of electrodes to recognize the conductivity changes in the field of interest like a mixing tank (Seagar et al., 1987). Sensors are always in continuous contact with the electrolyte inside the vessel. There are several important parameters in regards to the electrodes such as the low cost, ease of installation, resistance to corrosion effects, good conductivity (more than electrolyte), and resistance to the process operation environment such as temperature, pressure, and electrical fire hazards. (Williams & Beck, 1995). Electrodes must be fabricated from gold coated platinum, stainless steel, braces, silver (Tapp & Williams, 2000), or silver palladium alloy and they are available commercially in a screw form and can easily be threaded into the process vessel (Dickin & Wang, 1996).

The reconstruction algorithm basically depends on the position of electrodes that they are located at defined intervals to outline the maximum amount of information from inside of the vessel (Dickin & Wang, 1996). The quantitative algorithm is more sensitive to the electrodes placement problems whereas in case of qualitative reconstruction algorithm position is less sensitive to the position of electrodes because they can be normalized with respect to the reference data (Mann et al., 1997). During the measurement of electric field distribution, size of electrodes is one of the other important factors (Mann et al., 1996). To inject enough current into the vessel, a large surface is needed for the current injecting electrodes (Dickin & Wang, 1996) whereas the voltage measuring electrodes are required to be as small as possible (Paulson et al., 1992).

Another most important factor is the number of electrodes used for the measurements. The time required to collect data as well as reconstruct the image is a function of number of electrode (N) which usually affects the number of independent measurements (M) whereas the spatial resolution is proportional to $M^{1/2}$ (Williams & Beck, 1995). Electrodes needs to be attached to the wall of process vessel by drilling holes into the vessel in order to fit the electrodes. But in few cases, this kind of attachment doesn't work, so the electrode can be retrofitted in vertical tubes or in a circular conduit, which are then attached to the wall of the vessel and this method is known as retrofitting method, by which the plastic tubes can also be reused in other process vessels.

Generally, the electrodes which are fitted throughout the vessel boundary at fixed locations, generate electrical contact with the fluid inside the vessels and are connected to the data-acquisition system by short length of signal-carrying co-axial cables to minimize the channels of electromagnetic noisiness, which are common in process environments (Dickin & Wang, 1996).

3.2.2 The Data Acquisition System (DAS)

The DAS is used for obtaining the quantitative data which describe the state of the conductivity distribution inside the vessel. The DAS is placed in a portable unit, which is connected to each of the electrode and then also in contact with the host image reconstruction computer.

If a complete set of independent measurements is not collected misleading images can be rebuilt and to overcome this problem some good data collection strategies is an important factor (Dickin & Wang, 1996). It is very important to choose the scheme which consists of a good distinguishability and high sensitivity to conductivity changes in the process. Distinguishability is one of the important parameter which is used to check, if the strategy used has the ability to distinguish between two conductivities (Gisser et al., 1987)

$$\delta = \delta(i) = \frac{\|R(\sigma_1) - R(\sigma_2)\|}{\|i\|} \geq \varepsilon \tag{3.1}$$

where *i,* ε, σ_1 and σ_2 are current, precision of measurements, and two conductivities respectively and R donates non-linear functional associated with the resultant boundary voltage. The strategy includes the adjacent, conducting boundary, diagonal and opposite measurement strategies **(Figure 3.2)**. Among all the aforementioned strategies, the adjacent method is one of the most common measuring protocol which involves two neighboring electrodes to supply current as well as for the measurement of voltages repeatedly at the same time. The procedure is followed by other combinations of adjacent pairs of electrodes for the entire ring of electrodes (Seager et al., 1987). The total number of independent measurements *M* can be calculated as:

$$M = \frac{N(N-3)}{2} \tag{3.2}$$

In the above equation, number of electrodes are denoted by N. The adjacent strategy is most popular due to its requirement of minimal hardware for implementation alongwith an important

feature of recording a conductivity signal output (Abdullah, 1993). Also, the image reconstruction can be achieved fast with the use of minimal resources (Dickin & Wang, 1996).

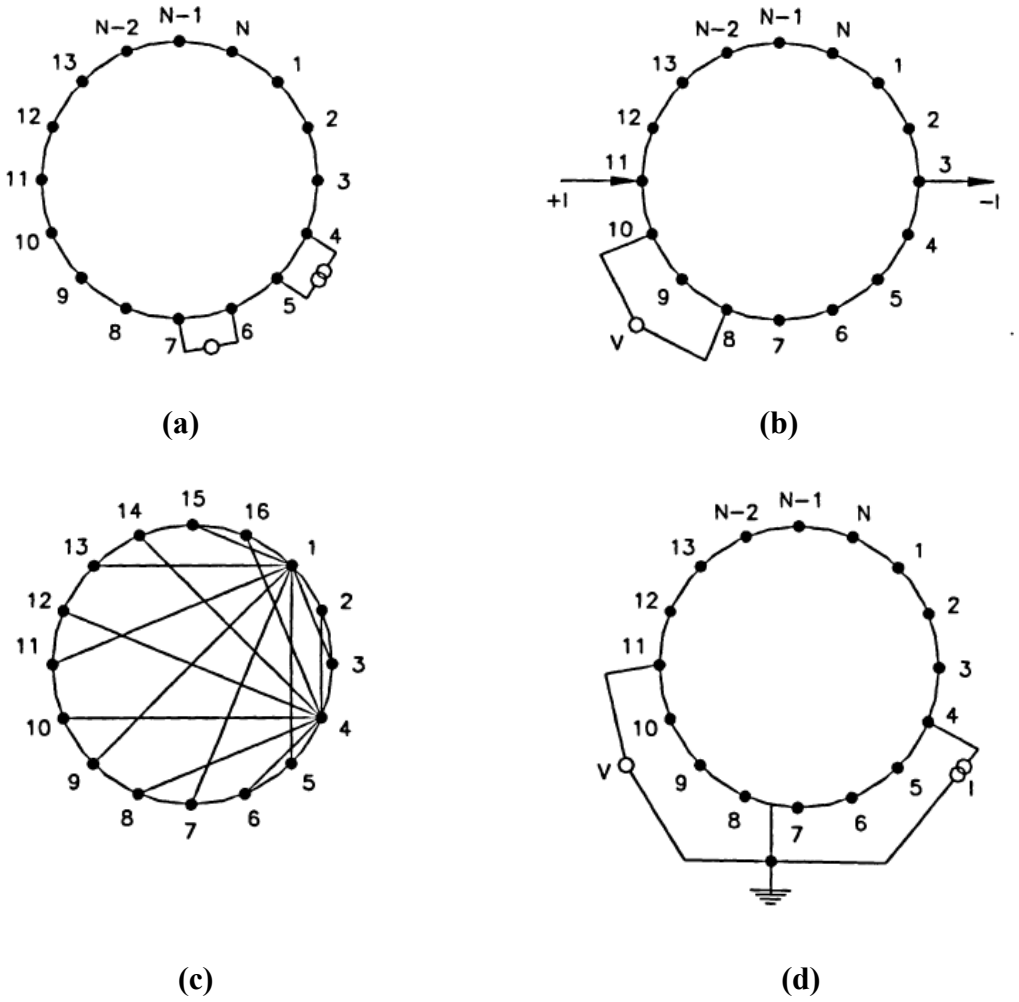

Figure 3.2. Data Collection Strategies (a) The adjacent measurement strategy (b) The opposite measurement strategy (c) The diagonal measurement strategy (d) Conducting boundary strategy.

3.2.3 Image Reconstruction System

The acquisition of data from the boundary of the system is required to process by using a suitable image reconstruction algorithm. The image which is reconstructed contains the information on the cross-sectional distribution of a parameter, which basically depends on the physical principle of the sensing system such as, electrical resistance tomography. Depending on the reconstruction

time, the algorithm can be used either on-line, or off-line. Generally, there are two types of algorithm: iterative and non-iterative. Also, the image reconstruction algorithm is a selection between accuracy of image and time required for reconstruction.

3.3 Recent Developments and Applications of ERT

ERT is used in both medical and engineering industry, development of body scanners in the medical industry have improved diagnostics and treatment as well as in chemical engineering ERT technique usually employed to determine different mixing procedure in reactors or vessels (Fransolet et al., 2001, Razzak et al., 2007, Pakzad et al., 2008). The efficiency of mixing usually depends on the type of impeller used, time, geometry of vessel and fluid viscosity (Gumery et al., 2011). During mixing process, ERT technique enhance the knowledge which is used to make improvements in designing the equipment and processes. The ERT technique is used by GlaxoSmithKline (a pharmaceutical company) for the production of paracetamol by controlling the synthesis of active pharmaceutical ingredient (API) online (Ricard et al., 2005). The following technique made them successful to determine the performance of various reactor geometries and demonstrated that ERT technique can be used for the development of API process.

After the discovery of ERT in 1980s, several creative research and influenced works have been showed by various researches all over the world. A new flow pattern identification algorithm for common two-phase flow based on ERT system measurements, principle component analysis-general regression neural network (PCA-GRNN) and principle component analysis-support vector machine (PCA-SVM) presented by Zhang et al. (2011) & (2012). ERT can also be used to study the development during nylon polymerization (Dyakowski et al., 2000). To overcome the harsh conditions such as high temperature and high pressure, electrodes were fabricated by using the plasma technology and fitted into the boundary of the vessel. By using the ERT technique various stages of nylon polymerization can be determined. During the heating up stage, the ERT displayed the material distribution, the effect of opening the valve which controls pressure and distribution of permittivity at the last step of polymerization (Dyakowski et al., 2000).

A dual plane ERT technique was developed by Yang et al. (2012) to provide a real-time measurement of air volume fraction distribution within its sensing region. Jin et al. (2013)

discovered the gas hold-up in multistage bubble column. A study on flow and velocity profile of several milk solutions in horizontal and vertical pipes and 3D- monitoring by using ERT technique was discovered by Sharifi & Young (2011) & (2012).

Few years ago, it was difficult to explain the mechanism of separation of fluids in hydrocyclone because of turbulence, swirling and need of on-line measuring techniques which can provide authentic experimental data for modelling (Dyakowski & Williams, 1998). Dong et al. (2012), Tan et al. (2010), Zhang et al. (2011) belongs to the same research group from Tianjin University, and developed a new ERT system which is completely programmable as well as reconfigurable FPGA (field programmable gate array) based compact PCI (peripheral component interconnect) bus. However, Dong et al. (2012) investigate the oil/gas/water whereas Tan et al. (2011) demonstrated the water flow through the gas flow dynamics simulations. Lastly Zhang et al. (2011) performed their experiments by using the tap water. Their research developed more computational power through parallel implementation which is then compared with the traditional instruction- driven digital signal processor. However, when this advanced technology applied to ERT system so it results in high bandwidth and good precision. By the use of FPGA chips, debugging and upgrading become easier.

The ERT system can also be applied to determine the mixing quality of an industrial pulp mixer (Yenjaichon et al., 2011). A parallel ERT system based on Compact PCI for multiphase flow measurement was proposed by Xu et al., 2011. To evaluate the mixing of micron-sized polymeric particles in a slurry reactor ERT system can be employed (Tahvildarian et al., 2011). Kourunen et al., 2011 employed 3D ERT system determine gas holdup distribution in a laboratory floatation cell. Therefore, other researchers such as Jin et al. (2010); Yang et al. (2012); Jin et al. (2013); Jin et al. (2007); Scott et al. (2005); Toye et al. (2005); and Fransolet et al. (2005) determined gas hold up in bubble column by using ERT system.

The ERT system was combined with a Venturimeter to measure the mass flow rate of an air-water two phase flow (Meng et al., 2009, 2010). Later, a feasibility study has been done by Kowalski et al., 2010 to evaluate the use of ERT in formulated products. Few research papers related to the ERT imaging of concrete were also presented by Karhunen et al. (2010) and Seppanen et al. (2008). The ERT system can be used to determine the solid-liquid mixing in an agitated tank equipped with a top-entering axial-flow impeller (Hosseini et al., 2010). By using the ERT system

along with differential pressure method with two axial locations in a gas-liquid-solid, the mean phase holdup and radial gas holdup distributions were discussed by Jin et al. (2010).

A study on twin plane ERT system on gas-liquid two-phase flow in a vertical pipe was demonstrated by Cui et al. (2010) which provides the information related to the online monitoring of flow regime classification as well as gas hold-up computation. The cross-correlation velocity of oil-water two phase flow in horizontal pipe by a dual-plane ERT was demonstrated by Tan et al. (2010). In accordance to reconstruct the conductivity distribution of ERT, electrical capacitance tomography (ECT) was applied by Cao et al. (2010). By using ERT system as well as V-cone meter, studies on gas-water two phase in a horizontal pipe were demonstrated by Tan & Dong, (2009). The ERT system was also used for slug flow measurement of gas-liquid two-phase flow in horizontal pipes (Xu et al., 2009). A study on liquid-solid two-phase system in a liquid-solid circulating fluidized bed (LSCFB) for flow characteristics was demonstrated by Razzak et al. (2009).

Pakzad et al. (2008) studied the ERT system to measure the mixing time of xanthan gum solution with the yield stress stirred in a baffled tank. To measure the liquor flow with the help of model chip digester Ruzinsky & Bennington (2007) applied ERT. To visualize and analyze the mixing of two miscible liquids with different conductivities in a stirred vessel, ERT was applied by Kim et al. (2006). The following table **(Table 3.1)** shows the summary of recent developments and applications of ERT.

Table 3.1. Summary of recent developments and applications of ERT.

No.	References	Applications
1.	Dyakowski & Williams (1998)	Hydrocyclone flow modelling
2.	Dyakowski et al. (2000)	Imaging of nylon polymerization process
3.	Fransolet et al. (2001)	ERT measurements on bubble column
4.	Fransolet et al. (2005)	Gas holdup in bubble column with non-Newtonian fluids
5.	Ricard et al. (2005)	Monitoring of multiphase pharmaceutical process
6.	Toye et al. (2005)	Applications in hydrodynamics of bubble column
7.	Kim et al. (2006)	Mixing
8.	Razzak et al. (2007)	Flow characterization of three-phase
9.	Ruzinsky & Bennington. (2007)	liquor flow aspects
10.	Jin et al. (2007)	Gas holdup profile measurements in gas-liquid concurrent bubble column
11.	Wang et al. (2007)	Analysis of bubbles in bubble column
12.	Pakzad et al. (2008)	Investigation of mixing process
13.	Seppanene et al. (2008)	Imaging of concrete
14.	Meng et al. (2009)	Measurement of flowrate of two-phase
15.	Razzak et al. (2009)	Flow characterization in LSCFB riser
16.	Tan & Dong. (2009)	Recognition of flow regime
17.	Xu et al. (2009)	Slug flow measurement
18.	Cao et al. (2010)	Using an ECT sensor
19.	Cui et al. (2010)	Twin-plane ERT system
20,	Hosseini et al. (2010)	Solid-liquid mixing in agitated tanks
21.	Jin et al. (2010)	Gas-liquid counter-current operation on gas holdup
22.	Karhunen et al. (2010)	Assessment of cracks in concrete
23.	Karhunen et al. (2010)	Localizing reinforcing bars in concrete
24.	Kowalski et al. (2010)	Physical stability in liquid compositions
25.	Meng et al. (2010)	Measurement of flow rate of air-water by Venturimeter with ERT sensor
26.	Tan et al. (2010)	Monitoring velocity of flow of two-phase
27.	Gumery et al. (2011)	Mixing characteristics of draft tube airlift bioreactor
28.	Kourunen et al. (2011)	Gas holdup distribution in laboratory floatation cell
29.	Tahvildarian et al. (2011)	Mixing of micron-sized particles in slurry reactor
30.	Yenjaichon et al. (2011)	Mixing quality of pulp in industries
31.	Zhang et al. (2011)	Visualization of multiphase flow
32.	Dong et al. (2012)	Visualization of multiphase flow
33.	Sharifi & Young (2012)	Qualitative and quantitative studies of milk flow
34.	Sharifi & Young (2012)	3D monitoring of tanks for milk processing
35.	Yang et al. (2012)	Void fraction measurements
36.	Zhang et al. (2012)	Two phase flow regime identification
37.	Jin et al. (2013)	Gas holdup measurements in multistage bubble column

4. Methodology

The following chapter is mainly described five sections including experimental set-up, rheology of fluid, experimental procedure, error analysis, and relevant experimental conditions.

4.1 Experimental Set-up

In the following study, the experimental set-up consists of three parts including a mixing vessel, the mixers and the ERT system. As described in previous chapter that ERT system has three different parts which are named as electrodes, data acquisition system (DAS), and a host computer.

4.1.1 Mixing Vessel

In **Figure (4.1)**, a mixing vessel is shown as a flat-bottomed cylindrical tank with an inner diameter (T) of 200mm. The Fluid height (H) was equal to the tank diameter providing a total volume of about 6 lit.

4.1.2 Mixer Configuration

The tank was equipped with single top shaft. Three impellers were employed as **(a)** an axial/radial impellers ARI (A200/Rushton impeller), **(b)** a mixed flow impeller called ASI (A200 and the Scaba impeller), and **(c)** a radial impeller named as Rushton turbine (a disc style flat blade turbine) with diameter of 90mm (D_C) attached to a top shaft. The central impeller was driven using a 0.2 hp (150 Watts) direct driven motor. Each impeller was centrally positioned at an off-bottom clearance (C_C) of 45mm and attached with a single top shaft. The impeller speed and torque were determined through the impeller rotational speed and torque display mounted on the mixer motor (CaframoBDC1850), respectively. The air was also sparged into the vessel through cross-shaped sparger fitted at the bottom of the tank with six arms of 78mm long and each arm had 4 holes of 1mm diameter. A rotameter (Acrylic Rotameter, Omega) was employed to apply the pre-set amount of air into the vessel. Further details regarding geometrical characteristics of central impellers and experimental setup are shown in **Figure 4.1** and **Figure 4.2**.

4.1.3 ERT System

The ERT system for this study consists of the electrodes, ITS P2000 data acquisition system and a host computer. The main objective to employ the ERT system is to determine the value of conductivity distribution within the mixing vessel. The numerous electrodes fitted on the periphery of the tank can be utilized to measure the current or voltages after injection of current which provides an idea about conductivity distribution inside the mixing tank.

4.1.3.1 Electrodes

The mixing vessel was equipped with two sensor planes as shown in **Figure 4.1** and each plane was comprised of 16 stainless steel electrodes bounded non-invasively at equal intervals around the periphery of the tank. Each rectangular electrode has a dimension of 8mm high and 7mm wide and 1mm thick. The features of the electrodes are a function of the different factors such as reactor diameter, fluid conductivity, fluid viscosity (Babaei et al., 2015(b)). The sensor planes are numbered from top downward (Plane 1 and 2). Electrodes bounded with the vessel were connected to the ITS P2000 DAS using a coaxial cable.

4.1.3.2 Data Acquisition System (DAS)

DAS is responsible for obtaining the quantitative data on fluid conductivity inside the vessel. DAS is also responsible for coordinating the desired measurement protocol. In this study, a P2+ ERT system (version 8, Industrial tomography system-ITS, Manchester, UK) makes use of an adjacent strategy (Barber at al., 1983) by which a current is applied between two adjacent electrodes and measuring the resultant voltage between all other adjacent electrode pairs (Pakzad et al., 2008)). The procedure was repeated until a full rotation is completed for injecting current to other combination of electrodes and resultant voltage was measured. The main specifications of DAS utilized and kept constant in this study for frequency, injection current range, frame speed, output voltage range, voltmeter sensitivity of tomography were as follows, $\pm$0.5%(at 9.6 KHz), 20mA, 20 mS/frame, -10V to +10V, 4.88uV at gain$\times$1000. The DAS was connected to a computer with nine-pin communication port for control, image recognition, and data storage.

4.1.3.3 Host Computer

The host computer was responsible for data processing by employing an image reconstruction algorithm. It utilized a non-iterative algorithm (Linear Back Projection- LBP) which provides the 2D conductivity maps for each plane by reconstructing the raw voltage measurements. Although, this algorithm makes use of voltage difference (change in conductivity before and after) to convert the raw voltage measurements into average conductivity signals on each sensors plane. Due to its low computational requirements, LBP is easy, quick and simple (Barber and Brown, 1984).

The non-iterative algorithm provides qualitative data on the conductivity change and their tomographic image includes 20×20 pixel array which gives 400 spatial elements. The circular reconstructed image includes 316 pixels out of 400 pixel square grid. However, in this work a mixing tank equipped with two tomographic planes was employed which resulted in 632 non-intrusive conductivity probes.

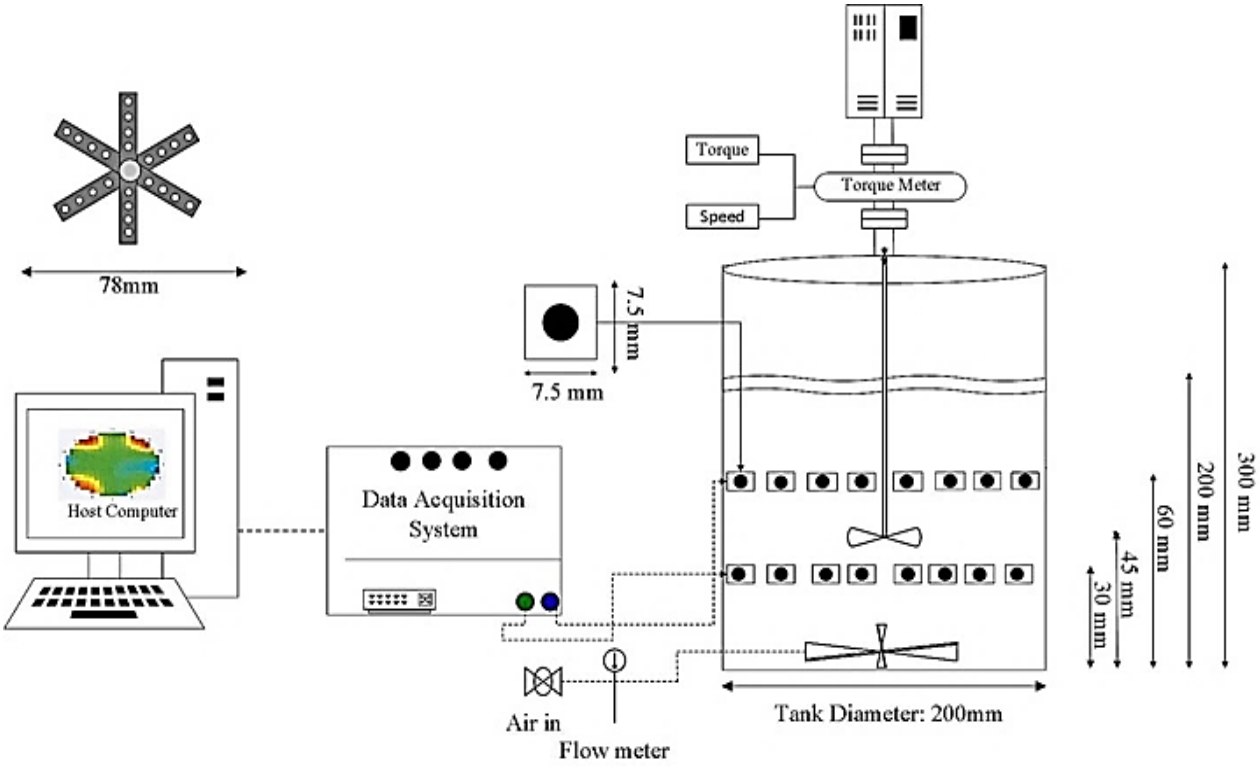

Figure 4.1. Schematic diagram of experimental set-up (dimensions in mm).

(i) ARI
(combination of A200 and Rushton impeller)

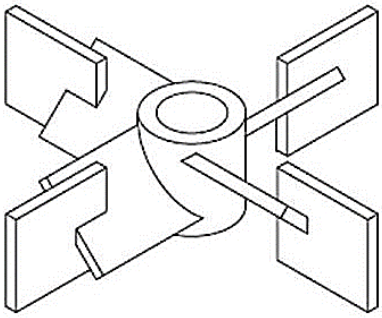

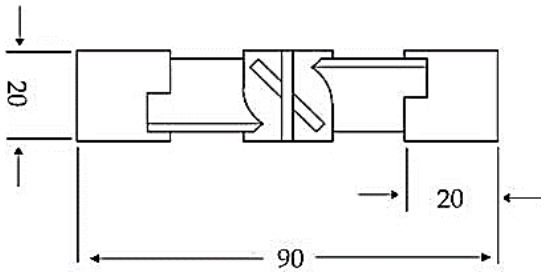

(ii) ASI
(combination of A200 and Scaba impeller)

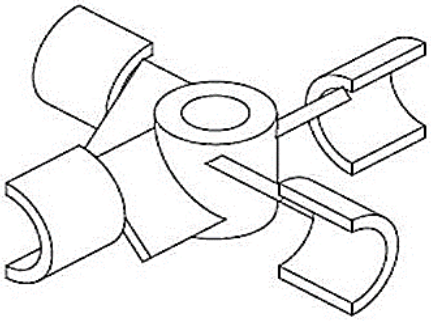

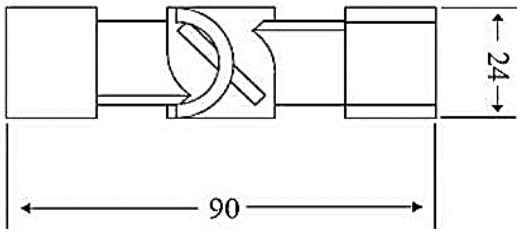

(iii) Rushton impeller
(fully radial impeller)

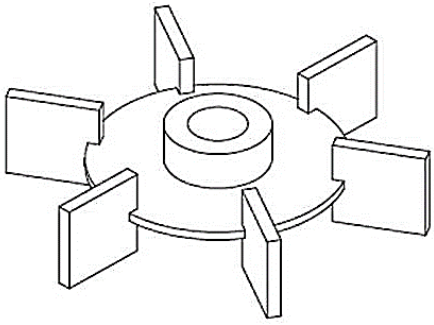

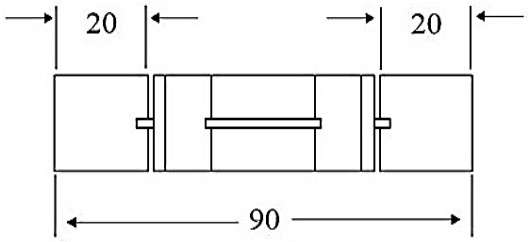

Figure 4.2. Impellers geometry (dimensions in mm).

4.2 Fluid Rheology

The fluid utilized for this work was the activated sludge which possesses the pseudoplastic properties of non-Newtonian fluid category. It exhibits complex rheology depending on several different parameters such as pH, temperature, particle dimensions, concentration of solid, fluid consistency coefficient, yield stress, and sludge treatment process (Novarino et al., 2010). An activated sludge is widely employed in wastewater treatment system to degrade organics and eliminate nutrients from wastewater for the production of high quality effluent (Eawag et al., 2014). The activated sludge consists of flocs of active bacteria which are capable of eliminating biodegradable organic substance from screened and pre-settled wastewater. However, while wastewater treatment process mixing and aeration are required to ensure that wastewater is mixed and aerated inside the mixing tank (Eawag et al., 2014). **Figure 4.3** shows the actual experimental set-up of the following study in which mixing tank (filled with activated sludge) was equipped with ERT planes which were connected to Data acquisition system and computer.

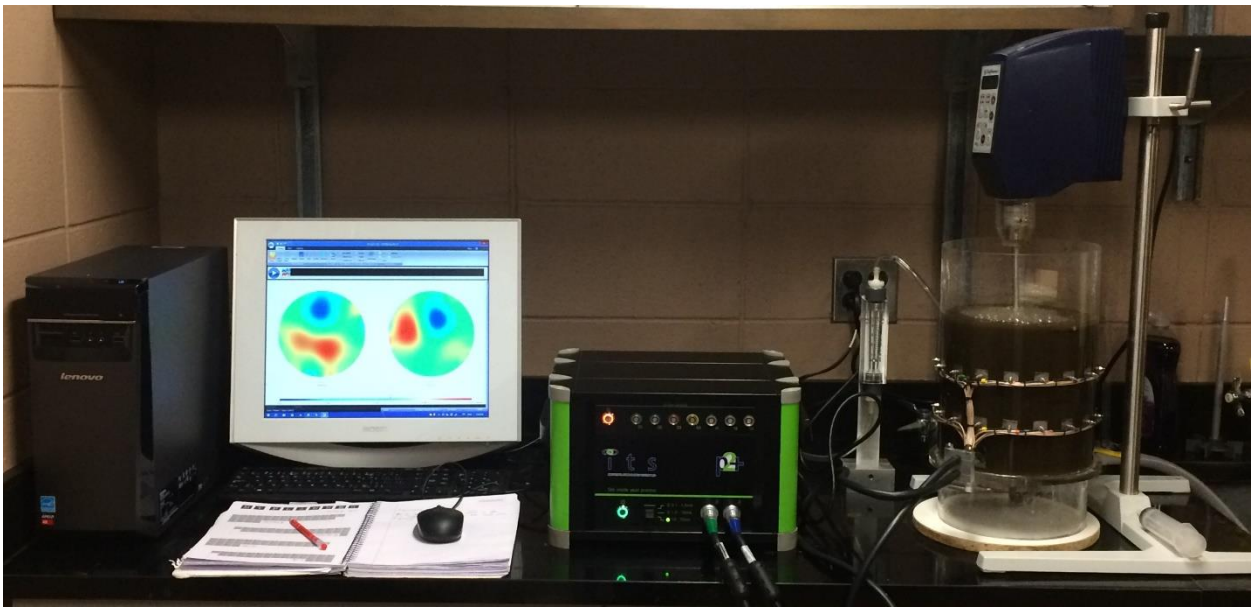

Figure 4.3. Actual Experimental Set-up.

The activated sludge with 7-10wt% of solid content was used from Resolute Forest, Thunder Bay, ON, Canada. Rheological properties of activated sludge samples were measured at the bulk fluid temperature (25 ± 0.5°C) by utilizing a DHR2 (Discovery Hybrid Rheometer-1) rheometer (TA

instruments, USA) through a bob and cup measuring system. Three samples of activated sludge (from the same batch) were taken and three measurements were recorded for each sample with three repeats. The range of shear rate, set in the rheometer corresponds to the shear rate encountered in the aerated mixing tank. The rheology of the activated sludge was modeled with high regression coefficient (R^2=0.98) using the power law rheological model as shown in **Figure 4.4.** The equation of power law model is as follows:

$$\tau = K\dot{\gamma}^n \tag{4.1}$$

where $\dot{\gamma}$ is the shear rate, K and n are shear rate independent constants. The rheological characteristics of the activated sludge are K= 1.73 Pa.s^n and n= 0.27.

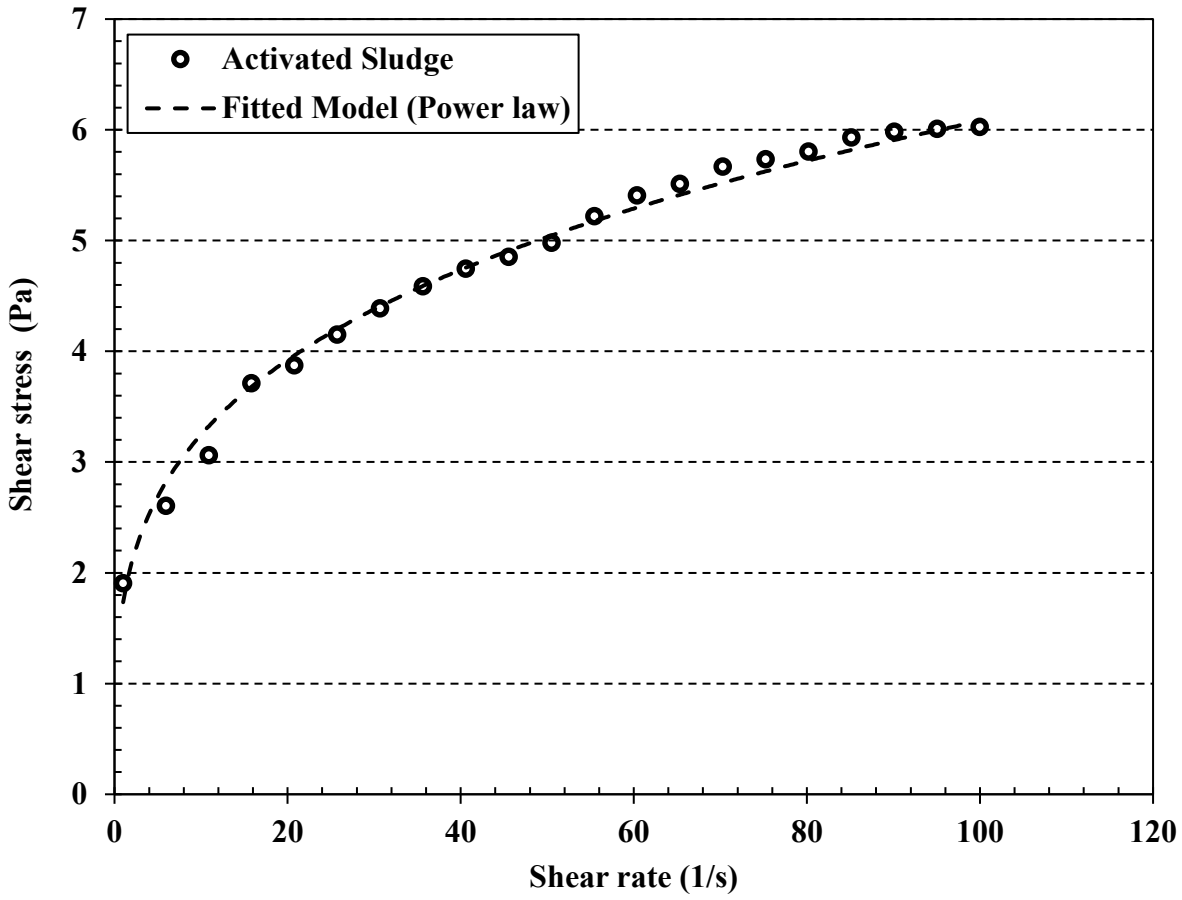

Figure 4.4. Shear stress versus shear rate for activated sludge used in this study.

4.3 Experimental Procedure

The experimental procedure involves various steps such as, stirring of activated sludge before transferring it into the mixing vessel, which requires great care as solid particles settle down very quickly at the bottom of the container. Also, care should be taken while pouring it into the ERT mixing tank to avoid spills on the electrodes (bounded on the walls of mixing vessel), injection of air, mixing time measurement, and power measurement.

4.3.1 Specific Power Measurement

The impeller speed and torque were determined through the impeller rotational speed and torque display mounted on the mixer motor (CaframoBDC1850), respectively. Specific power consumption is the ratio of total power input to the total volume of the mixing tank. It was calculated by utilizing various steps which involves the measurement of torque for every single run. The friction torque (measured when the vessel was empty) was subtracted from the measured torque:

$$T_{corrected} = T_{friction} - T_{measured} \tag{4.2}$$

where T denotes the torque (N. m). Power consumption was then calculated using the following equation:

$$P = 2\pi NT \tag{4.3}$$

where P, N, and T shows the Power, impeller rotational speed in seconds, and torque, respectively.

Therefore, to evaluate the specific power consumption the calculated power **(Equation 4.3)** can be divided by the total volume of the mixing vessel. The equation can be presented as follows:

$$P_{tot} = \frac{P}{V} \tag{4.4}$$

where P_{tot}, P, and V denoted the specific power consumption, power and total volume of the mixing tank.

By utilizing the Metzner and Otto approach (1975) the corresponding Re numbers to the impeller rotational speeds were calculated using the apparent viscosity (η_{app}) of the activated sludge modeled as a power-law fluid as follows:

$$\eta_{app} = \frac{\tau}{\dot{\gamma}_{ave}} = K(\dot{\gamma}_{ave})^{n-1} \tag{4.5}$$

The Reynolds number for non-Newtonian fluids can be defined as:

$$Re = \frac{\rho D^2 N^{2-n}}{K K_s^{n-1}} \tag{4.6}$$

where η_{app}, τ , $\dot{\gamma}_{ave}$, *N, D,* ρ, K , n, and K_s are apparent viscosity, shear stress, averaged shear rate, impeller speed, impeller diameter, fluid density, shear rate independent constants and Metzner-Otto constant, respectively.

4.3.2 Mixing Time Measurement

The mixing tank was equipped with a cross-shaped sparger and an impeller with the bottom clearance (C_C) set at 45mm, filled with the activated sludge to a volume of about 6 lit. The conductivity of activated sludge and brine were measured by employing a conductivity meter (Thermo Scientific, Orion Star A212) which was 4.24 mS/cm for activated sludge and 75.60 mS/cm for brine. These conductivity values were kept constant in all the experiments or on ERT system. Pre-set amount of air was applied through the system by a rotameter (Acrylic Rotameter, Omega) via sparger. Mixing time measurements were performed in the mixing tank by the addition of 10ml saline tracer (NaCl). **Figure 4.5** shows the injection and monitoring planes used for measuring of the mixing time.

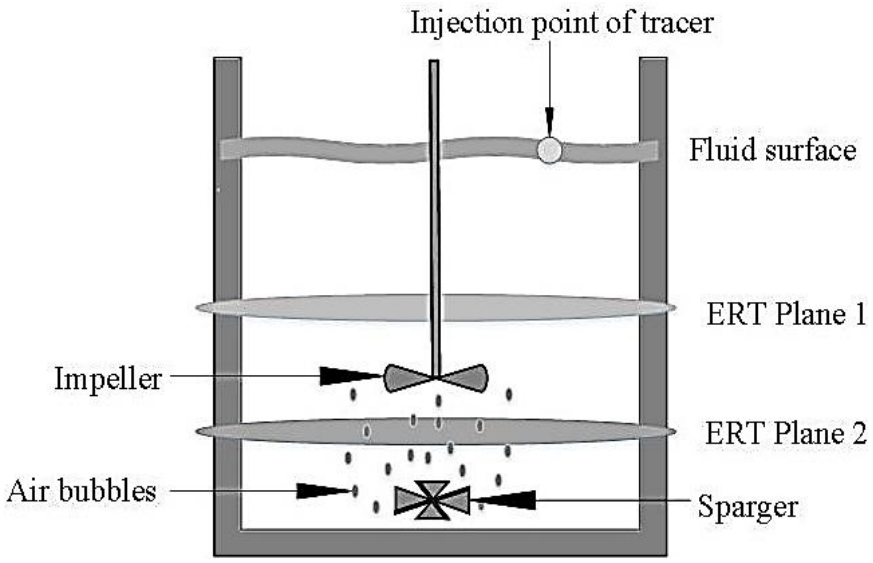

Figure 4.5. Geometry of ERT mixing tank with a point of injection.

To measure the mixing time using ERT, after about 12-15 frames 10ml of 30% saline solution was injected 20mm below the liquid surface. Prior to the data collection, the reference state was measured in order to eliminate the effects of the impeller and shaft. Also, it was necessary to calibrate the instrument current source, gains map and performance of electrodes before conducting a mixing time test. In order to increase signal to noise ratio, the multiple reference frame approach was applied. Therefore, for each experiment 100 frames were recorded and average of them was used as the reference frame. Each experiment regarding mixing time was repeated three times at least to make sure that the data is identical to each other and average of them was used as the mixing time. The mixing time was defined as the time required reaching 98% of the steady state conductivity value at both monitoring planes as shown in **Figure 4.6**. However, after the injection of tracer at about 6 seconds, electrodes of the ERT system recorded a peak in conductivity readings for both planes (Planes 1 and 2) until they reach to the level of homogeneity at time 8.41 seconds to determine the mixing time.

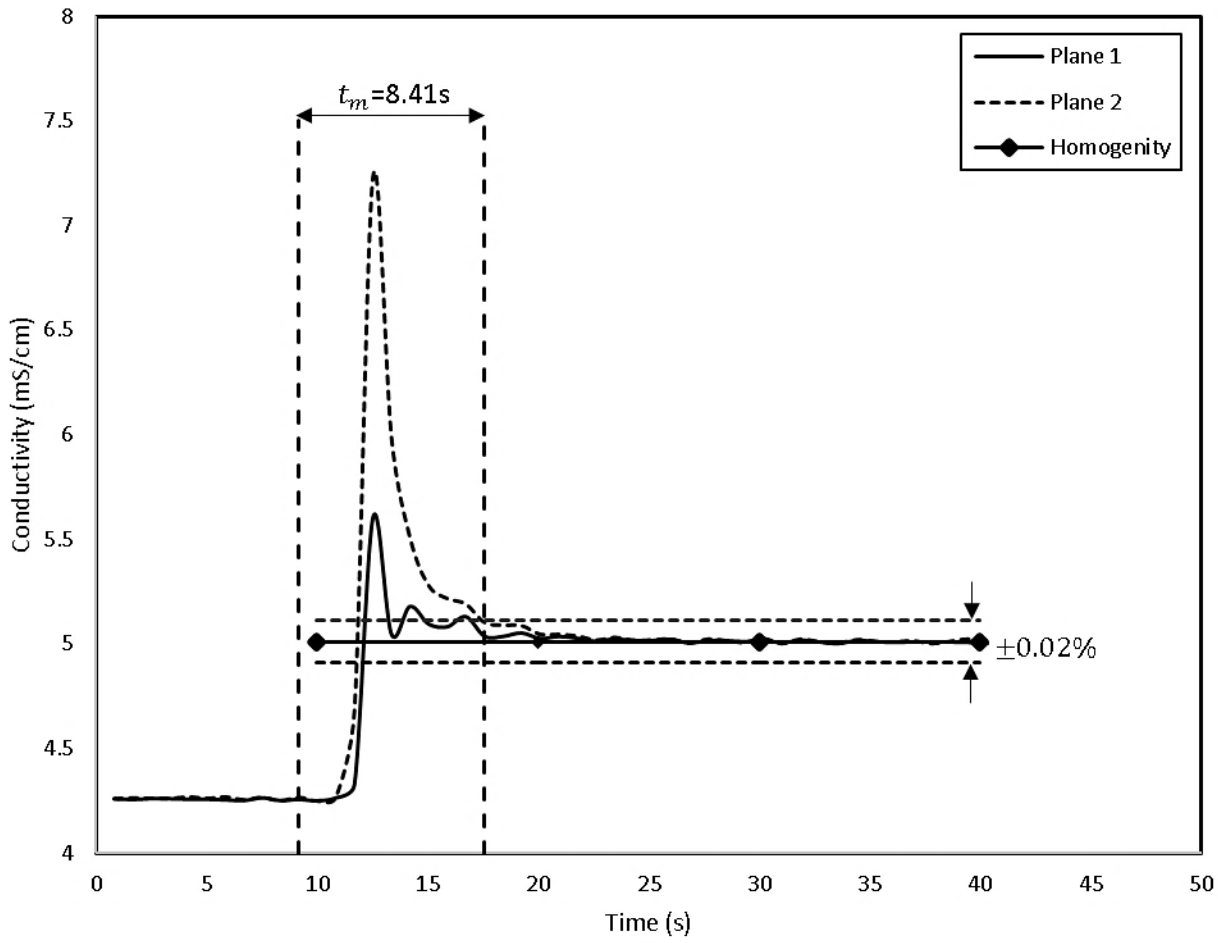

Figure 4.6. Mean conductivity measured using ERT as a function of time for activated sludge agitated by ASI at *N*=100 rpm with absence of gas flow.

4.3.3 Gas Flow Number Measurements

In this study, gas flow number was calculated for all the impellers employed during this experimental work at different gas flow rate by using the following equation:

$$Fl_g = \frac{Q_g}{ND^3} \tag{4.7}$$

where Fl_g is the gas flow number, Q_g is the rate of flow, N is impeller speed and D is the diameter of the impeller.

4. 4 Experimental Conditions

The effects of impeller speed, impeller type (fully radial and hybrid axial-radial impellers), and amount of aeration on the mixing of activated sludge in an aerated tank were studied in terms of power consumption, mixing time and flow pattern. The experimental conditions followed in this study are listed in **Table 4.1**.

Table 4.1. Experimental conditions.

No.	Description	Range and Type
1.	Impeller speed (rpm)	50, 75, and 100
2.	Impeller type (-)	ARI, ASI, and Rushton
3.	Gas flow rate (m^3/min)	No air, 0.011, 0.014

4.5 Error Analysis

As per the accuracy of torque sensors and ERT system, the errors can be analyzed as follows. **Table 4.2** shows the corresponding Reynolds number by using modified equation for Reynolds number **(Equation 4.6)**. The following Reynolds numbers (21 (the minimum) to 73 (the maximum)) were used to predict the flow behavior of activated sludge as transitional flow regime.

Table 4.2. Power Number and corresponding Reynolds Number (using **Equations 2.15** and **4.6**, respectively).

Run No.	Impeller Type	Impeller Speed (rpm)	Power Number (-)	Reynolds Number (-)
1	ARI	50	68.07	22.00
2	ARI	100	23.09	72.98
3	Rushton	50	72.93	21.33
4	Rushton	100	23.09	70.75
5	ASI	50	68.07	21.06
6	ASI	100	19.45	69.85
7	ASI	50	72.93	21.06
8	ASI	100	20.66	69.85
9	ARI	75	47.54	44.37
10	Rushton	75	45.38	43.01
11	ARI	75	45.38	44.37
12	Rushton	75	45.38	43.01
13	ASI	75	47.54	42.46
14	ASI	75	45.38	42.46
15	ASI	75	45.38	42.46

4.5.1 Torque Sensor Precision Analysis

Due to the electronic fluctuation, mechanical disturbance and friction in rotating shaft, torque sensor may cause some random errors in the collected data. Such random errors of torque sensor (CaframoBDC1850) can be defined by using the following equation of standard deviation:

$$SD = \sqrt{\frac{1}{N-1}\sum_{i=1}^{N}(M_i - \bar{M})^2} \tag{4.8}$$

where N is the number of measurements, M is the torque variable and $\bar{M}$ is the mean value of the torque measurements.

A graph was plotted **(Figure 4.7)** for torque versus all fifteen runs for which torque was measured and found that errors shown by the standard deviation (SD < 0.5 %) was small enough which signifies that torque measurements were accurate. **Figure 4.7** shows the respective graph for torque measurements for all experimental runs.

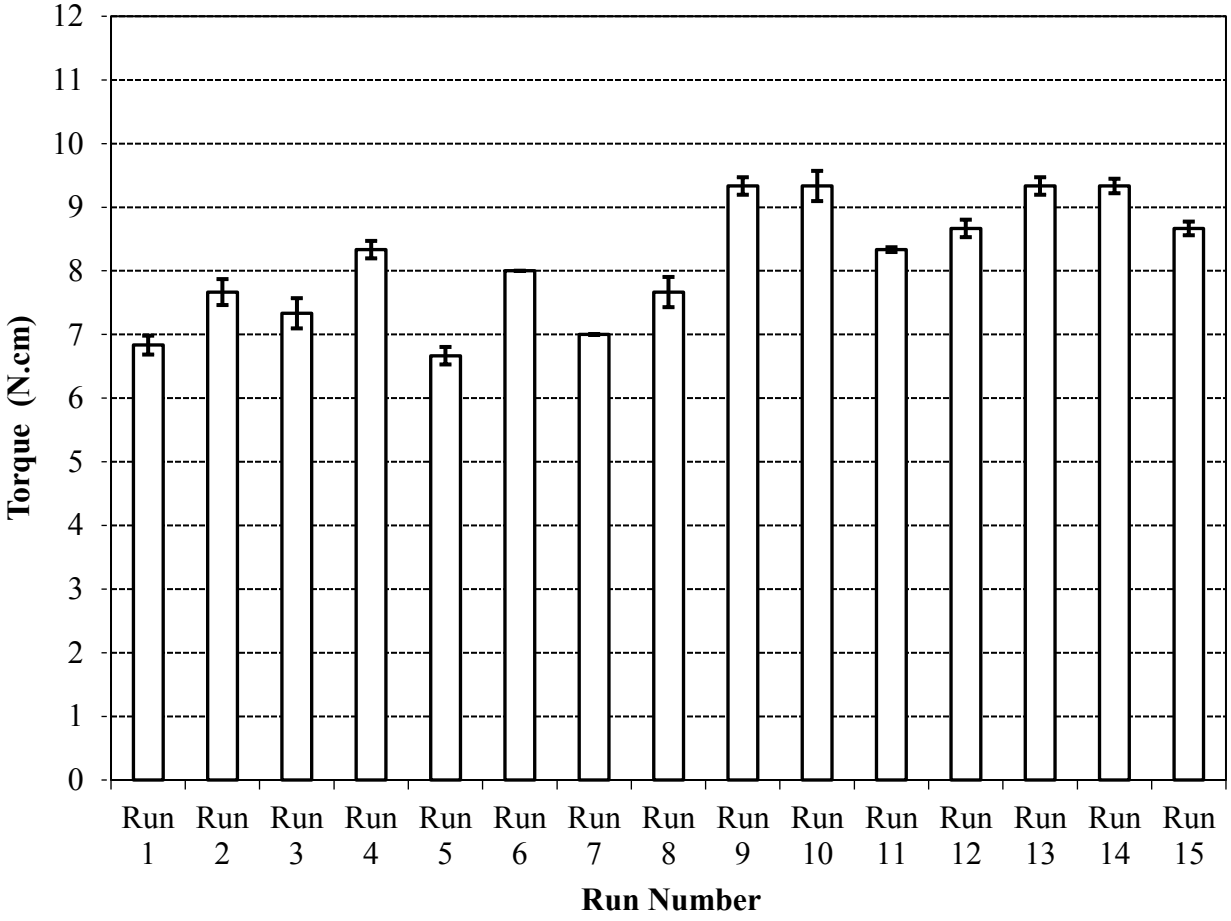

Figure 4.7. Torque measurement for activated sludge from Run 1 to 15.

4.5.2 ERT Measurements Precision Analysis

To confirm the accuracy of mixing time measurements a graph was plotted (mixing time versus experiment runs) by using the standard deviation equation **(Equation 4.8).** Therefore, the results of standard deviation (SD<0.3 %) shows that the mixing time measurements are error independent which also confirms that the experimental results have a good repeatability and reproducibility characteristics. Although, from **Figure 4.8** it can be easily observed that the mixing time measurements in the current study were error insignificant.

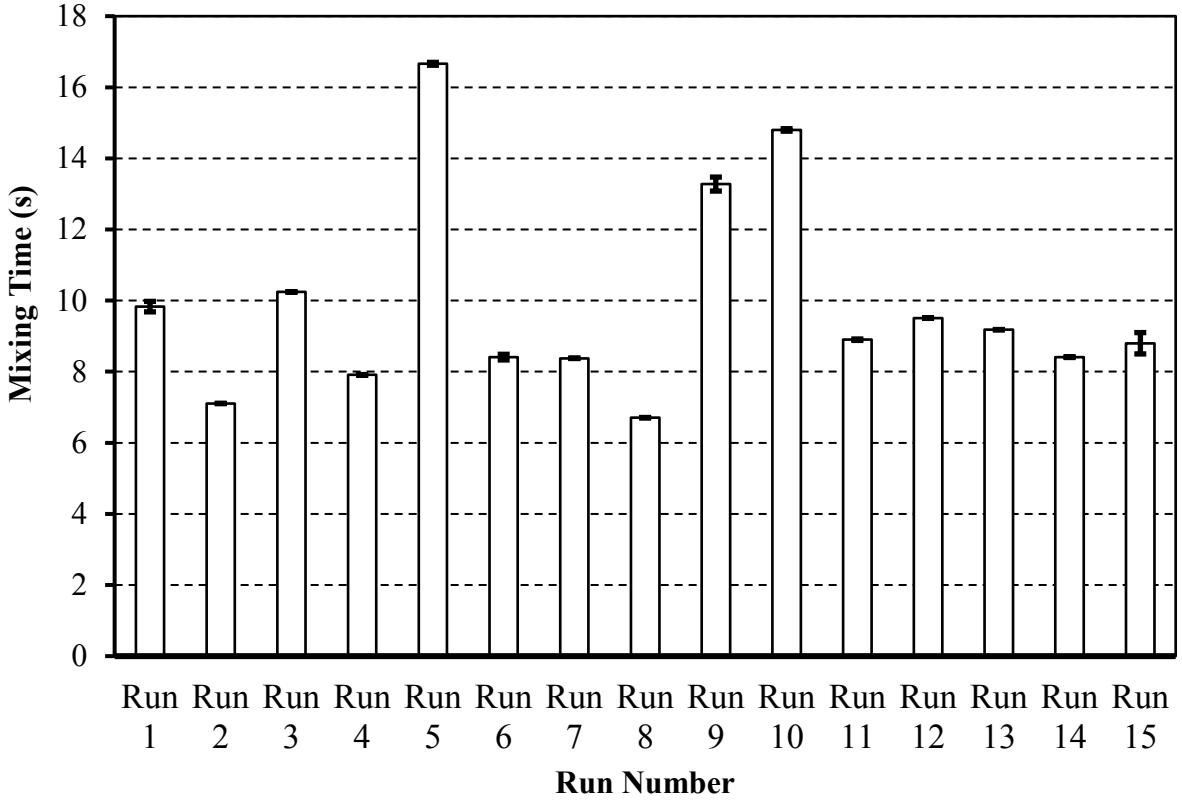

Figure 4.8. Mixing time measurements from Run 1 to 15.

As mentioned earlier (section 4.3.2) that ERT system was calibrated before taking any measurements. To confirm the accuracy of collected data, each measurement was repeated three time and standard deviation was determined as SD < 0.3% which signifies a good agreement of repeatability and reproducibility of the experiments.

5. Results and Discussions

5.1 Introduction

In this experimental study, electrical resistance tomography (ERT) and response surface methodology (RSM) were utilized to assess the performance of independent variables in presence or absence of air in agitation of activated sludge in a mixing tank in terms of three responses called mixing time, specific power consumption and gas flow number. After evaluating the results for each response, the data was analyzed with the help of analysis of variance (ANOVA)[1] and RSM which determined the individual and interactional effect of independent variables on each response significantly.

In this chapter, first experimental design are presented. Then, results from response surface methodology, comparisons, individual and interaction effects of independent variables with the help of plots, and three-dimensional response surface are presented. To study the behavior of independent variables such as impeller speed, impeller type, and gas flow rate 2D tomograms from electrical resistance tomography were obtained and presented.

5.2 Analysis of Hydrodynamics Characteristics of Activated Sludge in a Mixing Tank Agitated by an Impeller with or without Aeration through Response Surface Methodology (RSM)

Based on the aspects regarding applications of RSM and tomography, no empirical work has been done to evaluate the performance of a novel impeller named as ASI (a combination of the A200 and Scaba impeller) (Pakzad et al., 2013) in the agitation of activated sludge in presence or absence of gas and limited work has been done regarding performance and comparison of different impellers in agitation of activated sludge with or without gassing in a mixing tank. In consideration of the following facts, in the present work, with the help of a statistical- based experimental design 15 experiments were performed to evaluate the individual, interactive and comparable effects of

[1] **ANOVA**: collection of statistical models which was developed by Ronald Fisher in 1918.

three different type of impellers with different geometry at three rotational speeds (50, 75, and 100 rpm) with or without different gas flow rate (0.011 and 0.014m^3/min).

The classic method of changing one variable at a time to assess the effect of all variables on the objectives is time consuming especially for such multivariable system as the aerated mixing system. To analyze the performance of all the considered variables, response surface methodology (RSM), known as statistical method was utilized. Three-level factorial design, central-composite design (CCD) (Box and Wilson, 1951), Box-Behnken (Box and Behnken, 1960), and D-optimal (Myers and Montgomery, 2004) are the four types of RSM design. Multiple regression analysis is more desirable to be utilized in RSM (Kocabas, 2001). The statistical design of experiments determining the interaction among different variables requires less experiments to be conducted and can be utilized for the system optimization.

The description of variables and operating conditions are listed in **Table 5.1.** As can be seen in this table the independent variables were the impeller speed (X_1), impeller type (X_2), and gas flow rate (X_3). The low, center, and high levels of each variables were coded as -1, 0, and +1, respectively. The analytical selection of such maximum and minimum ranges for each independent variables were selected based on the preliminary experiments.

Table 5.1. Experimental range and levels of independent variables (Box-Behnken Design).

Variables	Symbol	-1	0	1
Impeller speed (rpm)	X_1	50	75	100
Impeller type (-)	X_2	ARI	ASI	Rushton
Gas flow rate (m^3/min)	X_3	No air	0.011	0.014

Since, in this study three variables were considered, for which a modified central composite experimental design known as Box-Behnken Design (BBD)[1], a statistical design method was utilized. In BBD, the level of one of the variables is fixed at the center level while interactions of all other variables are applied (Kocabas, 2001; Myers and Montgomery, 2004). In addition, BBD requires less runs of the experiments and optimize the main interaction and quadratic effects

[1] **Box-Behnken Designs:** These are the experimental designs devised by George E. P. Box and Donald Behnken in 1960.

(Hashemi et al., 2016) and it is rotatable (approximately). By using aforementioned method, impact of these variables was demonstrated in detail.

The response objectives were three significant parameters in mixing process i.e. mixing time (Y_1), specific power consumption (Y_2) and gas flow number (Y_3) as can be seen in **Table 5.2**. This table shows that based on three-level and three-factors experimental Box-Behnken Design there were total fifteen experiments performed along with three replicates at the center of the design. To analyze experimental data, response surface methodology (RSM) was utilized by using Design of Experiments (trail version of Design Expert software; version 10) which generates 3D surface plots.

Table 5.2. Three-factor, three-level Box-Behnken design (BBD) for response surface methodology (RSM) and the observed responses.

Run no.	Coded Variables			Responses		
	X_1	X_2	X_3	$t_m(s)$	$P_{tot}/V(Wm^{-3})$	$Fl_g(-)$
1	-1	-1	0	9.83	38.89	0.31
2	1	-1	0	7.11	105.56	0.16
3	-1	1	0	10.25	41.67	0.31
4	1	1	0	7.91	105.56	0.16
5	-1	0	-1	16.66	38.89	0.00
6	1	0	-1	8.41	105.56	0.00
7	-1	0	1	8.38	41.67	0.39
8	1	0	1	6.71	94.44	0.19
9	0	-1	-1	13.28	91.67	0.00
10	0	1	-1	14.8	87.50	0.00
11	0	-1	1	8.9	87.50	0.26
12	0	1	1	9.51	104.17	0.26
13	0	0	0	9.19	91.67	0.21
14	0	0	0	8.41	87.50	0.21
15	0	0	0	8.80	87.50	0.21

Note: $1, 0,$ and -1 shows the levels of independent variables shown in Table 5.1.

5.2.1 Statistical Analysis using Box-Behnken Design (BBD)

Regarding the analysis of experimental data, the second-order polynomial model with quadratic function was employed **(Equation 5.1)**:

$$Y = B_0 + \sum_{i=1}^{k} B_i X_i + \sum_{i=1}^{j-1} \sum_{j=1}^{k} \beta_{ij} X_i X_j + \sum_{i=1}^{k} \beta_{ii} X_i^2 + e_i \quad (5.1)$$

where Y, X_i, X_j, β_0, β_i, β_{ij}, β_{ii}, K, and e_i refers to the predicted response, independent variables, constant coefficient or intercept parameter, influence of independent variables, influence of interaction among variables, quadratic effect, number of variables studied and error residuals.

By applying the multiple regression analysis, the response functions for mixing time (Y_1), specific power consumption (Y_2) and gas flow number (Y_3) were obtained with the quadratic equations as follows:

$$Y_1 = 9.95 - 2.38X_1 + 0.49X_2 - 2.46X_3 + 0.095X_1X_2 + 1.70X_1X_3 - 0.25X_2X_3 - 0.80X_1^2 + 0.78X_2^2 + 0.89X_3^2 \quad (5.2)$$

$$Y_2 = 90.39 + 28.17X_1 - 0.57X_2 + 0.69X_3 - 0.69X_1X_2 + 2.74X_1X_3 + 1.33X_2X_3 - 19.44X_1^2 + 3.47X_2^2 + 5.32X_3^2 \quad (5.3)$$

$$Y_3 = 0.13 - 0.048X_1 + 0.00X_2 + 0.14X_3 + 0.00X_1X_2 - 0.049X_1X_3 + 0.00X_2X_3 + 0.020X_1^2 + 0.24X_2^2 - 0.19X_3^2 \quad (5.4)$$

where (X_1), (X_2), and (X_3), are the coded terms of three independent variables representing impeller speed, impeller type, and gas flow rate sparged into the column, respectively.

5.2.2 Model Coefficient and Interaction Analysis

The second-order polynomial model with quadratic and interaction coefficients; i.e. **Equation (5.2), (5.3)** and **(5.4)** can be applied to fit the coded values of experimental data. **Table (5.3)**, **(5.4)**, and **(5.5)** represents the results of quadratic regression equation for responses (Y_1), (Y_2), and (Y_3) from analysis of variance (ANOVA). In addition, ANOVA also confirms the adequacy of the

equations for all three responses by analyzing the F-value[1]. Therefore, the greater F-value and the lower P-value shows the more significant coefficient.

The models F-values of 149.22, 33.00, and 252.01 show that models reasonably describing the mixing time, specific power consumption and gas flow number, respectively. There is only 0.01% chance that an F-values these larges could occur due to noises. However, if the value of Prob>F is <0.0500, the model is considered to be significant whereas if the Prob>F value is >0.1000 the model is considered insignificant. The Prob>F values for all responses are <0.0500 indicating that the models were significant.

Table 5.3. ANOVA test for response function (mixing time) $Y_1 = 9.95 - 2.38X_1 + 0.49X_2 - 2.46X_3 + 0.095X_1X_2 + 1.70X_1X_3 - 0.25X_2X_3 - 0.80X_1^2 + 0.78X_2^2 + 0.89X_3^2$.

Source	Sum of Squares	Degree of freedom	Mean Square	F-ratio	p-value Prob>F
Models	112.37	9	12.49	149.22	<0.0001
X_1	39.43	1	39.43	471.24	<0.0001
X_2	1.69	1	1.69	20.24	0.0064
X_3	48.27	1	48.27	576.84	<0.0001
X_1X_2	0.036	1	0.036	0.43	0.5403
X_1X_3	13.69	1	13.69	163.60	<0.0001
X_2X_3	0.30	1	0.30	3.54	0.1185
X_1^2	2.39	1	2.39	28.51	0.0031
X_2^2	2.24	1	2.24	26.76	0.0035
X_3^2	1.03	1	1.03	12.29	0.0172

Note: $R^2 = 0.9963$, $R^2_{adj} = 0.9896$, C.V.%= 2.93, Adequate Precision[2]= 40.98

[1] **F-value**: Test for comparing the variance associated with that term with the residual variance.
[2] **Adequate Precision:** signal to noise ratio. Ratio greater than 4 indicates adequate model discrimination.

Table 5.4. ANOVA test for response function (specific power consumption) $Y_2 = 90.39 + 28.17X_1 - 0.57X_2 + 0.69X_3 - 0.69X_1X_2 + 2.74X_1X_3 + 1.33X_2X_3 - 19.44X_1^2 + 3.47X_2^2 + 5.32X_3^2$.

Source	Sum of Squares	Degree of freedom	Mean Square	F-ratio	p-value Prob>F
Models	9403.81	9	1044.87	33.00	0.0004
X_1	7072.91	1	7072.91	223.38	<0.0001
X_2	4.12	1	4.12	0.13	0.7646
X_3	2.16	1	2.16	0.068	0.6972
X_1X_2	1.93	1	1.93	0.061	0.7820
X_1X_3	23.64	1	23.64	0.75	0.2669
X_2X_3	68.07	1	68.07	2.15	0.5716
X_1^2	1371.08	1	1371.08	43.30	0.0005
X_2^2	40.21	1	40.21	1.27	0.2197
X_3^2	2.19	1	2.19	0.069	0.2589

Note: $R^2 = 0.9865$, $R^2_{adj} = 0.9623$, C.V.%= 6.08, Adequate Precision= 17.447

Table 5.5. ANOVA test for response function (gas flow number) $Y_3 = 0.13 - 0.048X_1 + 0.00X_2 + 0.14X_3 + 0.00X_1X_2 - 0.049X_1X_3 + 0.00X_2X_3 + 0.020X_1^2 + 0.24X_2^2 + 0.19X_3^2$.

Source	Sum of Squares	Degree of freedom	Mean Square	F-ratio	p-value Prob>F
Models	0.22	9	0.025	252.01	<0.0001
X_1	0.016	1	0.016	161.60	<0.0001
X_2	0.000	1	0.000	0.000	1.0000
X_3	0.15	1	0.15	1535.93	<0.0001
X_1X_2	0.000	1	0.000	0.000	1.0000
X_1X_3	0.011	1	0.011	113.81	0.0001
X_2X_3	0.000	1	0.000	0.000	1.0000
X_1^2	1.477E-003	1	1.477E-003	15.00	0.0117
X_2^2	9.231E-005	1	9.231E-005	0.94	0.3774
X_3^2	1.979E-005	1	1.979E-005	0.20	0.6727

Note: $R^2 = 0.9978$, $R^2_{adj} = 0.9938$, C.V.%= 5.57 %, Adequate Precision= 47.715

Table 5.3 and **Table 5.5** demonstrates that two variables, i.e. impeller speed (rpm) and gas flow rate (m^3/min) shows the greatest F-values and the lowest P-values, suggesting that these two

variables have strongly affected the mixing time and gas flow number. On the other hand, **Table 5.4** suggests that impeller speed affected the specific power consumption significantly.

Table 5.3 and **Table 5.5** also demonstrates that among the variables interactions, i.e. X_1X_2, X_1X_3, and X_2X_3, the interaction effect of the X_1X_3 (impeller speed and gas flow rate) exhibited a significant effect on both mixing time and gas flow number while the interaction effect of X_1X_2 (impeller speed and impeller type) and X_2X_3 (impeller type and gas flow rate) did not show any significant effects on the mixing time as well as gas flow number. In addition, all the quadratic functions (X_1^2, X_2^2, and X_3^2) has significant effects on the mixing time and gas flow number. ANOVA results also enabled us to examine the interaction among variables affecting the response function of specific power consumption presented in **Table 5.4**. Although due to the Prob>F value (higher than 0.1), the interaction effects of such variables of (X_1X_2), (X_1X_3), and (X_2X_3) are not significant on the specific power consumption. It is worth mentioning that among all quadratic functions, the impeller speed (X_1^2) is the only quadratic function which has a significant effect on specific power consumption.

On the basis of statistical design of the following study, interactional plots were obtained for all the responses which illustrates the contribution of each factor to the respective response variables. From the above mentioned ANOVA results it can be analyzed that the mixing time and gas flow number displays somehow similar characteristics in terms of effected by independent variables.

Although, **Figure 5.1** and **Figure 5.2** shows the interaction plots among three factors for the mixing time and gas flow number respectively. These figures represent if one variable was reliant on the other variable. The following plots depict that the interaction effects on the mixing time and gas flow number between impeller speed and impeller type (X_1X_2), impeller type and gas flow rate (X_2X_3) were not significant as mentioned earlier. The parallel graphs presented in **Figures 5.1 and 5.2(a)** and **Figures 5.1 and 5.2(c)** signify that these variables are self-reliant and considered insignificant in the mixing time and gas flow number model (**Equations (5.2) and (5.4)**). However, the interaction effect between impeller speed and gas flow rate (X_1X_3) is significant as the plots were tending to cross for both responses.

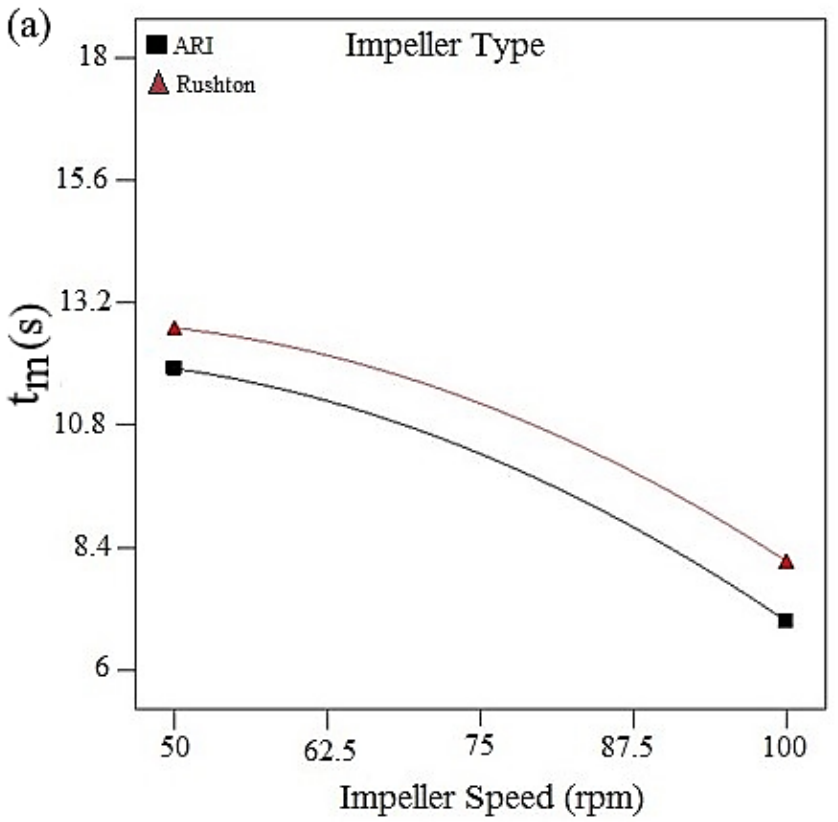
(a)
ARI
Rushton
Impeller Type
18
15.6
13.2
10.8
8.4
6
t_m (s)
50
62.5
75
87.5
100
Impeller Speed (rpm)

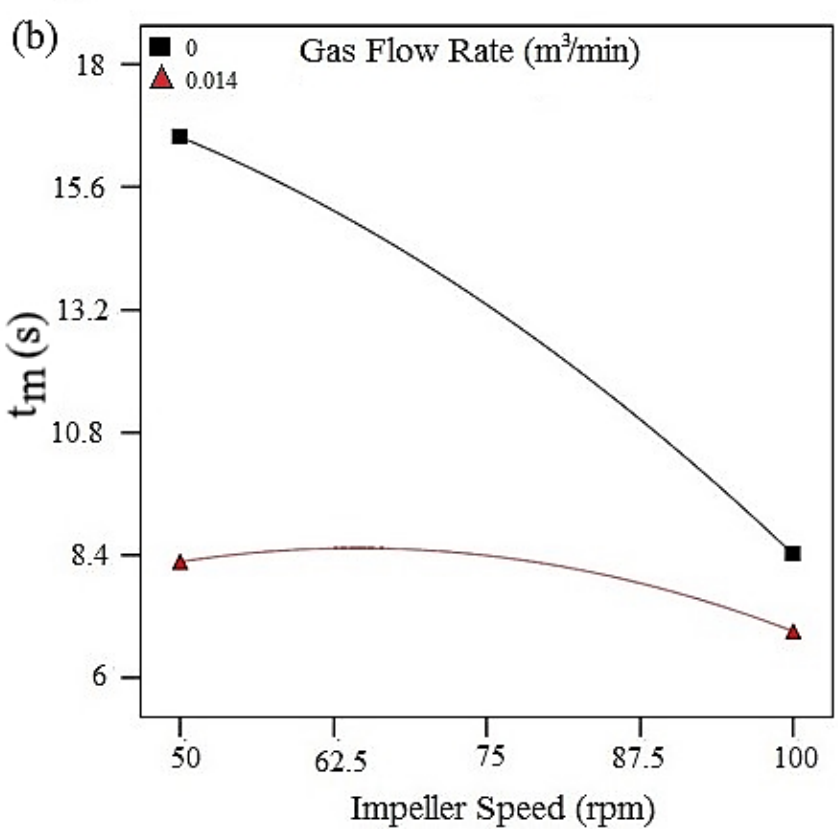
(b)
0
0.014
Gas Flow Rate (m^3/min)
18
15.6
13.2
10.8
8.4
6
t_m (s)
50
62.5
75
87.5
100
Impeller Speed (rpm)

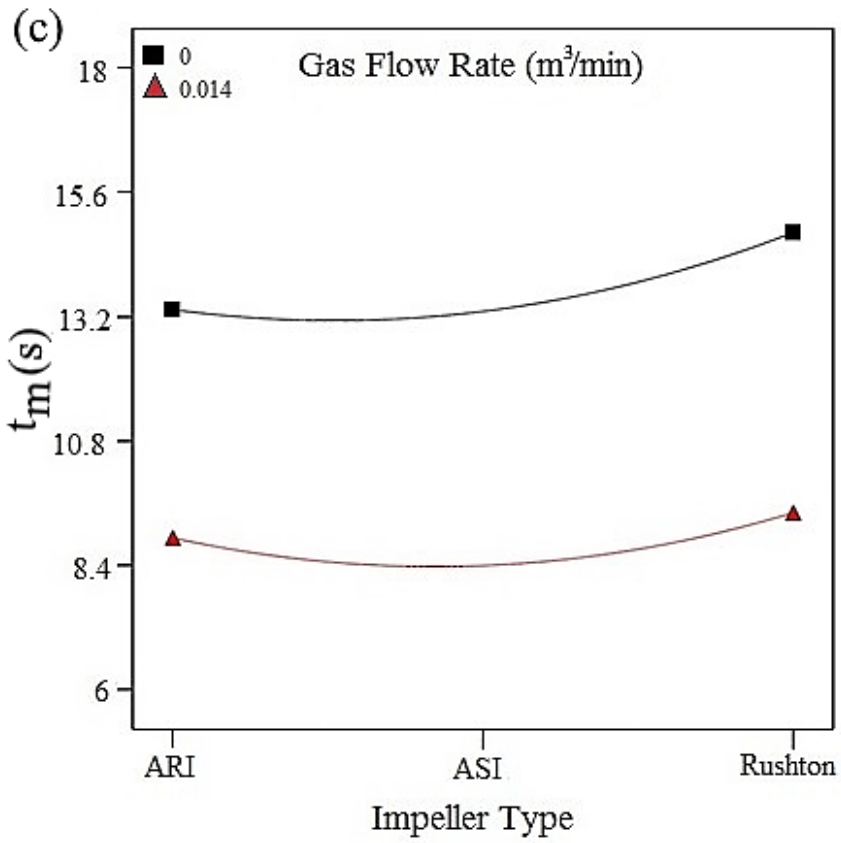

Figure 5.1. Interaction plots for mixing time (s): **(a)** impeller speed and impeller type (X_1X_2), **(b)** impeller speed and gas flow rate (X_1X_3), and **(c)** impeller type and gas flow rate (X_2X_3).

The interaction effects of three independent variables on the power consumption (**Figure 5.3 (a)**) shows the parallel plots for impeller speed and impeller type (X_1X_2) which confirms that the above mentioned variables are not reliant on each other. Although, the plots of the interaction effect on the specific power consumption between impeller speed and gas flow rate (X_1X_3), and between impeller type and gas flow rate (X_2X_3) were slightly crossed, **(Figure 5.1 (b)** and **(c))** the Fisher's F test suggested that the value of Prob>F was higher than 0.1 as shown in **Table 5.4**. Therefore, these two interactions have no significant effect on the specific power consumption.

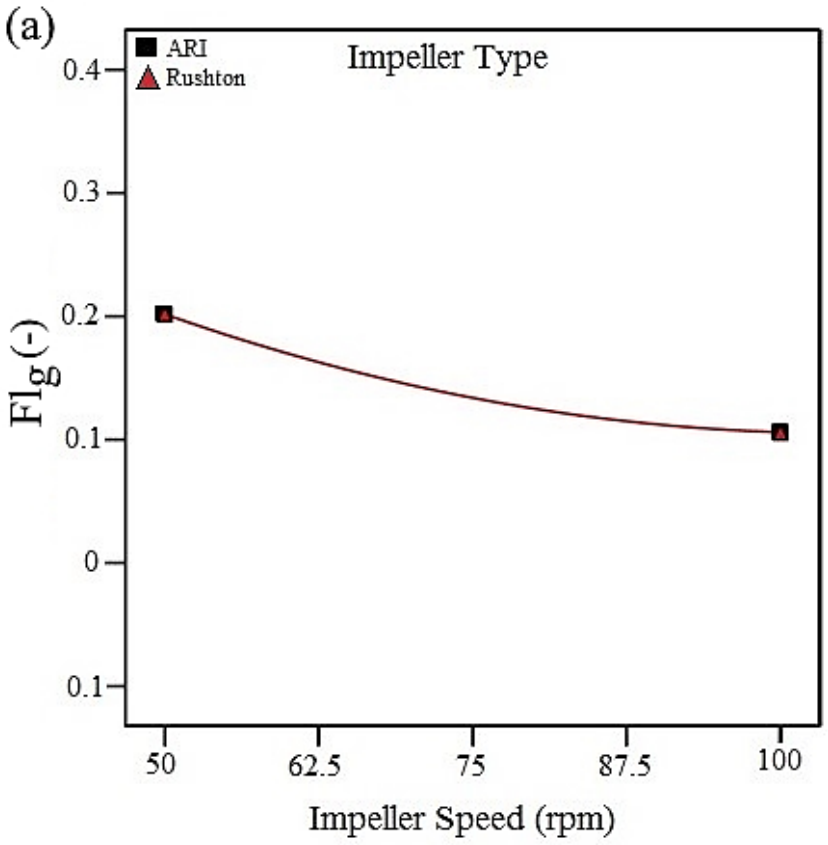
(a)
ARI
Rushton
Impeller Type
0.4
0.3
0.2
0.1
0
0.1
Fl_g(-)
50
62.5
75
87.5
100
Impeller Speed (rpm)

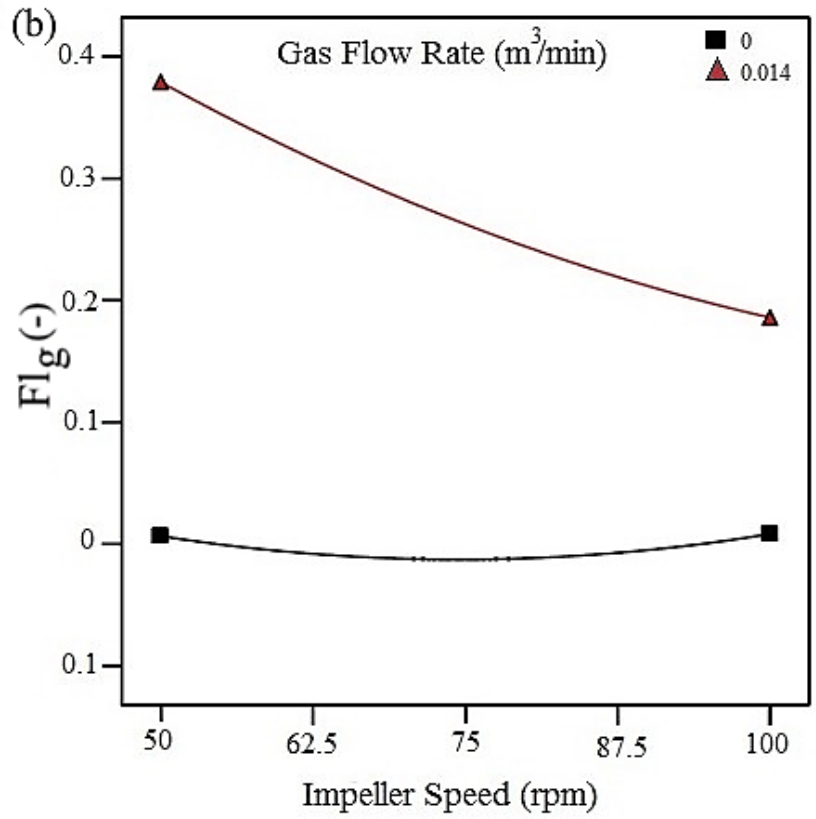
(b)
Gas Flow Rate (m^3/min)
0
0.014
0.4
0.3
0.2
0.1
0
0.1
Fl_g(-)
50
62.5
75
87.5
100
Impeller Speed (rpm)

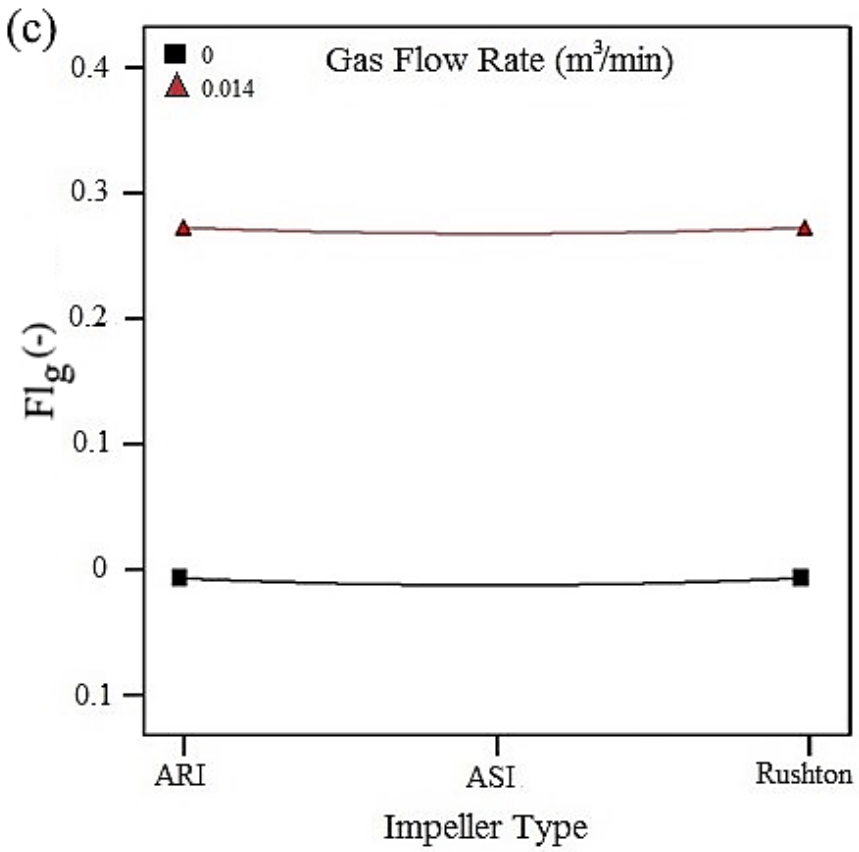

Figure 5.2. Interaction plots for gas flow number (-): **(a)** impeller speed and impeller type (X_1X_2), **(b)** impeller speed and gas flow rate (X_1X_3), and **(c)** impeller type and gas flow rate (X_2X_3).

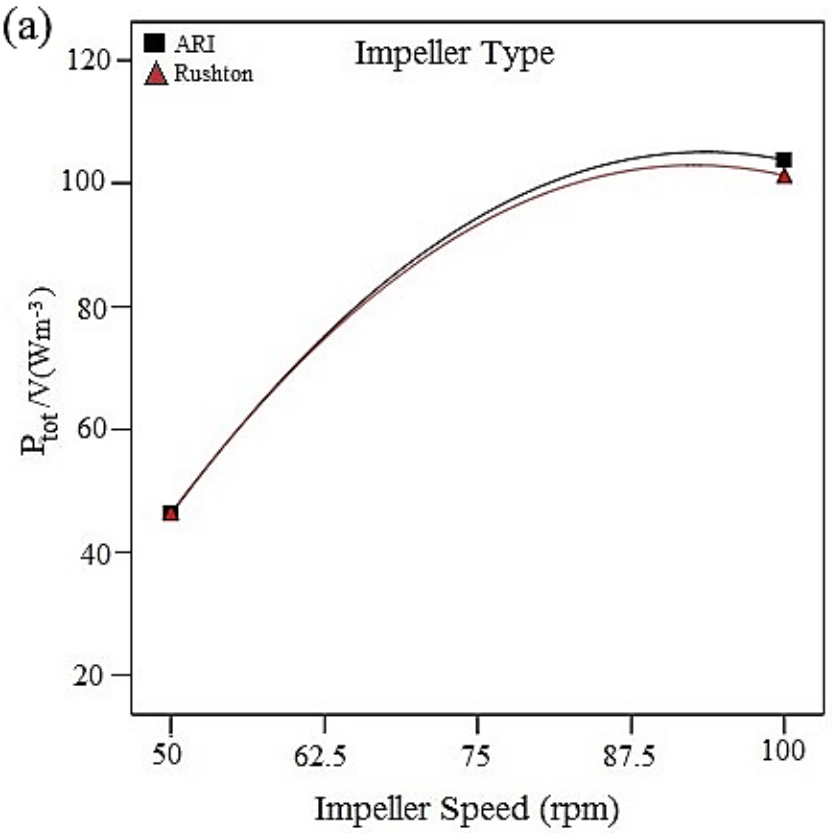
(a)
ARI
Rushton
Impeller Type
120
100
80
60
40
20
$P_{tot}/V(Wm^{-3})$
50
62.5
75
87.5
100
Impeller Speed (rpm)

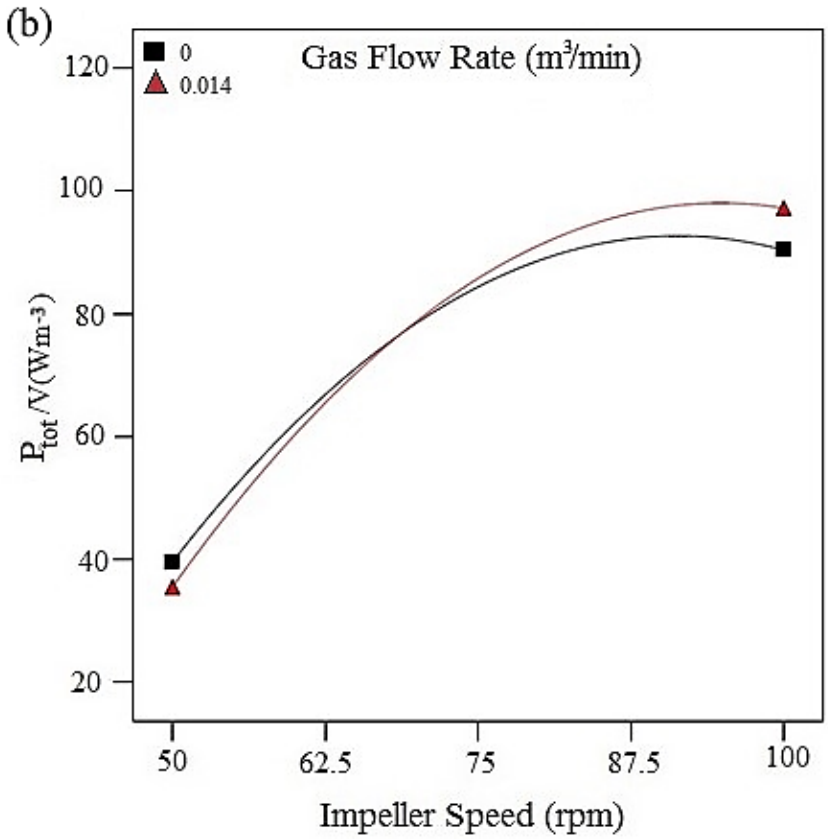
(b)
0
0.014
Gas Flow Rate (m^3/min)
120
100
80
60
40
20
$P_{tot}/V(Wm^{-3})$
50
62.5
75
87.5
100
Impeller Speed (rpm)

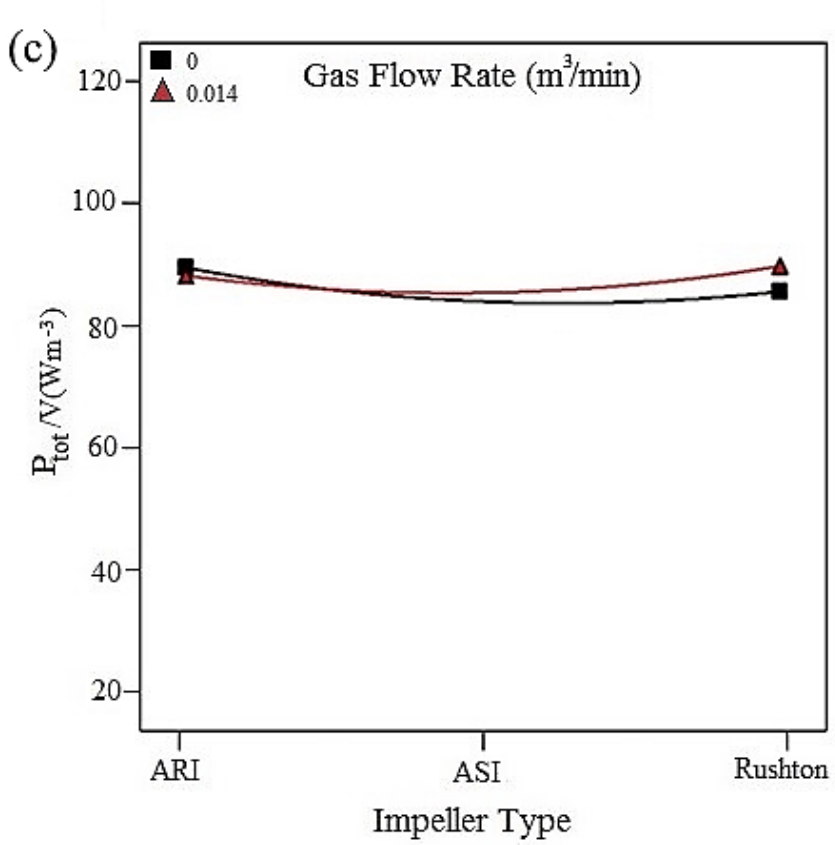

Figure 5.3. Interaction plots for specific power consumption (Wm^{-3}): **(a)** impeller speed and impeller type (X_1X_2), **(b)** impeller speed and gas flow rate (X_1X_3), and **(c)** impeller type and gas flow rate (X_2X_3).

5.2.3 Goodness of Fit of the Models

The goodness of fit of the quadratic functions for experimental data was determined by utilizing analysis of variance (ANOVA). The coefficient of determination ($R^2 = 0.9896$ for mixing time, 0.9536 for specific power consumption and 0.9978 for gas flow number) confirmed that the goodness of fit of the models. Therefore, these results depict that only 1.04%, 4.64%, 0.22% of the variability for mixing time, specific power consumption and gas flow number were not explained by the RSM equations (**Equations (5.2), (5.3),** and **(5.4))**, respectively.

Figure 5.4 shows that the predicted output values measured using **Equation (5.2), (5.3),** and **(5.4)** for mixing time, specific power consumption and gas flow number were in good agreement with the experimental data for the ranges listed in **Table 5.1** for the independent variables.

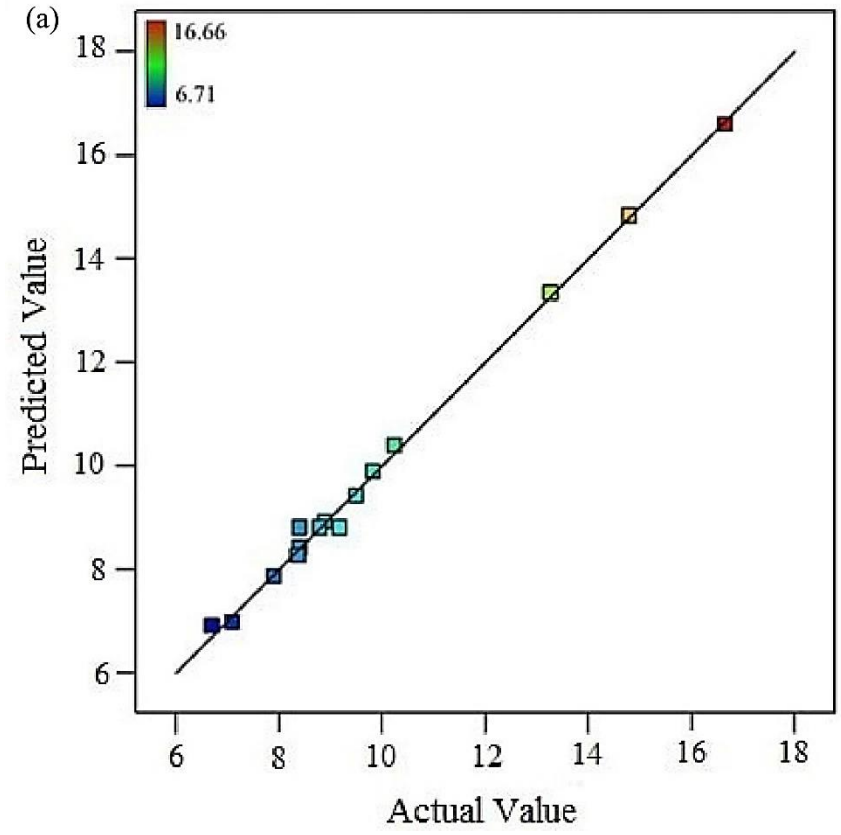
(a)
16.66
6.71
Predicted Value
Actual Value
6
8
10
12
14
16
18

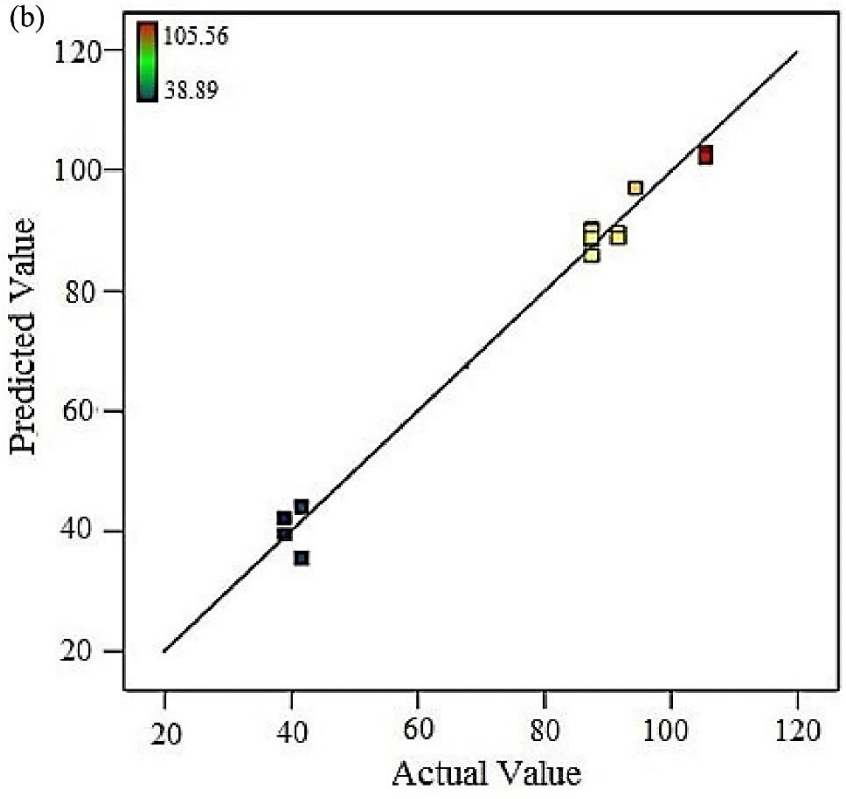
(b)
105.56
38.89
Predicted Value
Actual Value
20
40
60
80
100
120

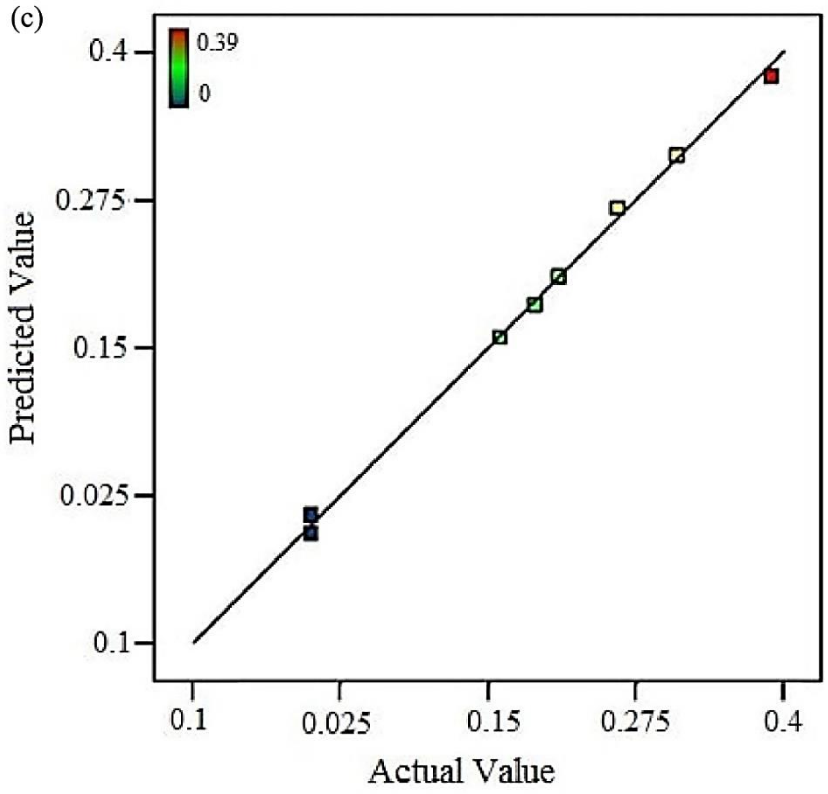

Figure 5.4. Predicted values versus the computed data for: **(a)** mixing time (s), **(b)** specific power consumption (Wm^{-3}), and **(c)** gas flow number (-).

Figure 5.5 demonstrates the normal probability of the residuals which examines if the errors are normally distributed and if the error variance shows homogeneity. The normal probability plots of residuals validate the normal conclusions. In addition, these evaluations proves that RSM equation for all responses (Y_1 , Y_2, Y_3) for the given ranges of independent variables provides good evaluation as well as confirms the normality assumptions.

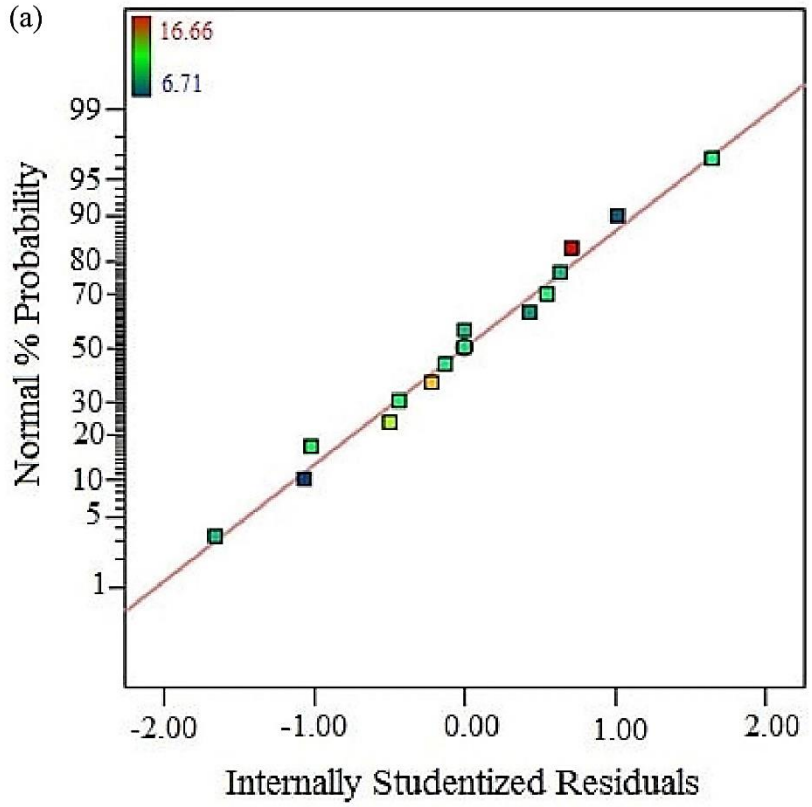
(a)
16.66
6.71
Normal % Probability
99
95
90
80
70
50
30
20
10
5
1
-2.00
-1.00
0.00
1.00
2.00
Internally Studentized Residuals

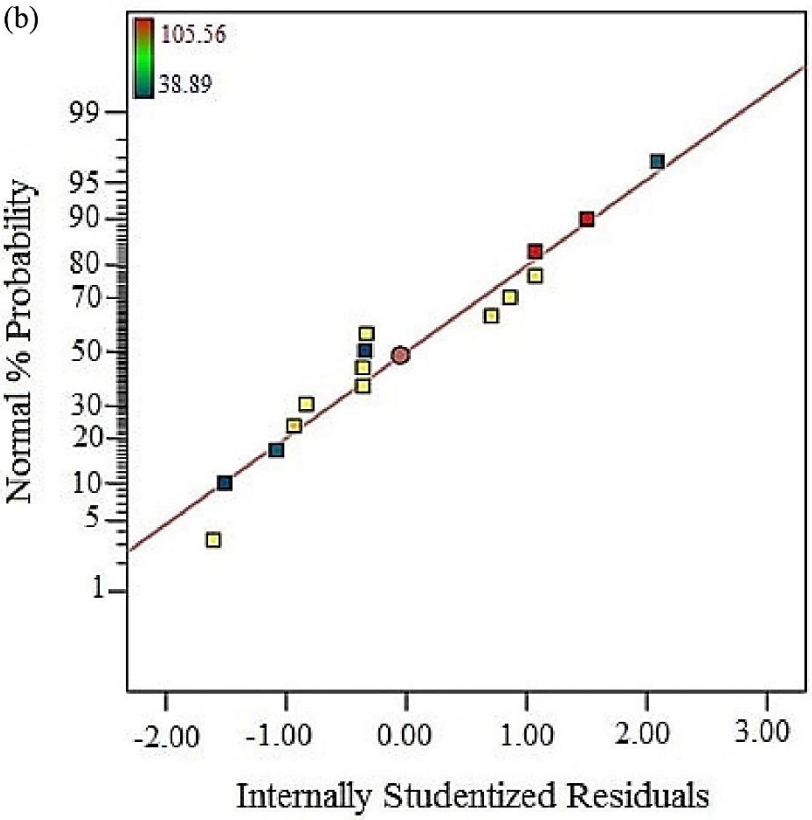
(b)
105.56
38.89
Normal % Probability
99
95
90
80
70
50
30
20
10
5
1
-2.00
-1.00
0.00
1.00
2.00
3.00
Internally Studentized Residuals

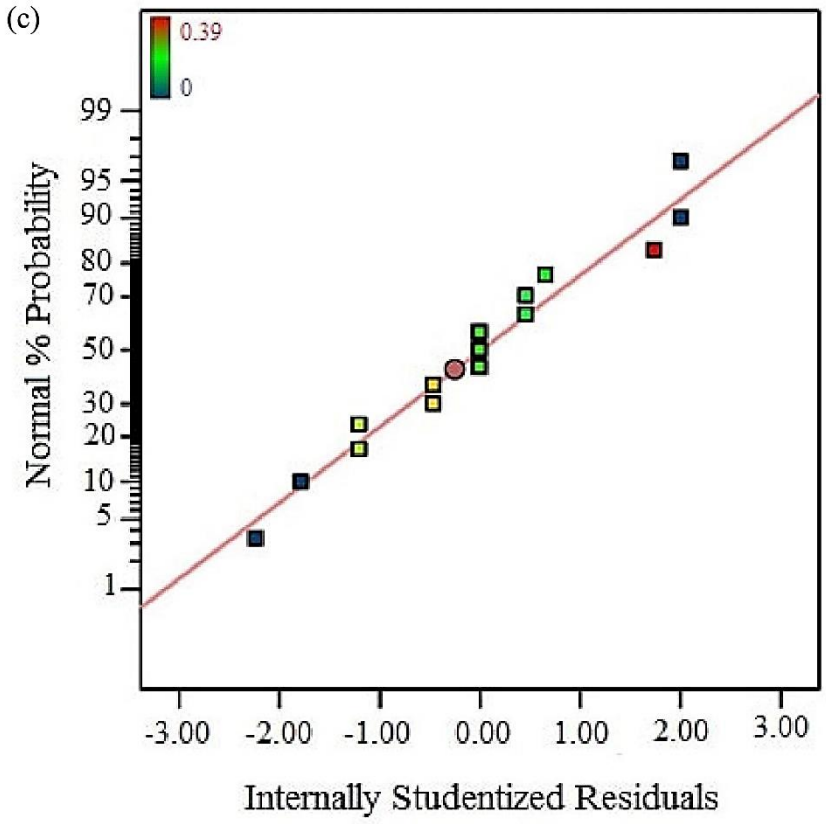

Figure 5.5. Normal probability plot of internally studentized residuals for: **(a)** mixing time (s), **(b)** specific power consumption (Wm^{-3}), and **(c)** gas flow rate (-).

5.2.4 Analysis of Three-Dimensional Response Surface Plots

5.2.4.1 Mixing Time

In order to determine the effect of independent variables on quadratic responses, three-dimensional response surface graphs were plotted as a function of two variables at a time while other variables are kept constant. The results of the experimental design for the effect of independent variables ($X_1, X_2, and\ X_3$) on mixing time, specific power consumption and gas flow number by using quadratic equations **(Equations 5.2, 5.3,** and **5.4)** were visualized in three-dimensional response surface plots.

Figure 5.6(a) depicts the response surface of effect of impeller speed and type. It was observed that at lower impeller speed, the interaction of both variables was not significant. It means that impeller type has higher effect on mixing time at the higher impeller speed. As illustrated in

Figure 5.6(b) the mixing time was significantly influenced by impeller speed and the amount of air sparged into the vessel. It was observed that with high aeration (0.014 m^3/min) and high impeller speed (100 rpm) the mixing time reduced significantly. Also, it can be depicted by ANOVA results in **Table 5.3** that the interaction of these two variables was the most significant to the mixing time model in comparison with other interactions.

Figure 5.6 presents that mixing time was affected mostly by both impeller speed and gas flow rate. As can be seen in **Figure 5.6(a)-(c)** mixing time reduced at higher impeller speed and high degree of gas flow levels. Nonetheless, mixing time does not influenced by impeller types. It may because that all impellers selected in this study were radial (Rushton turbine) or axial-radial impeller (ARI and ASI). Therefore, same impeller flow pattern was expected. However, ASI shows slightly better performance in terms of mixing time. **Table 5.4** also confirms the above mentioned statement.

Figure 5.6(c) shows the response surface for impeller type and gas flow rate on the mixing time. As mentioned earlier the amount of aeration has significant effect on the mixing time while impeller type has the least impact. In fact **Figure 5.6(a)** and **(c)** shows that mixing time were slightly influenced by different types of impeller although the changes were not substantial. It is known that impeller is responsible for the flow pattern generated within the tank by which the efficiency of mixing system can be affected (Chhabra & Richardson, 2008).

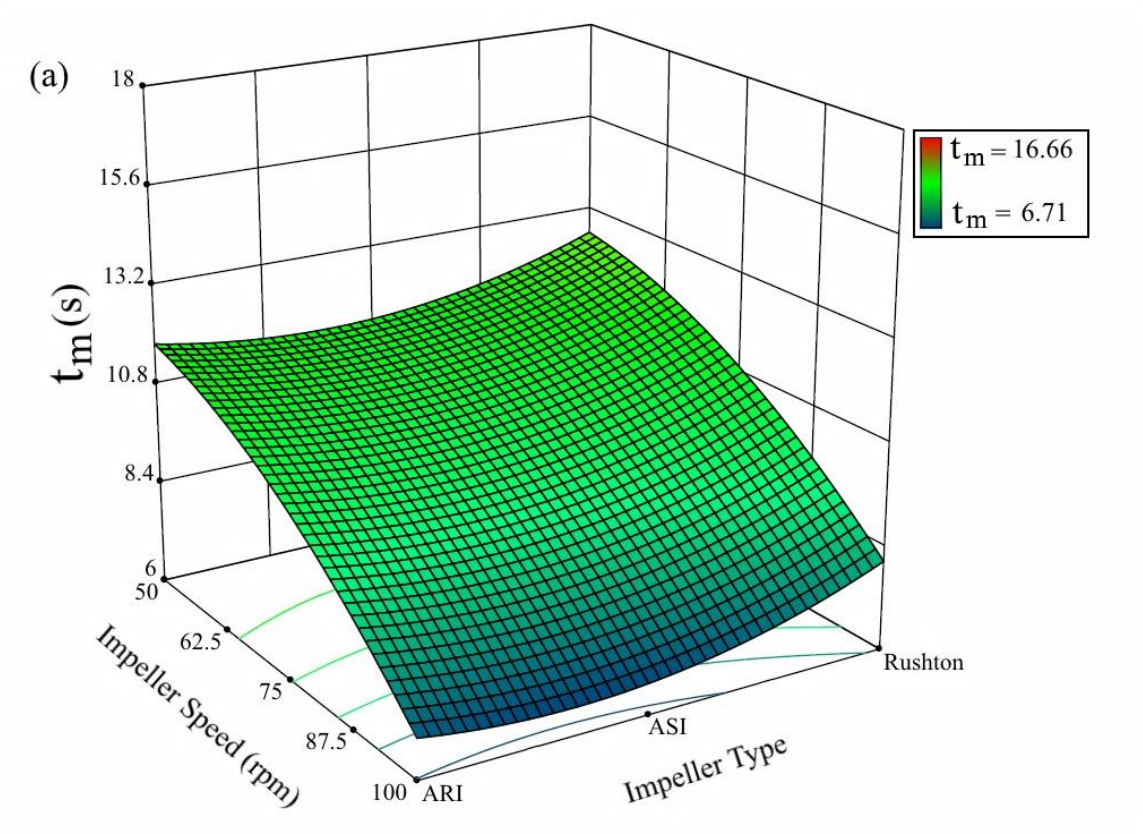
(a)
18
15.6
13.2
10.8
8.4
6
t_m (s)
t_m = 16.66
t_m = 6.71
50
62.5
75
87.5
100
Impeller Speed (rpm)
ARI
ASI
Rushton
Impeller Type

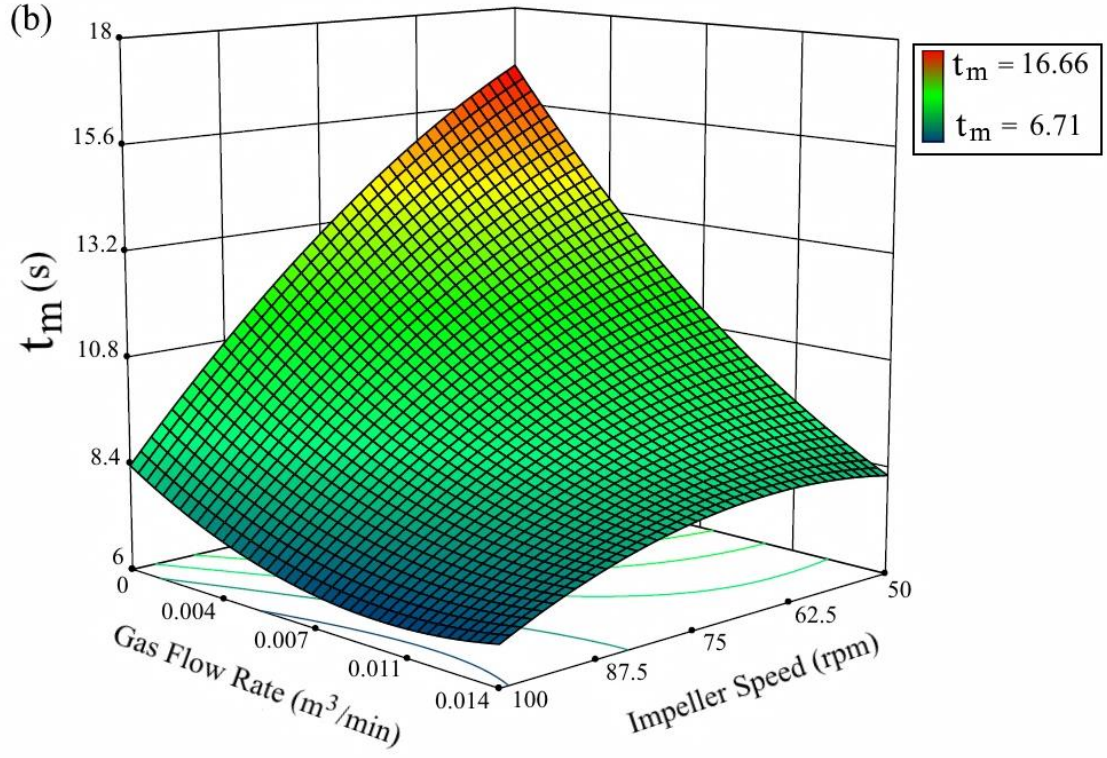
(b)
18
15.6
13.2
10.8
8.4
6
t_m (s)
t_m = 16.66
t_m = 6.71
0
0.004
0.007
0.011
0.014
Gas Flow Rate (m^3/min)
100
87.5
75
62.5
50
Impeller Speed (rpm)

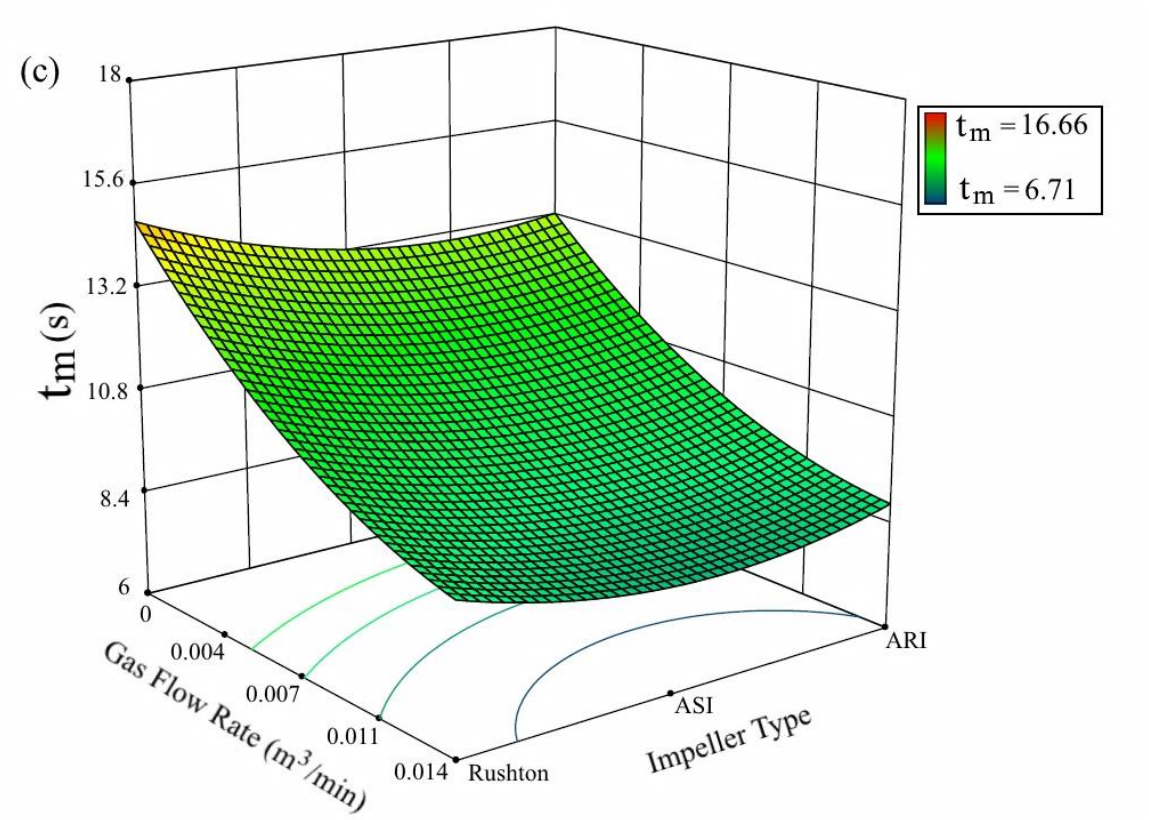

Figure 5.6. Response surface methodology showing mixing time as a function of two independent variables: **(a)** impeller speed and impeller type (X_1X_2), **(b)** impeller speed and gas flow rate (X_1X_3), and **(c)** impeller type and gas flow rate (X_2X_3).

5.2.4.2 Specific Power Consumption

The effect of all three factors and their interaction on specific power consumption have been illustrated in **Figure 5.7**. In **Figure 5.7(a)** and **(b)** it can be easily demonstrated that specific power consumption was increased with the increase in impeller speed as expected. Generally, more power was required for high degree of mixing. Therefore, impeller type and aeration were not significant and does not influence the specific power consumption respectively **(Figure 5.7(c))**. Power consumption of the impeller is an important parameter in order to select and design the drive unit as well as characterizing the transport phenomena within the vessel (Yoshida et al., 2002). Usually, the reduction in power consumption depends on the impeller type and combination of impellers utilized (Karimi et al., 2015, Albaek et al., 2008).

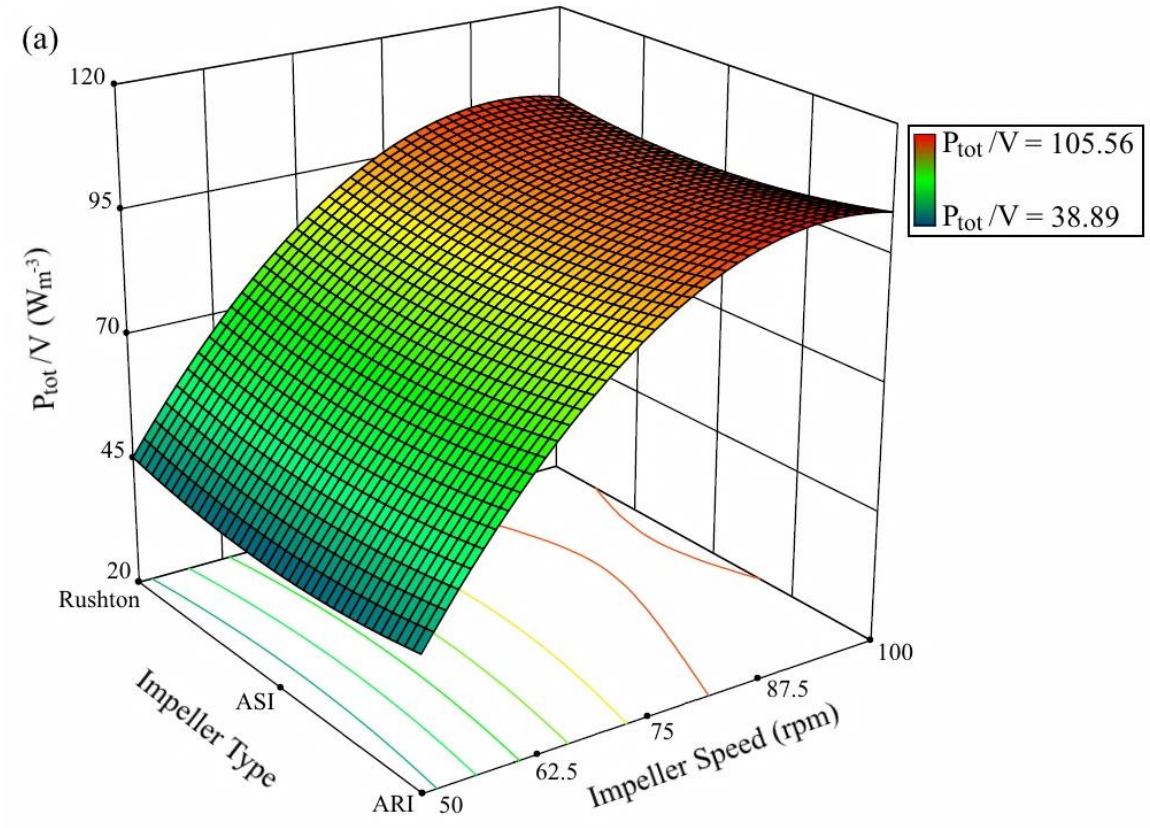
(a)
120
95
70
45
20
P_{tot} /V (W_m^{-3})
P_{tot} /V = 105.56
P_{tot} /V = 38.89
Rushton
ASI
ARI
Impeller Type
50
62.5
75
87.5
100
Impeller Speed (rpm)

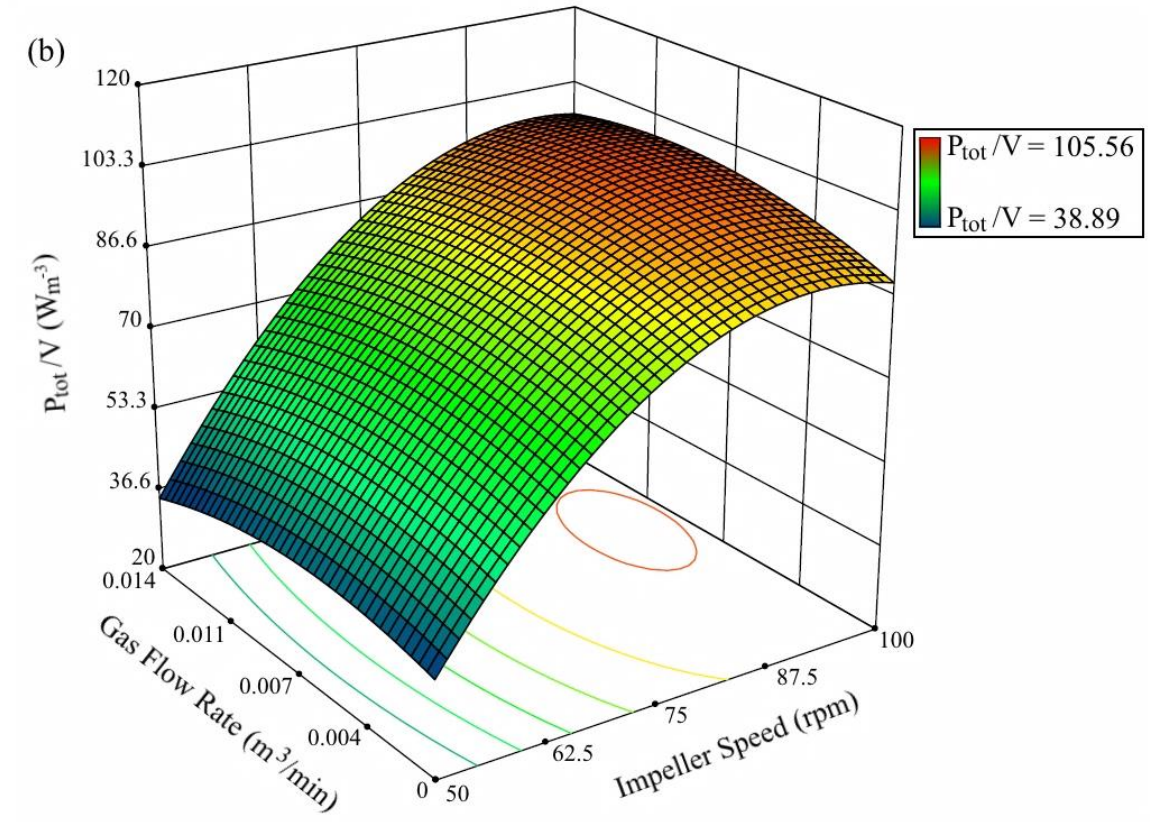
(b)
120
103.3
86.6
70
53.3
36.6
20
P_{tot} /V (W_m^{-3})
P_{tot} /V = 105.56
P_{tot} /V = 38.89
0.014
0.011
0.007
0.004
0
Gas Flow Rate (m^3/min)
50
62.5
75
87.5
100
Impeller Speed (rpm)

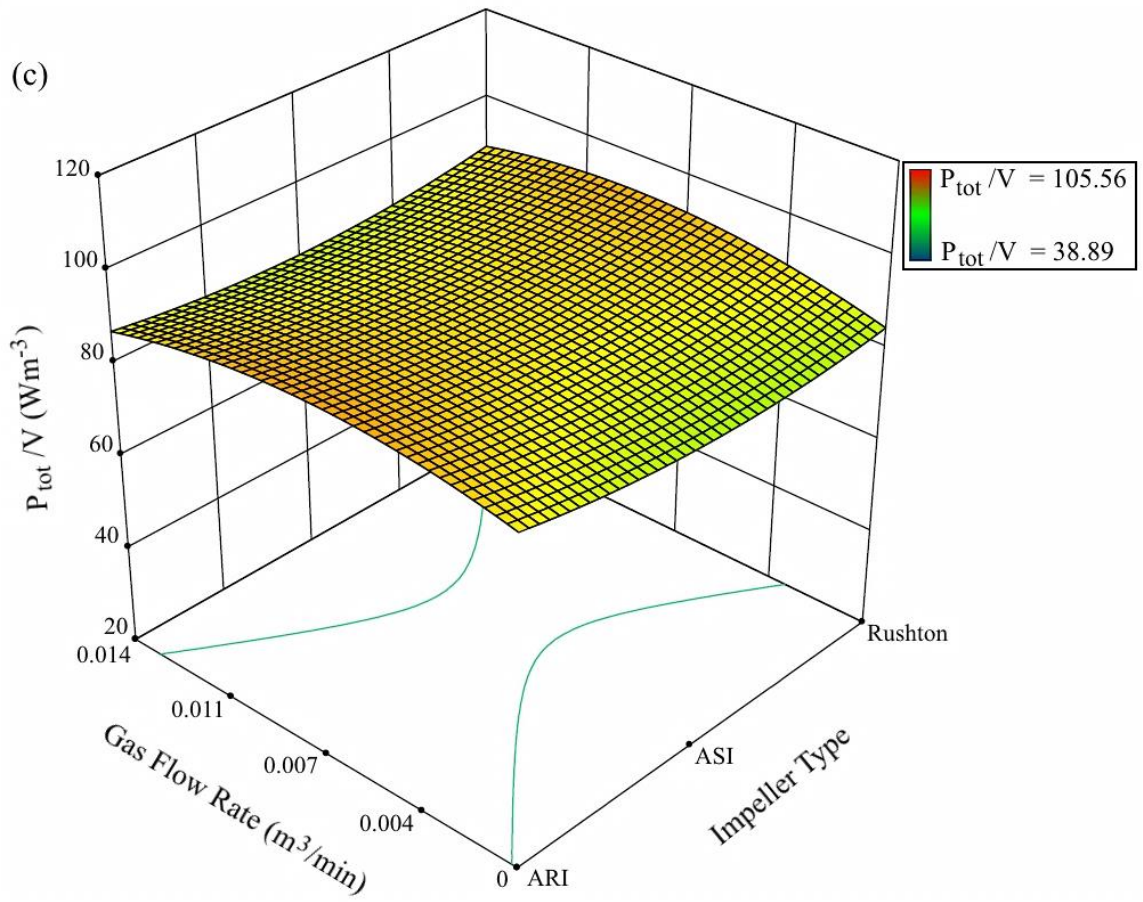

Figure 5.7. Response surface methodology showing specific power consumption as a function of two independent variables: **(a)** impeller speed and impeller type (X_1X_2), **(b)** impeller speed and gas flow rate (X_1X_3), and **(c)** impeller type and gas flow rate (X_2X_3).

5.2.4.3 Gas Flow Number

As it can be depicted that results of mixing time and gas flow number are identical to each other and somewhat shows the same characteristics features in regards to impact of independent and interactional variables. It can be easily seen that among all the independent variables, gas flow number also effected by the impeller speed and gas flow rate only.

With the help of 3D response surface **(Figure 5.8 (b))** it can be depicted that gas flow number is a function of gas flow rate as gas flow number increases with the increase in gas flow rate whereas high impeller speed decreases the gas flow number significantly. This fact is in a good agreement of previous studies (Ali, 2014) which demonstrates that with high impeller speed the gas dispersed throughout the mixing vessel and gives the less gas flow number. However, like as mixing time, gas flow number was also effected by impeller type very slightly and does not show much effect. Although, **Figure 5.8 (a)** and **(c)** signifies that gas flow number also does not impacted by impeller type.

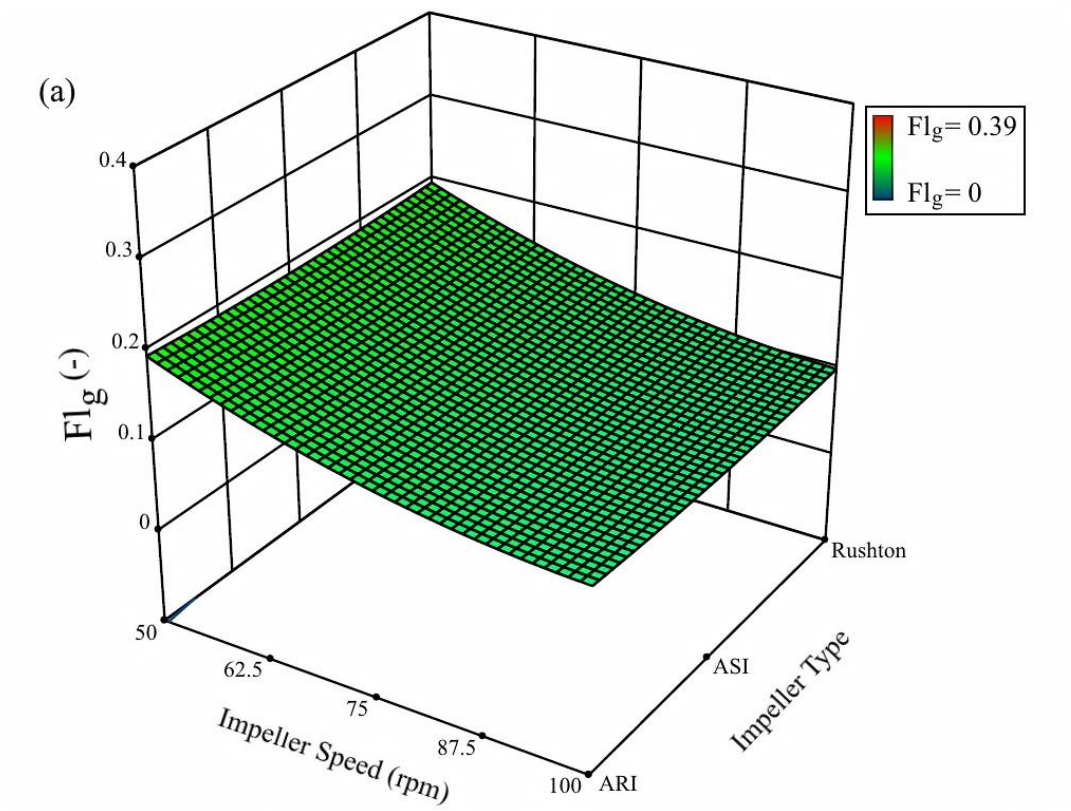
(a)
Flg= 0.39
Flg= 0
Flg (-)
0.4
0.3
0.2
0.1
0
50
62.5
75
87.5
100
Impeller Speed (rpm)
ARI
ASI
Rushton
Impeller Type

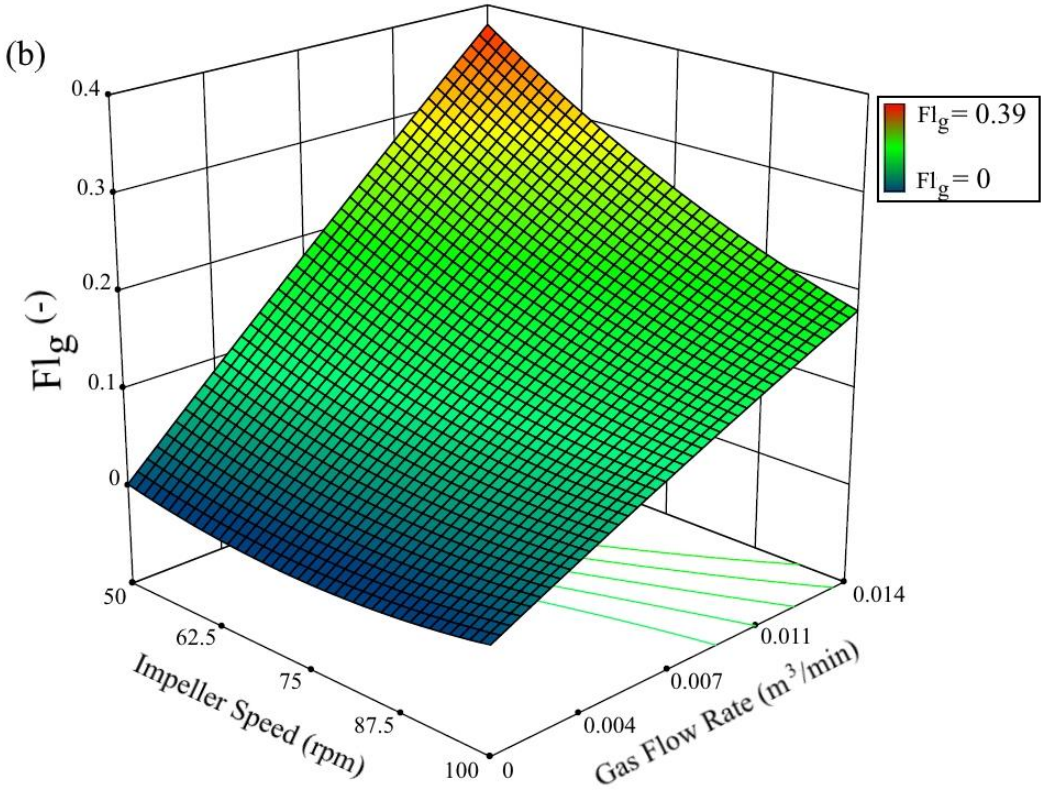
(b)
Flg= 0.39
Flg= 0
Flg (-)
0.4
0.3
0.2
0.1
0
50
62.5
75
87.5
100
Impeller Speed (rpm)
0
0.004
0.007
0.011
0.014
Gas Flow Rate (m3/min)

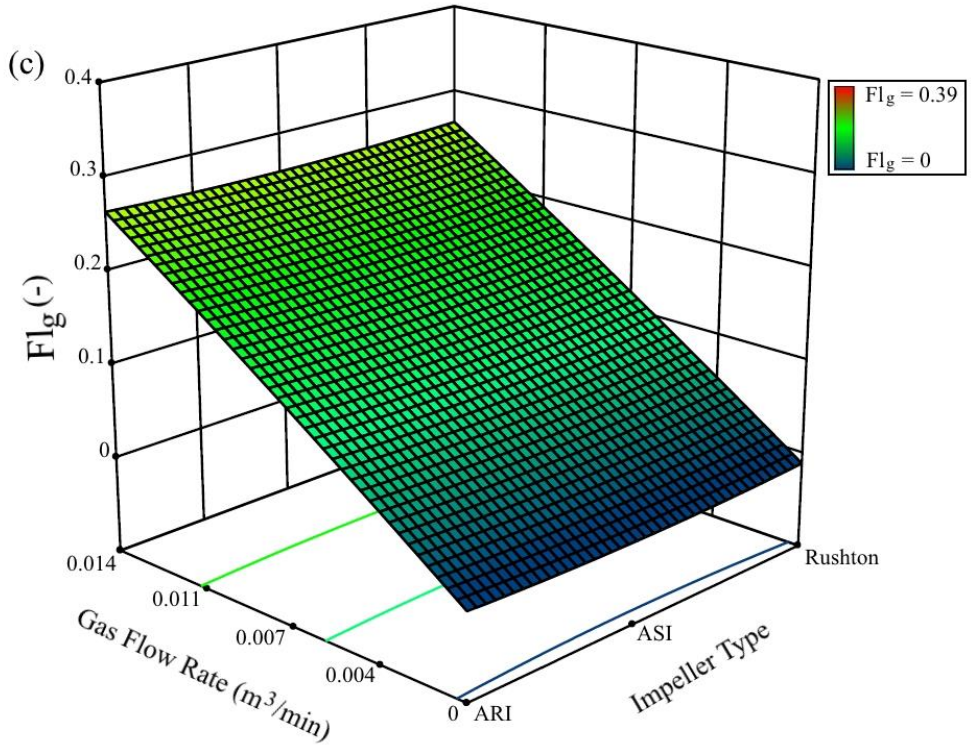

Figure 5.8. Response surface methodology showing gas flow number as a function of two independent variables: **(a)** impeller speed and impeller type (X_1X_2), **(b)** impeller speed and gas flow rate (X_1X_3), and **(c)** impeller type and gas flow rate (X_2X_3).

5.3 Numerical Process Optimization

To determine the optimum condition in the current study all the responses (mixing time, specific power consumption, and gas flow number) as a Y function in **Equations (5.2), (5.3), (5.4)** were minimized first which were presented as a desirability function by the Design-Expert 10 software to evaluate the minimum response values. However, the process optimization suggested the following ideal amount to attain the minimum mixing time and specific power consumption: the ASI impeller, at impeller speed (N) = 50 rpm, with 0.014 m^3/min gas flow rate and gas flow number as 0.379. Under such ideal conditions, the best local minimum values are as follows: 8.25 sec for the mixing time and 35.5 Wm^{-3} for specific power consumption and 0.38 for gas flow number. Then the aforementioned optimum conditions were applied through an experiment and following responses were determined as 8.38 ± 0.06 sec and 41.67 ± 0.20 Wm^{-3} (mean ± SD of three replicates) for mixing time and specific power consumption, respectively. The corresponding flow number to the gas flow rate was 0.38. All responses were in good agreement with the optimized values. **Figure 5.9** shows the optimization results for the mixing time.

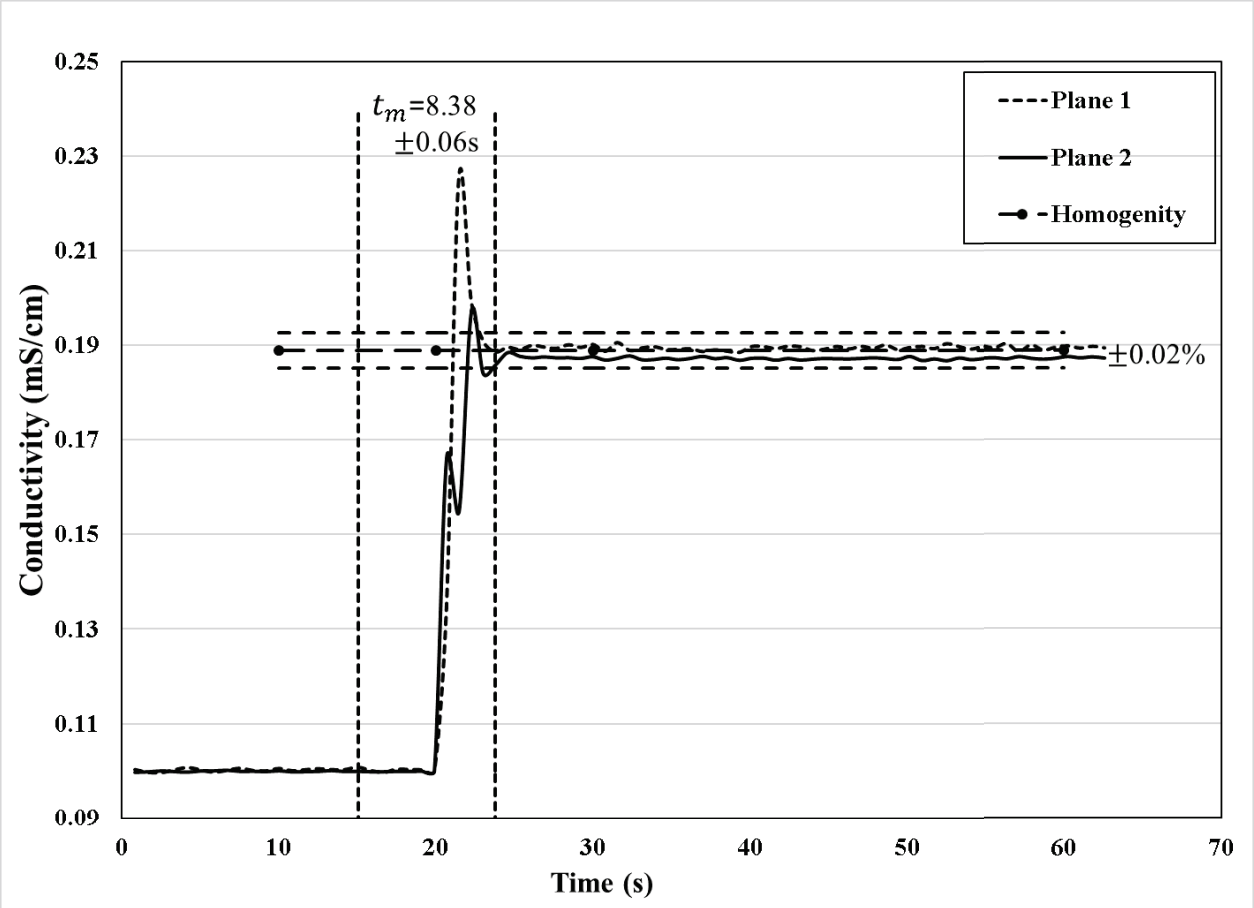

Figure 5.9. Mean conductivity measured using ERT as a function of time for activated sludge agitated by ASI at N= 50 rpm with 0.014 m^3/min gas flow rate.

5.4 Analysis of Flow Patterns and Homogenization inside Mixing Tank with the help of Electrical Resistance Tomography (ERT)

5.4.1 Introduction

The ability of ERT in performing local and global measurements in a non-intrusive manner made it possible to examine the effect of radial and axial-radial impellers on flow patterns and homogenization of non-Newtonian fluids. ERT is an advanced and non-invasive flow visualization technique which is applicable to opaque fluid and has the ability to perform on-line measurements which shows the effect of aeration within the mixing tank. Therefore, in this study ERT collected some relevant results which demonstrates the impact of impeller speed, impeller type and performance of impeller in presence or absence of aeration on hydrodynamics of activated sludge.

The homogenization characteristics of a mixing tank effected by several parameters such as impeller geometry, impeller rotational speed, fluid viscosity (Paul et al., 2004). In this experimental study three impellers were employed at different speeds with different gas flow rate or without gas flow rate. The flow patterns created by the impellers and aeration inside the mixing tank were studied with the help of conductivity plots, two-dimensional tomograms and three-dimensional stacked images obtained by electrical resistance tomography. For the first time, the formation and destruction of cavern inside the mixing tank filled with activated sludge and agitated by ASI was assessed at different conditions which provides very stimulating results. By employing ERT, the performance of aeration on destruction of cavern was also assessed which gives a strong consideration that mixing of non-Newtonian fluids is possible without agitators which can reduce the power consumption at industrial levels.

5.4.2 Effect of Radial Impeller Flow Pattern versus Axial/Radial Flow Pattern on Homogenization

ERT is an advanced flow visualization technique with the ability of collecting high speed data in both transparent and opaque fluids (Babaei et al., 2015(b)) and in this study it assessed the performance of three different type of impellers. **Figure 5.10** illustrates the corresponding tomograms obtained by employing two different impellers: **(i)** Rushton impeller (at N = 75 rpm, no air) and **(ii)** ASI (at N =75 rpm, no air). As Rushton is a fully radial impeller and ASI is a

combination of A200 impeller (axial) and Scaba impeller (radial) which has axial/radial geometry. The corresponding 2D tomograms are shown in **Figure 5.10** which shows the flow pattern of the above mentioned impellers and homogenization characteristics in agitation of activated sludge. As shown in the scale bar **(Figure 5.10)** the blue color shows the lower conductivity while high conductivity shown by the red color in the corresponding tomograms of ERT plane 1 and plane 2. To analyze the flow patterns and homogenization throughout the mixing tank 10ml of 30% brine was injected on plane 1. As can be seen after brine injection, the tracer (red zone) was observed immediately on plane 1 in both conditions (Rushton and ASI at 75 rpm) while the tracer on plane 1 enlarged at the same time in case of ASI. After 4.5 sec it could be easily demonstrated that the tracer was being swept in a clockwise direction on plane 1 and partially on plane 2. Since Rushton impeller is a fully radial impeller which has the ability to discharge the fluid at right angles towards the tank walls. In such impellers, centrifugal force produced by the impellers which depend on the diameter and speed of impeller. Although due to such radial behavior tracer was dispersed only near the walls of plane 1 and plane 2.

On the other hand, ASI dispersed the tracer throughout the mixing tank after 4.5 sec of tracer injection. It can be easily depicted in **Figure 5.10 ((ii) (c))** which shows the complete dispersion of tracer and relatively high conductivity on both plane 1 and 2. As ASI has a axial/radial geometry which discharge the fluid perpendicular to the axis of the impeller through which it enters. At the same time, it pumps the fluid from downward to upward direction or vice versa as well as at the right angles towards the tank walls.

However, after a further 8.5 sec of injection the change in color from red to green shows the homogeneity or steady state within the mixing vessel in case of both impeller conditions **((i), (ii)).** It should be mentioned that when Rushton impeller was employed, tracer (red zone) near the wall can be seen easily on plane 1 which shows that tracer was still present near the tank wall while homogeneity takes place on plane 2. Therefore, after comparing the performance of both impellers (Rushton and ASI) with the help of 2D tomograms it is clear that ASI shows the better mixing performance in agitation of activated sludge within the mixing tank.

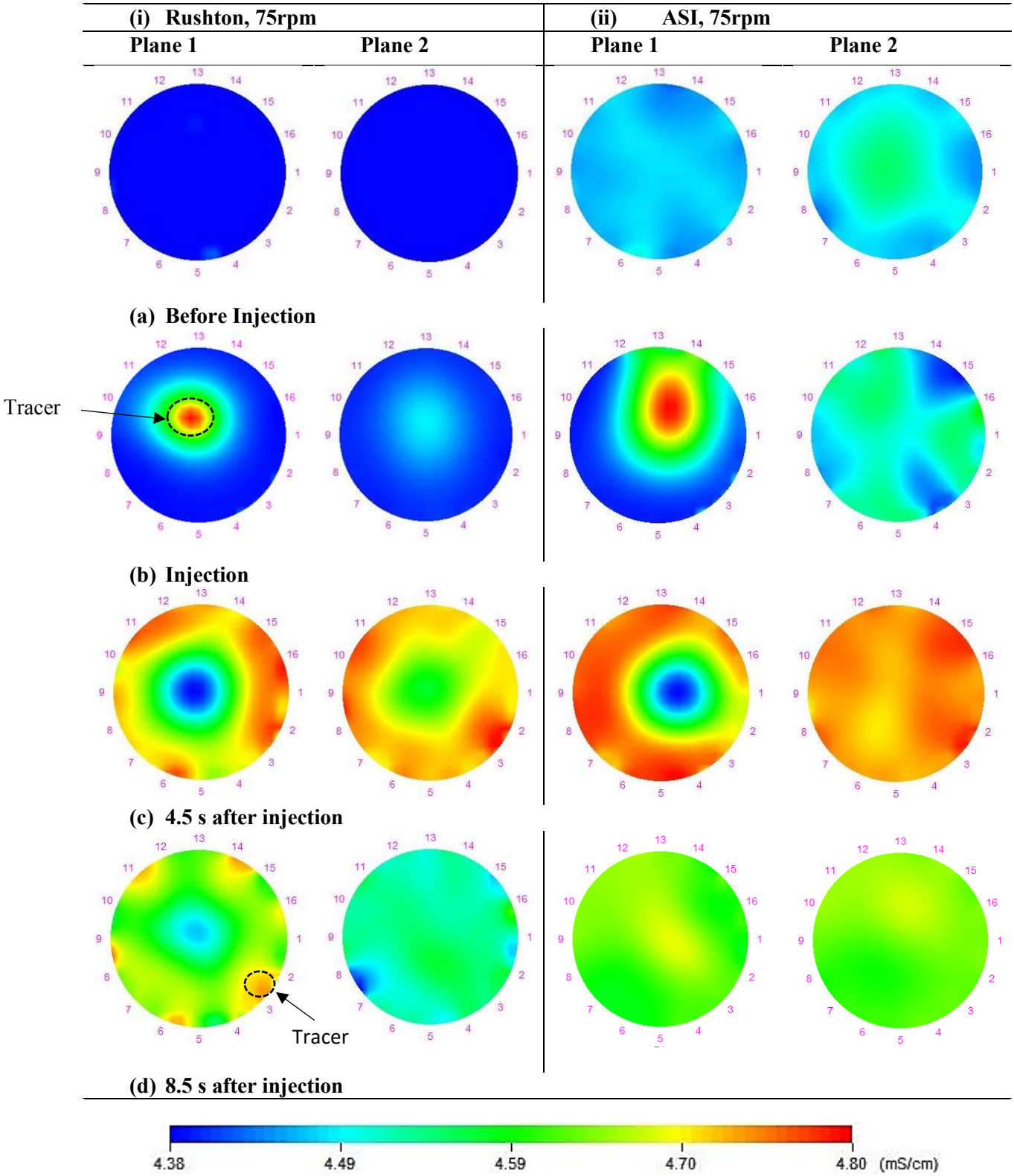

Figure 5.10. Sequence of reconstructed ERT images (based on conductivity, mS/cm) showing the dispersion of tracer: **(i)** Rushton impeller at N=75rpm, no air, and **(ii)** ASI at N=75rpm, no air.

5.4.3 Effect of Impeller Speed

To understand the impact of impeller speed **Figure 5.11** shows a comparable graph which was plotted with the help of mean conductivity of plane 1 and plane 2 versus time. By employing ERT, based on conductivity distribution within the mixing tank 2D tomograms were also obtained which can be seen on the top and bottom of corresponding ERT planes. To study the effect of impeller speed, ASI was employed firstly at 20 rpm and then 75 rpm in absence of aeration.

Figure 5.11 illustrates that to influence the mixing and hydrodynamics throughout the mixing vessel an appropriate impeller rotational speed is required. In the following test, when impeller (ASI) was rotating at 20 rpm rotational speed tracer was injected close to the impeller hub to visualize the impact of impeller rotation on mixing time very clearly. The conductivity plot of plane 2 reached at peak which shows the increment in conductivity after the injection of tracer.

It can be depicted that at 20 rpm **(Figure 5.11 (a) and (b))** the mixing inside the vessel was totally in a dead zone (as the tracer is stable after injection) which shows that there is not enough motion inside the mixing tank to circulate the tracer from one plane to another. Although by observing the conductivity plot **(Figure 5.11 (b))** it can be easily seen that both planes pretending a steady state position. On the other hand, after increasing the impeller rotational speed from 20 rpm to 75 rpm the size of tracer enlarged and dispersed within the vessel **(Figure 5.11 (c))**. However, after few seconds of increment in impeller rotational speed (from 20 rpm to 75 rpm) it was observed that both planes on conductivity plot as well as 2D tomograms (completely green color) reached 98% homogenization throughout the mixing tank. In previous studies, it was investigated that the conductivity of the fluid suddenly increases in some regions after injection of tracer and decreases significantly due to the homogeneity throughout the mixing vessel (Gumery et al., 2011, Bolton et al., 2004) which is in a good agreement of present study.

It is obvious that the rotation of impeller at high speed consumes high amount of power. As discussed earlier that aeration effects the mixing time in a positive manner. However, the high-power consumption can be controlled by utilizing aeration inside the vessel with or without combination of an impeller. Also, Issa, (2016) reported that the power consumption is relatively low in an aerated system as compare to non-aerated systems which was in agreement with the obtained results in the current work.

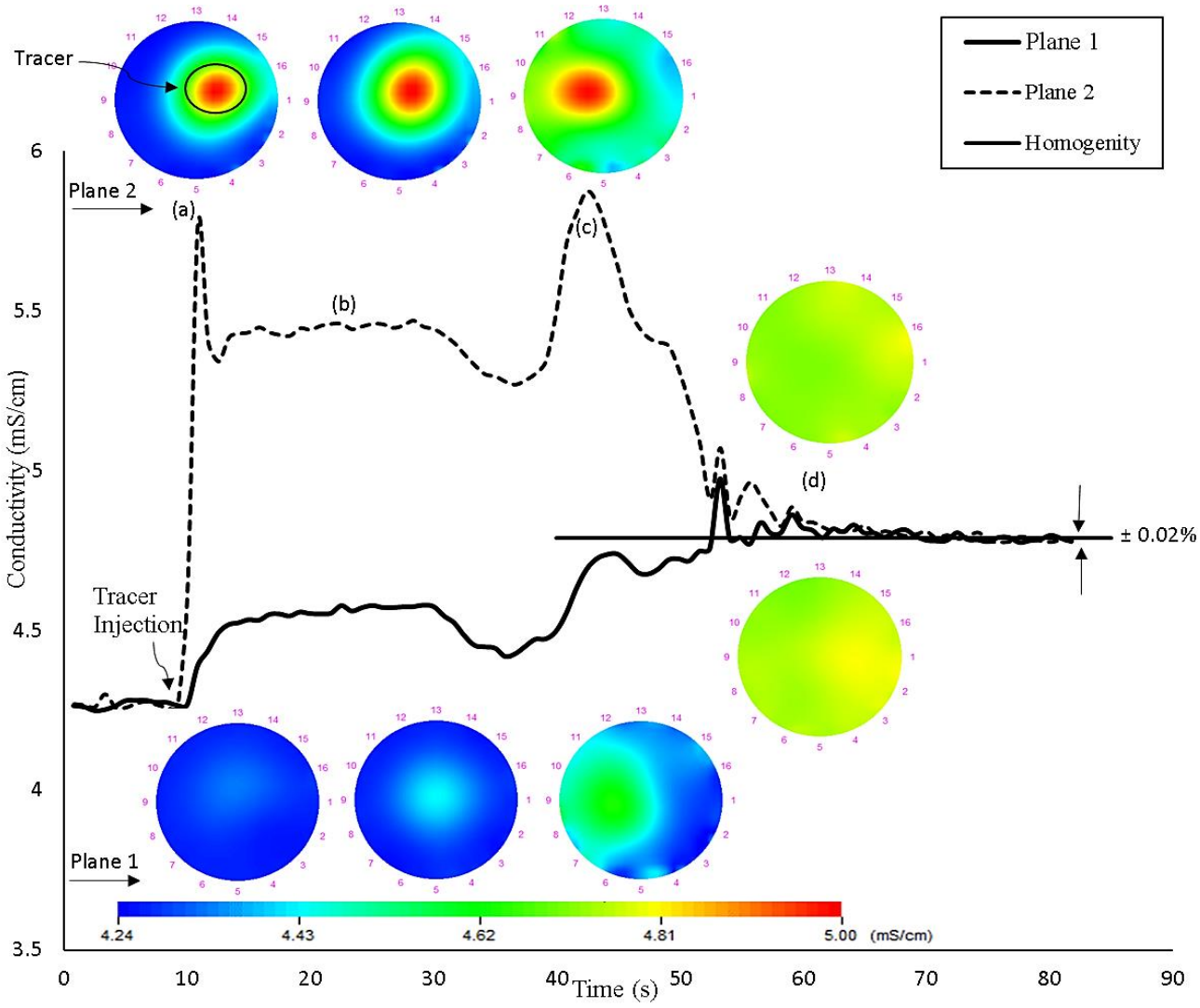

Figure 5.11. Sequence of 2D tomograms showing the effect of impeller speed on level of homogeneity within the mixing tank filled with activated sludge and agitated by ASI **(a)** & **(b)** at N=20rpm and **(c)** & **(d)** at N= 75rpm.

5.4.4 Effect of Gas Flow Rate

In comparing two experimental studies **(Figure 5.12 (i)** and **(ii))** the effect of aeration on flow pattern and level of homogenization can be demonstrated. To demonstrate the flow pattern inside the mixing vessel, **Figure 5.12** provides a sequence of 2D and stacked ERT images which were obtained by injecting 10ml of 30% saline into the activated sludge agitated by ASI impeller. In this study, the liquid phase (activated sludge) was conductive and gas phase (air) was non-conductive distributed within the vessel. The 2D tomograms interprets the comparison between conductivity distribution inside the mixing tank **(i)** at impeller speed (N=100rpm) without aeration and **(ii)** at impeller speed (N=100rpm) with 0.014(m^3/min) gas flow rate. The blue color shows the regions with less conductivity whereas higher conductivity regions are exhibited by red color. It is a known fact that the conductivity of saline solution is higher than the activated sludge (as mentioned in section 4.3.2 i.e. 4.24 mS/cm for activated sludge and 75.60 mS/cm for brine), thus the region with higher conductivity depicts the accumulation of saline in the mixing tank (Gumery et al., 2011, Pakzad et al., 2008, Bolton et al., 2004, Hamood-ur-Rehman, 2012).

Figure 5.12 shows that after few seconds of tracer injection (on plane 1), axial/radial impeller (ASI) rotation forced it towards plane 2 and increased the conductivities of both planes (red color of tomograms for plane 1 and plane 2). However, the axial /radial flow of impeller distributed the tracer within the vessel while at t= 6.71sec (in presence of air) and at t= 8.41sec (in absence of air) the tomographic planes changes to green color which represents the dispersion of saline solution in the whole vessel and reached homogeneity. Therefore, 98% homogeneity was attained after 6.71sec of brine injection with air and 8.41sec without air. It should be mentioned that due to the more motion in presence of aeration homogeneity was achieved faster than in absence of aeration. However, some researchers found that the aeration increases the mixing times (Blakebrough & Sambamurthy, 1996; Einsele & Finn, 1980). On the other side, it was also reported that the mixing time totally depends on the hydrodynamics existing inside the mixing tank (Abardi et al., 1990). Aeration can have positive, negative and neutral effect on the mixing time depending on the flow patterns induced by an impeller, aeration or combination of both impeller and air (Vasconselos et al., 1995). Although the present work was in agreement of the positive effect of aeration on mixing time as shown in **Figure 5.12**.

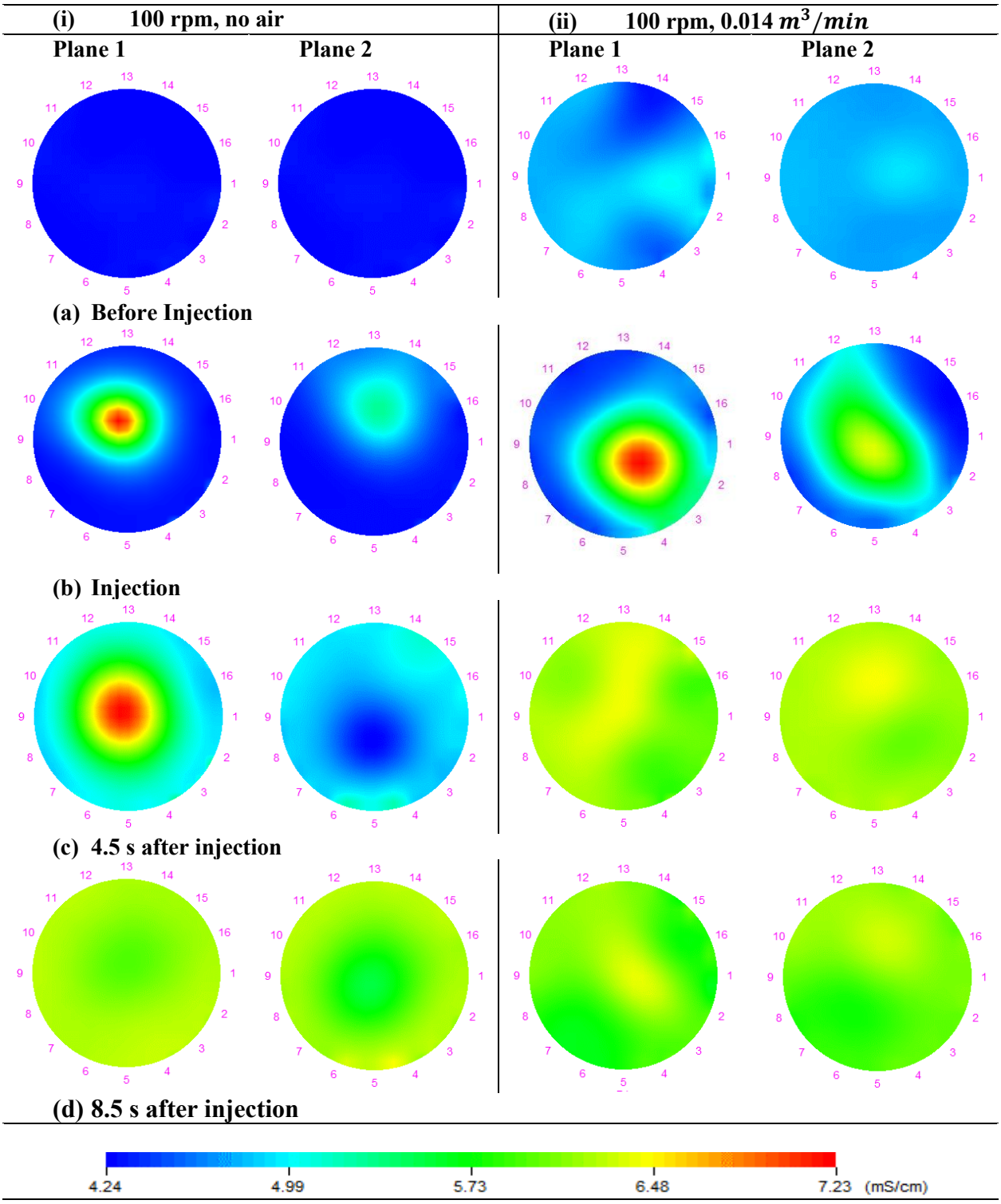

Figure 5.12. Sequence of 2D and stacked ERT images (based on conductivity, mS/cm) showing the level of homogeneity of activated sludge agitated by the ASI: **(i)** at *N*= 100 rpm, no air, and **(ii)** *N*=100 rpm, with gas at 0.014 m^3/min.

5.4.5 Formation and Destruction of Cavern

The formation and destruction of cavern confirms that the fluid in the mixing tank is in motion and has significant homogenization characteristics. Wichterle & Wein (1975) demonstrated the movable zone near the impeller which was flexible in non-Newtonian fluids and such zone is termed as 'cavern'. Therefore, by conventional designing and operating agitation system it is desired to destroy such stagnant regions (Pakzad et al., 2008). **Figure 5.13** illustrates the formation and destruction of cavern achieved in this study in mixing of activated sludge.

Figure 5.13 shows the corresponding tomograms when 20ml of 30 % saline solution was added into the activated sludge (near the impeller hub) agitated by ASI at 20 rpm along with gassing at 0.006 m^3/min. These tomography results were employed to investigate the gassing effects on the mixing time inside a mixing tank. As it can be seen, ASI impeller rotational speed at 20rpm along with gassing at 0.06 m^3/min gas flow rate led to destruct the cavern formed around impeller. This figure shows that 20 sec after injection, the tracer cloud limited to the well mixed zone (cavern) since the rotational speed of 20 rpm did not provide enough motion inside the tank. Then air was started to be sparged at rate of 0.014 m^3/min into the tank and after 2 sec it could be easily seen that cavern size was enlarged in both radial and axial direction and consequently high conductivity region was observed in Plane 1 **(Figure 5.13 (b))**. This trend was continued as shown in **Figure 5.13 (c)**, i.e. 10 sec after air injections started, the cavern was destructed. After 2 more second passing, the tank reached homogeneity. However, the following test shows that by employing aeration in a mixing tank a well-mixed zone can be destructed throughout the tank which shows that aeration has the ability to achieve homogeneity inside the vessel in mixing of non-Newtonian fluids.

(i) Cavern formation

(a) 20 s after tracer injected

Plane 1

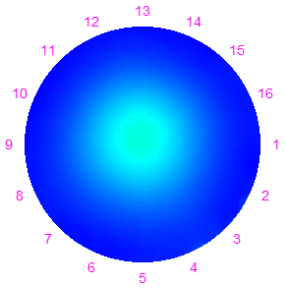

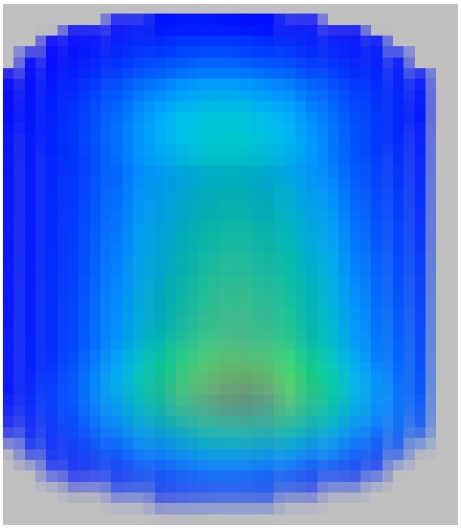

Plane 2

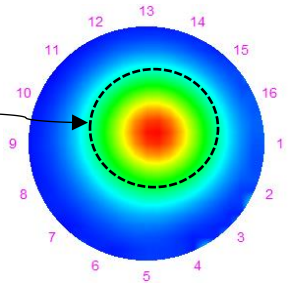

(ii) Cavern destruction

(b) 2 s after air injection started

Plane 1

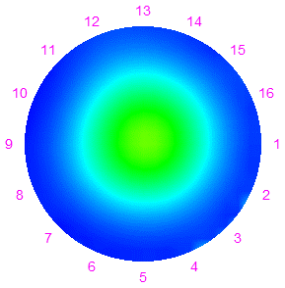

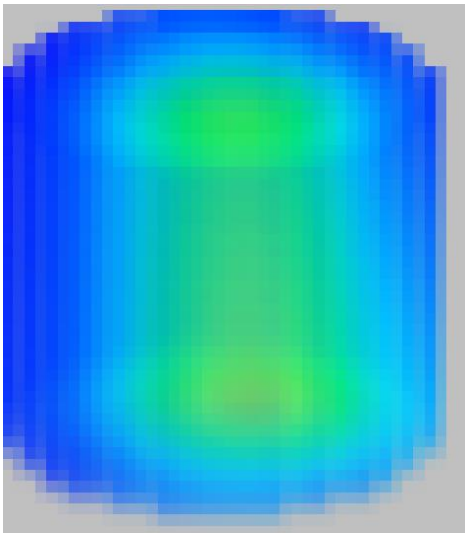

Plane 2

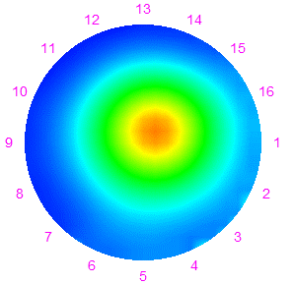

(c) 10 s after air injection started

Plane 1

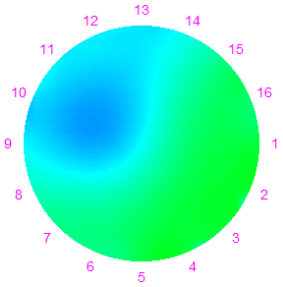

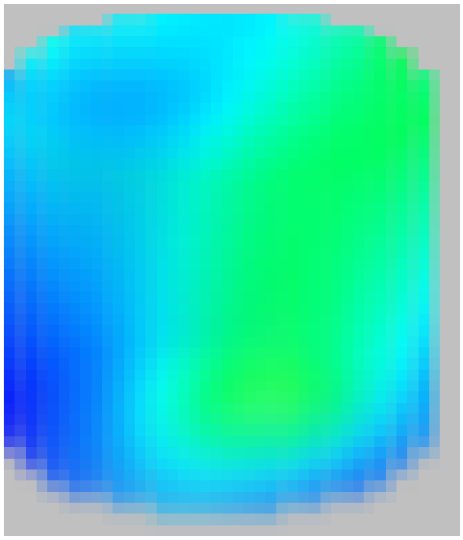

Plane 2

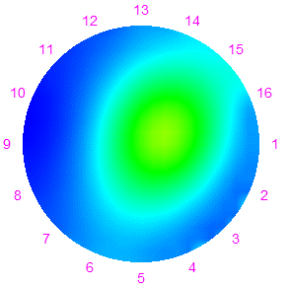

(d) 12 s after air injection started

Plane 1

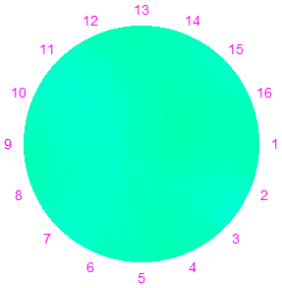

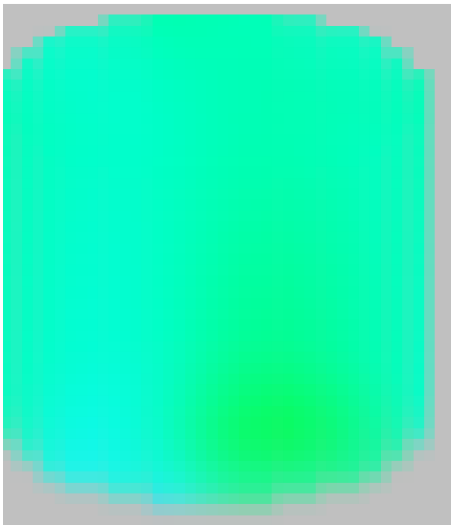

Plane 2

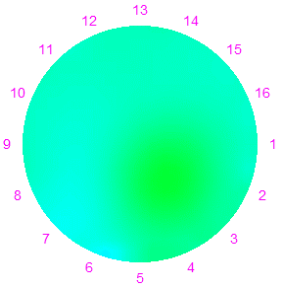

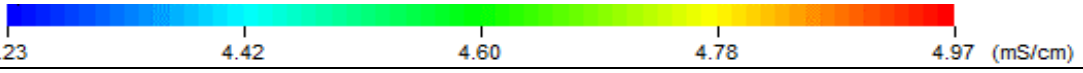

Figure 5.13. Effect of air on cavern destruction using 2D and 3D tomography images at **(i)** cavern formation at N=20rpm, 0.006 m^3/min, and **(ii)** cavern destruction (b, c, d) after 2sec, 10sec, 12sec of air injection at 0.014m^3/min.

6. Conclusions

In this study, with the help of electrical resistance tomography (ERT) and response surface methodology (RSM) various important means for non-invasive measurements for non-Newtonian fluid mixing parameters were observed. In the first section, accuracy of measurements of this study were obtained as well as generalized Reynolds numbers were evaluated for all the experimental runs. In the second section, RSM was employed to study the independent variables used in this study. Lastly in third section, with the help of ERT flow patterns within the mixing tank were analyzed and discussed in detail with the help of 2D and 3D images. The following main conclusions were drawn in the following experimental study:

- In this study, ERT was employed to determine the mixing performance of impeller type in presence and absence of aeration.
- For the first time, ERT was utilized to evaluate the performance of impeller type in agitation of activated sludge at different rotational speed with various gas flow rates.
- ERT was successfully utilized to evaluate the effects of different parameters and operating conditions such as employing impeller type, impeller speed, and gas flow rate in the mixing tank on different hydrodynamic parameters such as mixing time, specific power consumption and gas flow number for a two-phase (gas/liquid) system.
- For the first time, a multivariable technique called response surface methodology (RSM) was applied to evaluate the performance of independent variables and respective responses.
    - A statistical-based experimental design with RSM was employed to evaluate the individual and interactional effects of impeller speed, impeller type and gas flow rate on the mixing time, specific power consumption, and gas flow number.
    - The proposed second-order quadratic models for the mixing time, specific power consumption and gas flow number illustrated high coefficient of determination and the experimental values were in a good agreement with the predicted values.
    - By observing RESM equations for all responses for the given ranges of independent variables normality assumptions were confirmed.
    - It was revealed that among all the independent variables, impeller speed and gas flow rate was the most effective factor for the mixing time and gas flow number while for the specific power consumption the most effective factor was the impeller speed.

- It was found that the least effective factor was the impeller type for all responses.
- Among the interactional effects, the most common was the impeller speed and gas flow rate for all the studied responses in this study.
- For the first time, the performance of a novel impeller called ASI (a combination of A200 and Scaba impeller) was assessed and compared with ARI (a combination of A200 and Rushton impeller) and Rushton impeller in agitation of activated sludge in presence or absence of aeration.
- It was found that ASI was more efficient than other impeller type. From the results of ERT and RSM it can be illustrated that ASI performed slightly better performance as compare to ARI and Rushton impeller since ASI achieved homogenization in less time and consumed less power.
- The ability of ERT system to observe the flow pattern created by impeller types in presence or absence of aeration was demonstrated by monitoring the distribution of the tracer as 2-D and 3-D tomograms.
- This is the first time when ERT was applied to study the formation and destruction of cavern in the mixing of activated sludge and have been successfully monitored within the mixing tank.

6.1 Recommendations for Future Work

This experimental study can be expanded in several ways. The following recommendations have been made to enhance our knowledge of mixing of non-Newtonian fluids using non-invasive ERT technique:

- The proposed mixing tank equipped with an impeller and a sparger can be further investigated for other Newtonian fluids (sugar solutions) and non-Newtonian fluids (xanthan gum solution, tomato ketchup).
- Further work can be made to evaluate the effect of impeller type at different rotational speeds.
- Performance of impeller types can be evaluated by selecting different gas flow rates.

- Since crossed shaped sparger was used in this study. To determine the gas flow characteristics various sparger configuration can be used such as perforated pipe ladder type gas sparger, multiple orifice sparger, single orifice and annular ring sparger.
- Rheological properties of activated sludge can also be studied in detail.
- Since this study was related to two-phase (gas-liquid) mixing. To explore our knowledge two-phase (liquid-liquid) and three-phase mixing can be studied for the same system.
- Computational fluid dynamics (CFD) can be used to simulate and validate the mixing process.

Nomenclature

A	area, m^2
c	initial concentration of tracer (equation (2.22)
c_∞	main concentration of tracer (equation (2.22)
C_c	off-bottom clearance, mm
d	diameter of droplet, m (equation 2.11)
d_y	specific distance between two plates, m
dV_x	upper plate velocity, ms^{-1}
$dV_x/\ d_y$	uniform velocity gradient, ms^{-1}
D	impeller diameter, mm
D_C	impeller diameter, mm (figure 4.2)
E	activation energy, $Jmol^{-1}$
F	force, N
g	gravitational acceleration, ms^{-2}
H	tank height, mm
i	current, mA
K	consistency index, $Pa.s^n$
m	cross rate constant
M	independent measurements (equation 3.2)
M	torque variable, N.m (equation 4.8)
$\overline{M}$	mean value of torque measurements, N.m (equation 4.8)
N	impeller rotational speed, rps
N	number of electrodes (equation 3.1)
P	power, W
P_1	gas pressure at free space, Pa
P_2	gas pressure at the bottom of the vessel, Pa
P_{tot}/V	specific power consumption, Wm^{-3}
Q_g	gas flow rate, m^3/min
R	universal gas constant (8.314 $Jmol^{-1}K^{-1}$)

R	non-linear function of boundary voltage (equation 3.1)
t_m	mixing time, s
T	temperature, *K*
T	tank diameter, mm (figure 4.1)
V	volume, m^3
X_1	experimental factor 1, impeller speed, rpm
X_2	experimental factor 2, impeller type, dimensionless
X_3	experimental factor 3, gas flow rate, m^3/min
Y_1	response 1, mixing time, *s*
Y_2	response 2, specific power consumption, Wm^{-3}
Y_3	response 3, gas flow number, dimensionless

Greek letters

ε	precision of measurements
σ	standard deviation
$\dot{\gamma}$	shear rate, s^{-1}
$\dot{\boldsymbol{\gamma}}_{ave}$	averaged shear rate, s^{-1}
μ_∞	infinite rate apparent viscosity, *Pa.s*
μ_0	zero shear rate apparent viscosity, *Pa.s*
η_B	high shear thinning viscosity, $Pa.s^n$
η_{app}	apparent viscosity, *Pa.s*
τ	shear stress, *Pa*
τ_y	yield stress, *Pa*
ρ	fluid density $Kg\ m^{-3}$
λ	time constant, s
β_0, β_i, β_{ij},β_{ii}	constants coefficients of independent variables (equation 5.1)

Subscripts

i, j	variable
adj	adjusted
app	apparent
ave	average
g	gas
m	mixing
tot	total
y	yield stress

Dimensionless Groups

e_i	error, dimensionless (for mixing time, specific power consumption and gas flow number)
Fl_g	gas flow number, dimensionless
k	number of studied factors, dimensionless
K_s	Metzner-Otto constant for calculating shear rate, dimensionless
n	power-law index, dimensionless
N_P	power number, dimensionless
N_{Re}	Reynolds number, dimensionless
Re	generalized Reynolds number, dimensionless
R^2	coefficient of determination, dimensionless

Abbreviations

API	active pharmaceutical company
ANOVA	analysis of variance
BBD	Box-Behnken design
CCD	central-composite design
CMC	carboxy methyl cellulose
C.V.	coefficient of variation
DAS	data acquisition system

DOE	design of experiments
EALR	external air-lift reactor
ECT	electrical capacitance tomography
EIT	electrical impedance tomography
EMT	electrical magnetic tomography
ERT	electrical resistance tomography
FPGA	field programmable gate array
IALR	internal air-lift reactor
LBP	linear back projection
LSCFB	liquid-solid circulating fluidized bed
MLSS	mixed liquor suspended solids
PCA-GRNN	principle component analysis general regression neural network
PCA-SVM	principle component analysis support vector machine
PCI	peripheral component interconnect
RPM	revolution per minute
RSM	response surface methodology
sec	seconds
SD	standard deviation

References

A

Abardi, V., Rovero, G., Sicardi, S., Baldi, G., & Conti, R. (1990). Hydrodynamics of a gas–liquid reactor stirred with multi-impeller systems. *Trans Inst. Chem. Eng*, *68*, 516.

Ali, K. M. A. (2014). Parameters Influence on Mixing Time of Gas Liquid Agitation System.

Amiri, T. Y., Moghaddas, J. S., & Moghaddas, Y. (2011). A jet mixing study in two phase gas–liquid systems. *Chemical Engineering Research and Design*, *89*(3), 352-366.

Ascanio, G., Foucault, S., & Tanguy, P. A. (2003). Performance of a new mixed down pumping impeller. Chemical engineering & technology, 26(8), 908-911.

Aw, S. R., Rahim, R. A., Rahiman, M. H. F., Yunus, F. R. M., & Goh, C. L. (2014). Electrical resistance tomography: A review of the application of conducting vessel walls. *Powder Technology*, *254*, 256-264.

B

Babaei, R., Bonakdarpour, B., & Ein-Mozaffari, F. (2015(a)). The use of electrical resistance tomography for the characterization of gas holdup inside a bubble column bioreactor containing activated sludge. *Chemical Engineering Journal*, *268*, 260-269.

Babaei, R., Bonakdarpour, B., & Ein-Mozaffari, F. (2015(b)). Analysis of gas phase characteristics and mixing performance in an activated sludge bioreactor using electrical resistance tomography. *Chemical Engineering Journal*, *279*, 874-884.

Bakker, A., & Gates, L. E. (1995). Properly choose mechanical agitators for viscous liquids. *Chemical engineering progress*, *91*(12), 25-34.

Bakker, A., Smith, J. M., & Myers, K. J. (1994). How to disperse gases in liquids. *Chemical engineering*, *101*(12), 98.

Barber CD, Brown BH, Freeston IL (1983) Imaging spatial distributions of resistivity using

Barbot, E., Seyssiecq, I., Roche, N., & Marrot, B. (2010). Inhibition of activated sludge respiration by sodium azide addition: Effect on rheology and oxygen transfer. *Chemical Engineering Journal*, *163*(3), 230-235.

Barigou, M., & Greaves, M. (1991). A capillary suction prove for bubble size measurement. *Measurement Science and Technology*, *2*(4), 318.

Baudez, J. C., SLATTER, P. & ESHTIAGHI, N. 2013. The impact of temperature on the rheological behaviour of anaerobic digested sludge. Chemical Engineering Journal, 215–216, 182-187.

Bissell, E. S. (1938). *U.S. Patent No. 2,137,328*. Washington, DC: U.S. Patent and Trademark Office.

Blakebrough, N., & Sambamurthy, K. (1966). Mass transfer and mixing rates in fermentation vessels. *Biotechnology and Bioengineering*, *8*(1), 25-42.

Bolton, G. T., & Primrose, K. M. (2005). An overview of electrical tomographic measurements in pharmaceutical and related application areas.*AAPS PharmSciTech*, *6*(2), E137-E143.

Bouaifi, M., & Roustan, M. (2001). Power consumption, mixing time and homogenisation energy in dual-impeller agitated gas–liquid reactors. *Chemical Engineering and Processing: Process Intensification*, *40*(2), 87-95.

Box, G. E., & Behnken, D. W. (1960). Some new three level designs for the study of quantitative variables. *Technometrics*, *2*(4), 455-475.

Box, G.E.P., and Wilson, K.B. 1951. On the experimental attainment of optimum conditions. Journal of the Royal Statistical Society Series, B13(1): 1-45

Braak, E., Alliet, M., Schetrite, S., & Albasi, C. (2011). Aeration and hydrodynamics in submerged membrane bioreactors. *Journal of membrane science*, *379*(1), 1-18.

Bruun, H. H. (1996). Hot-film anemometry in liquid flows. *Measurement Science and Technology*, *7*(10), 1301.

Bujalski, J. M., Jaworski, Z., Bujalski, W., & Nienow, A. W. (2002). The influence of the addition position of a tracer on CFD simulated mixing times in a vessel agitated by a Rushton turbine. *Chemical Engineering Research and Design*, *80*(8), 824-831.

C

Campbell, H. W., & Crescuolo, P. J. (1982). The use of rheology for sludge characterization. *Water Science and Technology*, *14*(6-7), 475-489.

Cao, Z., Xu, L., Xu, C., & Wang, H. (2010, July). Electrical resistance tomography (ERT) by using an ECT sensor. In *Imaging Systems and Techniques (IST), 2010 IEEE International Conference on* (pp. 63-66). IEEE.

Chhabra, R. P. & Richardson, J. F. 2008. Non-Newtonian Flow and Applied Rheology - Engineering Applications (2nd Edition). Elsevier.

Cui, Z. Q., WANG, H. X., XU, Y. B., & FAN, W. R. (2010). Design of Twin-Plane Electrical Resistance Tomography System [J]. *Journal of Tianjin University*, *2*, 006.

D

Defrance, L., Jaffrin, M. Y., Gupta, B., Paullier, P., & Geaugey, V. (2000). Contribution of various constituents of activated sludge to membrane bioreactor fouling. *Bioresource technology*, *73*(2), 105-112.

Dentel, S. K. (1997). Evaluation and role of rheological properties in sludge management. *Water Science and Technology*, *36*(11), 1-8.

Devi, T. T., & Kumar, B. (2014). Scale up criteria for dual stirred gas-liquid unbaffled tank with concave blade impeller. *Korean Journal of Chemical Engineering*, *31*(8), 1339-1348.

Dickin, F., & Wang, M. (1996). Electrical resistance tomography for process applications. *Measurement Science and Technology*, *7*(3), 247.

Durán, C., Fayolle, Y., Pechaud, Y., Cockx, A., & Gillot, S. (2016). Impact of suspended solids on the activated sludge non-newtonian behaviour and on oxygen transfer in a bubble column. *Chemical Engineering Science*, *141*, 154-165.

Dyakowski, T. (1996). Process tomography applied to multi-phase flow measurement. *Measurement Science and Technology*, *7*(3), 343.

Dyakowski, T., & Williams, R. A. (1998). Hydrocyclone flow modelling-a continuous research challenge. *Chapter*, *5*, 61-73.

Dyakowski, T., York, T., Mikos, M., Vlaev, D., Mann, R., Follows, G., ... & Wilson, M. (2000). Imaging nylon polymerisation processes by applying electrical tomography. *Chemical Engineering Journal*, *77*(1), 105-109.

E

Einsele, A., & Finn, R. K. (1980). Influence of gas flow rates and gas holdup on blending efficiency in stirred tanks. *Industrial & Engineering Chemistry Process Design and Development*, *19*(4), 600-603.

F

Fan, H., Qi, L., Liu, G. H., Zhang, Y., Chen, X., & Wang, H. (2014). Promotion and inhibition of oxygen transfer under fine bubble aeration by activated sludge. *Water and Environment Journal*, *28*(3), 434-441.

Feng, D. O. N. G., Cong, X. U., ZHANG, Z., & Shangjie, R. E. N. (2012). Design of parallel electrical resistance tomography system for measuring multiphase flow. *Chinese Journal of Chemical Engineering*, *20*(2), 368-379.

Forster, C. F. (1982). Sludge surfaces and their relation to the rheology of sewage sludge suspensions. *Journal of chemical technology and biotechnology*, *32*(7-12), 799-807.

Forster, C. F. (2002). The rheological and physico-chemical characteristics of sewage sludges. *Enzyme and Microbial Technology*, *30*(3), 340-345.

Fransolet, E., Crine, M., L'Homme, G., Toye, D., & Marchot, P. (2001). Analysis of electrical resistance tomography measurements obtained on a bubble column. *Measurement Science and Technology*, *12*(8), 1055.

Fransolet, E., Crine, M., Marchot, P., & Toye, D. (2005). Analysis of gas holdup in bubble columns with non-Newtonian fluid using electrical resistance tomography and dynamic gas disengagement technique. *Chemical Engineering Science*, *60*(22), 6118-6123.

G

Galindo, E., & Nienow, A. W. (1993). Performance of the Scaba 6SRGT agitator in mixing of simulated xanthan gum broths. *Chemical engineering & technology*, *16*(2), 102-108.

Gibilaro, L. G., Davies, S. N., Cooke, M., Lynch, P. M., & Middleton, J. C. (1985). Initial response analysis of mass transfer in a gas sparged stirred vessel. *Chemical engineering science*, *40*(10), 1811-1816.

Gimbun, J., Rielly, C. D., & Nagy, Z. K. (2009). Modelling of Mass Transfer in Gas-Liquid Stirred Tanks Agitated by Rushton Turbine and CD-6 Impeller. In *13th Eur. Conf. Mixing, London*.

Gisser, D. G., Isaacson, D., & Newell, J. C. (1987). Current topics in impedance imaging. *Clinical Physics and Physiological Measurement*, *8*(4A), 39.

Grebe, A., & Fenge, C. Single-Use, Stirred-Tank Bioreactors: Efficient Tools for Process Development and Characterization.

Gresch, M., Armbruster, M., Braun, D., & Gujer, W. (2011). Effects of aeration patterns on the flow field in wastewater aeration tanks. *Water research*, *45*(2), 810-818.

Guibaud, G., Dollet, P., Tixier, N., Dagot, C., & Baudu, M. (2004). Characterisation of the evolution of activated sludges using rheological measurements. *Process Biochemistry*, *39*(11), 1803-1810.

Guillard, F., & Trägårdh, C. (2003). Mixing in industrial Rushton turbine-agitated reactors under aerated conditions. *Chemical Engineering and Processing: Process Intensification*, *42*(5), 373-386.

Gumery, F., Ein-Mozaffari, F., & Dahman, Y. (2009). Characteristics of local flow dynamics and macro-mixing in airlift column reactors for reliable design and scale-up. *International Journal of Chemical Reactor Engineering*, *7*(7), 4.

Gumery, F., Ein-Mozaffari, F., & Dahman, Y. (2011). Mixing characteristics of draft tube airlift bioreactor using electrical resistance tomography.*Bioprocess Biosyst. Eng*, *34*, 135-144.

Günther, A., Khan, S. A., Thalmann, M., Trachsel, F., & Jensen, K. F. (2004). Transport and reaction in microscale segmented gas–liquid flow. *Lab on a Chip*, *4*(4), 278-286.

H

Hamood-Ur-Rehman, M. (2012). Mixing Characteristics of External Loop Airlift Bioreactor using Electrical Resistance Tomography.

Hashemi, N., Ein-Mozaffari, F., Upreti, S. R., & Hwang, D. K. (2015). Experimental investigation of the bubble behavior in an aerated coaxial mixing vessel through electrical resistance tomography (ERT). *Chemical Engineering Journal*, *289*, 402-412.

Hashemi, N., Ein-Mozaffari, F., Upreti, S. R., & Hwang, D. K. (2016). Analysis of mixing in an aerated reactor equipped with the coaxial mixer through electrical resistance tomography and response surface method. *Chemical Engineering Research and Design*, *109*, 734-752.

Holland, F. A., & Chapman, F. S. (1966). *Liquid mixing and processing in stirred tanks*. Reinhold Pub. Corp.

Holley, C. A., & Albert, K. B. (1996). *U.S. Patent No. 5,580,170*. Washington, DC: U.S. Patent and Trademark Office.

Hosseini, S., Patel, D., Ein-Mozaffari, F., & Mehrvar, M. (2010). Study of solid–liquid mixing in agitated tanks through electrical resistance tomography. *Chemical Engineering Science*, *65*(4), 1374-1384.

Huang, S. M., Xie, C. G., Salkeld, J. A., Plaskowski, A., Thorn, R., Williams, R. A., ... & Beck, M. S. (1992). Process tomography for identification, design and measurement in industrial systems. *Powder technology*, *69*(1), 85-92.

I

Issa, H. M. (2016). Power consumption, mixing time, and Oxygen mass transfer in a gas-liquid contactor stirred with a dual impeller for different spacing. *Journal of Engineering*, *2016*.

J

Jaworski, Z., Bujalski, W., Otomo, N., Nienow, A.W., 2000. CFD study of homogenization with dual Rushton turbines-comparison with experimental results. Part I: Initial studies. Chem. Eng. Res. Des. 78, 327-333.

Jin, B., Yin, P., & Lant, P. (2006). Hydrodynamics and mass transfer coefficient in three-phase air-lift reactors containing activated sludge. *Chemical Engineering and Processing: Process Intensification*, *45*(7), 608-617.

Jin, H., Lian, Y., Qin, Y., Yang, S., & He, G. (2013). Distribution characteristics of holdups in a multi-stage bubble column using electrical resistance tomography. *Particuology*, *11*(2), 225-231.

Jin, H., Yang, S., He, G., Wang, M., & Williams, R. A. (2010). The effect of gas-liquid counter-current operation on gas hold-up in bubble columns using electrical resistance tomography. *Journal of chemical technology and biotechnology*, *85*(9), 1278-1283.

K

Kadić, A., Palmqvist, B., & Lidén, G. (2014). Effects of agitation on particle-size distribution and enzymatic hydrolysis of pretreated spruce and giant reed. *Biotechnology for biofuels*, *7*(1), 77.

Karhunen, K., Seppänen, A., Lehikoinen, A., Blunt, J., Kaipio, J. P., & Monteiro, P. J. (2010). Electrical resistance tomography for assessment of cracks in concrete. *ACI Materials Journal*, *107*(5), 523.

Kazemzadeh, A., Ein-Mozaffari, F., Lohi, A., & Pakzad, L. (2016). Effect of the rheological properties on the mixing of Herschel-Bulkley fluids with coaxial mixers: Applications of tomography, CFD, and response surface methodology. *The Canadian Journal of Chemical Engineering*, *94*(12), 2394-2406.

Kim, S., Nkaya, A. N., & Dyakowski, T. (2006). Measurement of mixing of two miscible liquids in a stirred vessel with electrical resistance tomography. International communications in heat and mass transfer, 33(9), 1088-1095.

Kocabaş, Z. (2001). An Application and interpretation of second order response surface model. *Ankara University Journal of Agricultural Sciences*, *7*, 121-128.

Kourunen, J., Niitti, T., & Heikkinen, L. M. (2011). Application of three-dimensional electrical resistance tomography to characterize gas holdup distribution in laboratory flotation cell. *Minerals Engineering*, *24*(15), 1677-1686.

Kowalski, A., Davidson, J., Flanagan, M., & York, T. (2010). Electrical resistance tomography for characterisation of physical stability in liquid compositions. *Chemical Engineering Journal*, *158*(1), 69-77.

Kraume, M., & Zehner, P. (2001). Experience with experimental standards for measurements of various parameters in stirred tanks: a comparative test. *Chemical Engineering Research and Design*, *79*(8), 811-818.

Kryłów, M., & Fryźlewicz-Kozak, B. (2007). Rheological properties of wastewater sludge.

Kuzmanić, N., & Ljubičić, B. (2001). Suspension of floating solids with up-pumping pitched blade impellers; mixing time and power characteristics. *Chemical Engineering Journal*, *84*(3), 325-333.

L

Lahey, R. T., & Ohkawa, K. (1989). An experimental investigation of phase distribution in an eccentric annulus. *International journal of multiphase flow*,*15*(3), 447-457.

Lamont, A. G. W. (1958). Air agitation and pachuca tanks. *The Canadian Journal of Chemical Engineering*, *36*(4), 153-160.

Li, H., & Prakash, A. (2000). Influence of slurry concentrations on bubble population and their rise velocities in a three-phase slurry bubble column. *Powder Technology*, *113*(1), 158-167.

Lotito, V., Spinosa, L., Mininni, G., & Antonacci, R. (1997). The rheology of sewage sludge at different steps of treatment. *Water Science and Technology*, *36*(11), 79-85.

Lutz, A. E., Kee, R. J., & Miller, J. A. (1988). *SENKIN: A FORTRAN program for predicting homogeneous gas phase chemical kinetics with sensitivity analysis* (No. SAND-87-8248). Sandia National Labs., Livermore, CA (USA).

M

Machon, V., & Jahoda, M. (2000). Liquid Homogenization in Aerated Multi-Impeller Stirred Vessel. *Chemical engineering & technology*, *23*(10), 869-876.

Mann, R., Dickin, F. J., Wang, M., Dyakowski, T., Williams, R. A., Edwards, R. B., ... & Holden, P. J. (1997). Application of electrical resistance tomography to interrogate mixing processes at plant scale. *Chemical engineering science*, *52*(13), 2087-2097.

Markis, F. (2015). *Sludge rheology: semi–empirical correlations to predict the apparent viscosity and yield stress of sludge mixtures* (Doctoral dissertation, RMIT University).

McFarlane, C. M., & Nienow, A. W. (1996). Studies of high solidity ratio hydrofoil impellers for aerated bioreactors. 4. Comparison of impeller types. *Biotechnology progress*, *12*(1), 9-15.

Meng, Z., Huang, Z., Wang, B., Ji, H., & Li, H. (2009, May). Flowrate measurement of air-water two-phase flow using an electrical resistance tomography sensor and a venturi meter. In *Instrumentation and Measurement Technology Conference, 2009. I2MTC'09. IEEE* (pp. 118-121). IEEE.

Meng, Z., Huang, Z., Wang, B., Ji, H., Li, H., & Yan, Y. (2010). Air–water two-phase flow measurement using a Venturi meter and an electrical resistance tomography sensor. *Flow Measurement and Instrumentation*,*21*(3), 268-276.

Metzner, A.B., Otto, R.E., 1957. Agitation of non-Newtonian fluids. AIChE J. 3, 3-11.

Middleton J.C., 1985, Gas-liquid dispersion and mixing. In: Mixing in the Process Industries, Eds. Harnby N., Edward M.F., Nienow A.W., Butterworth, Heidelberg, Germany, 322-355.

Mori, M., Seyssiecq, I., & Roche, N. (2006). Rheological measurements of sewage sludge for various solids concentrations and geometry. *Process Biochemistry*, *41*(7), 1656-1662.

Myers, R. H., Montgomery, D. C., Vining, G. G., Borror, C. M., & Kowalski, S. M. (2004). Response surface methodology: a retrospective and literature survey. *Journal of quality technology*, *36*(1), 53.

N

Nienow, A. W., & Miles, D. (1978). The effect of impeller/tank, configurations on fluid-particle mass transfer. *The Chemical Engineering Journal*, *15*(1), 13-24.

Novarino, D., Santagata, E., Dalmazzo, D., & Zanetti, M. (2010). Rheological characterization of sludge coming from a wastewater treatment plant. *American Journal of Environmental Sciences*, *6*(4), 329-337.

O

Onken, U., & Weiland, P. (1980). Hydrodynamics and mass transfer in an airlift loop fermentor. *European journal of applied microbiology and biotechnology*, *10*(1-2), 31-40.

P

Pakzad, L., Ein-Mozaffari, F., & Chan, P. (2008). Using electrical resistance tomography and computational fluid dynamics modeling to study the formation of cavern in the mixing of pseudoplastic fluids possessing yield stress. *Chemical Engineering Science*, *63*(9), 2508-2522.

Pakzad, L., Ein-Mozaffari, F., Upreti, S. R., & Lohi, A. (2013). A novel and energy-efficient coaxial mixer for agitation of non-Newtonian fluids possessing yield stress. *Chemical Engineering Science*, *101*, 642-654.

Papa, M., Pedrazzani, R., Nembrini, S., & Bertanza, G. (2015). Should rheological properties of activated sludge be measured? *Appl. Rheol*, *25*, 24590.

Paul, E. L., Atiemo-Obeng, V. A., & Kresta, S. M. (Eds.). (2004). *Handbook of industrial mixing: science and practice*. John Wiley & Sons.

Paulson, K., Breckon, W., & Pidcock, M. (1992). Electrode modelling in electrical impedance tomography. *SIAM Journal on Applied Mathematics*,*52*(4), 1012-1022.

Pittoors, E., Guo, Y., & WH Van Hulle, S. (2014). Modeling dissolved oxygen concentration for optimizing aeration systems and reducing oxygen consumption in activated sludge processes: a review. *Chemical Engineering Communications*, *201*(8), 983-1002.

Poitou, A., Racineux, G., & Burlion, N. (1997). Identification and measurement of pastes rheological properties–effects of water dissociation. *Water science and technology*, *36*(11), 19-26.

R

Raghav Rao, K. S. M. S., & Joshi, J. B. (1988). Liquid phase mixing in mechanically agitated vessels. *Chemical Engineering Communications*, *74*(1), 1-25.

Rao, M. A. (2010). *Rheology of fluid and semisolid foods: principles and applications: principles and applications*. Springer Science & Business Media.

Ratkovich, N., Horn, W., Helmus, F. P., Rosenberger, S., Naessens, W., Nopens, I., & Bentzen, T. R. (2013). Activated sludge rheology: a critical review on data collection and modelling. *Water research*, *47*(2), 463-482.

Razzak, S. A., Barghi, S., & Zhu, J. X. (2007). Electrical resistance tomography for flow characterization of a gas–liquid–solid three-phase circulating fluidized bed. Chemical Engineering Science, 62(24), 7253-7263.

Razzak, S. A., Barghi, S., & Zhu, J. X. (2009). Application of electrical resistance tomography on liquid–solid two-phase flow characterization in an LSCFB riser. *Chemical Engineering Science*, *64*(12), 2851-2858.

Ricard, F., Brechtelsbauer, C., Xu, X. Y., & Lawrence, C. J. (2005). Monitoring of multiphase pharmaceutical processes using electrical resistance tomography. Chemical Engineering Research and Design, 83(7), 794-805.

Roman, R. V., & Tudose, R. Z. (1996). Studies on transfer processes in mixing vessels: hydrodynamic of the modified Rushton turbine agitators in gas—liquid dispersions. *The Chemical Engineering Journal and The Biochemical Engineering Journal*, *61*(2), 83-93.

Rosenberger, S., Kubin, K., & Kraume, M. (2002). Rheology of activated sludge in membrane bioreactors. *Engineering in life sciences*, *2*(9), 269-275.

Ruzinsky, F., & Bennington, C. P. (2007). Aspects of liquor flow in a model chip digester measured using electrical resistance tomography. *Chemical Engineering Journal*, *130*(2), 67-74.

S

Sahinkaya, E., & Dilek, F. B. (2005). Biodegradation of 4-chlorophenol by acclimated and unacclimated activated sludge—evaluation of biokinetic coefficients. *Environmental Research*, *99*(2), 243-252.

Sanin, D. F. (2002). Effect of solution physical chemistry on the rheological properties of activated sludge. *Water Sa*, *28*(2), 207-212.

Sanin, F. D., Clarkson, W. W., & Vesilind, P. A. (2011). *Sludge engineering: the treatment and disposal of wastewater sludges*. DEStech Publications, Inc.

Scargiali, F. (2007). *Gas-liquid dispersions in mechanically agitated contactors* (Doctoral dissertation, PhD thesis, Universitá degli Studi di Palermo).

Schymanski, E. L., Jeon, J., Gulde, R., Fenner, K., Ruff, M., Singer, H. P., & Hollender, J. (2014). Identifying small molecules via high resolution mass spectrometry: communicating confidence.

Scott, D. M., & McCann, H. (Eds.). (2005). *Process imaging for automatic control*. CRC Press.

Seagar, A. D., Barber, D. C., & Brown, B. H. (1987). Theoretical limits to sensitivity and resolution in impedance imaging. *Clinical Physics and Physiological Measurement*, *8*(4A), 13.

Seppänen, A., Karhunen, K., Lehikoinen, A., Kaipio, J. P., & Monteiro, P. J. M. (2008, September). Electrical resistance tomography imaging of concrete. In *2nd International Conference on Concrete Repair, Rehabilitation and Retrofitting, ICCRRR* (pp. 231-232).

Shariati, S. R. P., Bonakdarpour, B., Zare, N., & Ashtiani, F. Z. (2011). The effect of hydraulic retention time on the performance and fouling characteristics of membrane sequencing batch reactors used for the treatment of synthetic petroleum refinery wastewater. *Bioresource technology*, *102*(17), 7692-7699.

Sharifi, M., & Young, B. (2011). 3-Dimensional spatial monitoring of tanks for the milk processing industry using electrical resistance tomography. *Journal of Food Engineering*, *105*(2), 312-319.

Sharifi, M., & Young, B. (2012). Qualitative visualization and quantitative analysis of milk flow using electrical resistance tomography. *Journal of Food Engineering*, *112*(3), 227-242.

Skelland, A. H. P. (1967). *Non-Newtonian flow and heat transfer*. Wiley.

Slatter, P. T. (1997). The rheological characterization of sludges. *Water Science and Technology*, *36*(11), 9-18.

Smith, J. M. (1990). Industrial needs for mixing research. *Chemical engineering research & design*, *68*(1), 3-6.

Sokolov, L. I. (2013). Rheology of sludges and residues of effluent waters. *Life Science Journal*, *10*(4).

Sterbacek, Z., Tausk, P., & Sterbacek, Z. (1965). Mixing in the chemical industry.

T

Tahvildarian, P., Ng, H., D'Amato, M., Drappel, S., Ein-Mozaffari, F., & Upreti, S. R. (2011). Using electrical resistance tomography images to characterize the mixing of micron-sized polymeric particles in a slurry reactor. *Chemical engineering journal*, *172*(1), 517-525.

Tan, C., & Dong, F. (2009, August). Gas-water two-phase flow regime recognition with data and feature fusion from a dual-plane ERT system. In*2009 Fifth International Conference on Natural Computation* (pp. 218-222). IEEE.

Tan, C., & Dong, F. (2010). Cross correlation velocity of oil-water two-phase flow by a dual-plane electrical resistance tomography system. In *Instrumentation and Measurement Technology Conference (I2MTC), 2010 IEEE* (pp. 766-770). IEEE.

Tapp, H. S., & Williams, R. A. (2000). Status and applications of microelectrical resistance tomography. *Chemical Engineering Journal*, *77*(1), 119-125.

Tatterson, G. B. (1991). Fluid Mixing and Gas Dispersion in Agitated Tanks, (1991). *Tatterson, GB, Fluid Mixing and Gas Dispersion in Agitated Tanks*, 359.

Tixier, N., Guibaud, G., & Baudu, M. (2003). Determination of some rheological parameters for the characterization of activated sludge. *Bioresource Technology*, *90*(2), 215-220.

Toye, D., Fransolet, E., Simon, D., Crine, M., L'Homme, G., & Marchot, P. (2005). Possibilities and limits of application of electrical resistance tomography in hydrodynamics of bubble columns. *The Canadian Journal of Chemical Engineering*, *83*(1), 4-10.

V

Vasconcelos, J. M., Alves, S. S., & Barata, J. M. (1995). Mixing in gas-liquid contactors agitated by multiple turbines. *Chemical engineering science*, *50*(14), 2343-2354.

Vincent, T. L., & Mason, J. D. (1967). *A new method for treating optimal trajectories with restricted segments* (No. 744). University of Arizona.

Vlaev, S. D., & Martinov, M. (1999). Shape effects on impeller power characteristic for mixing and gassing power law fluids. In *Institution of Chemical Engineers Symposium Series* (Vol. 146, pp. 253-262). HEMSPHERE PUBLISHING CORPORATION.

W

Wang, M., Dorward, A., Vlaev, D., & Mann, R. (2000). Measurements of gas–liquid mixing in a stirred vessel using electrical resistance tomography (ERT). Chemical Engineering Journal, 77(1), 93-98.

Warmoeskerken, M. M. C. G., Feijen, J., & Smith, J. M. (1981). Hydrodynamics and power consumption in stirred gas-liquid dispersions. *Fluid Mixing*, *64*, J1-J14.

Wilkes, J. O. (2006). *Fluid Mechanics for Chemical Engineers with Microfluidics and CFD*. Pearson Education.

Williams, R. A., & Beck, M. S. (Eds.). (1995). *Process tomography: principles, techniques, and applications*. Butterworth-Heinemann.

Williams, R. A., Jia, X., West, R. M., Wang, M., Cullivan, J. C., Bond, J. & Kostuch, J. A. (1999). Industrial monitoring of hydrocyclone operation using electrical resistance tomography. Minerals Engineering, 12(10), 1245-1252.

Wójtowicz, R., Lipin, A. A., & Talaga, J. (2014). On the possibility of using of different turbulence models for modeling flow hydrodynamics and power consumption in mixing vessels with turbine impellers. Theoretical Foundations of Chemical Engineering, 48(4), 360-375.

X

Xu, Y., Wang, H., Cui, Z., & Dong, F. (2009, May). Application of electrical resistance tomography for slug flow measurement in gas/liquid flow of horizontal pipe. In *Imaging Systems and Techniques, 2009. IST'09. IEEE International Workshop on* (pp. 319-323). IEEE.

Y

Yang, C., Wang, H., & Cui, Z. (2012, May). Application of electrical resistance tomography in bubble columns for volume fraction measurement. In *Instrumentation and Measurement Technology Conference (I2MTC), 2012 IEEE International* (pp. 1199-1203). IEEE.

Yang, F., Zhou, S., & An, X. (2015). Gas–liquid hydrodynamics in a vessel stirred by dual dislocated-blade Rushton impellers. *Chinese Journal of Chemical Engineering*, *23*(11), 1746-1754.

Yenjaichon, W., Pageau, G., Bhole, M., Bennington, C. P., & Grace, J. R. (2011). Assessment of mixing quality for an industrial pulp mixer using electrical resistance tomography. *The Canadian Journal of Chemical Engineering*, *89*(5), 996-1004.

Yoshida, M., Ito, A., Yamagiwa, K., Ohkawa, A., Abe, M., Tezura, S., & Shimazaki, M. (2002). Effect of impeller clearance on power consumption of unsteadily forward-reverse rotating multiple impellers in an unbaffled agitation vessel. *Latin American applied research*, *32*(2), 189-194.

Yu, Z. Z., Peyton, A. T., Beck, M. S., Conway, W. F., & Xu, L. A. (1993). Imaging system based on electromagnetic tomography (EMT). *Electronics Letters*, *29*(7), 625-626.

Z

Zhang, Y., & Chen, Y. (2012). A novel PCA-SVM flow pattern identification algorithm for electrical resistance tomography system. In *Advances in Future Computer and Control Systems* (pp. 357-362). Springer Berlin Heidelberg.

Zhang, Z., Dong, F., & Xu, C. (2011). Data acquisition system based on CompactPCI bus and FPGA for electrical resistance tomography. In*Control and Decision Conference (CCDC), 2011 Chinese* (pp. 3538-3543). IEEE.

Zhao, Z. F., Mehrvar, M., & Ein-Mozaffari, F. (2008). Mixing time in an agitated multi-lamp cylindrical photoreactor using electrical resistance tomography. *Journal of chemical technology and biotechnology*, *83*(12), 1676-1688.